



## รายงานการวิจัยฉบับสมบูรณ์ปีที่ 2

การพัฒนา การศึกษาคุณสมบัติ และการประยุกต์ใช้ ของถ่านกัมมันต์ที่ได้จาก แบคทีเรียเซลลูโลส

Development and characterization of activated carbon derived from bacterial cellulose

(สัญญาเลขที่ GB-A\_60\_035\_21\_06)

แหล่งทุน	ทุนอุดหนุนการวิจัยจากเงินรายได้ ประเภทเงินอุดหนุนการวิจัยจากรัฐบาล ประจำปีงบประมาณ 2561
หัวหน้าโครงการ	ศาสตราจารย์ ดร.เหมือนเดือน พิศาลพงศ์
ส่วนงาน	ภาควิชาวิศวกรรมเคมี คณะวิศวกรรมศาสตร์

## กิตติกรรมประกาศ

โครงการวิจัยนี้ได้รับทุนอุดหนุนการวิจัยจากจุฬาลงกรณ์มหาวิทยาลัยและสำนักงานคณะกรรมการ วิจัยแห่งชาติ (วช.) นอกจากนี้ ผู้วิจัยขอขอบคุณ นายรัชคนัย อัสวมงคลกุล และ นายเชียรพิเชฐ เพ็งใหญ่ นิสิตในที่ปรึกษาซีเนียร์โปรเจ็ค (Senior Project), นายมิฟตะห์ฟาริด อิบนูอัब्ดุลวาฮับ นิสิตในที่ปรึกษาวิทยานิพนธ์ระดับปริญญาโท และ นายอนนท์ จำแก้ว นิสิตในที่ปรึกษาวิทยานิพนธ์ระดับปริญญาเอก ภาควิชา วิศวกรรมเคมี คณะวิศวกรรมศาสตร์ จุฬาลงกรณ์มหาวิทยาลัย ที่มีส่วนสำคัญในการช่วยในการดำเนินการทดลองวิจัย อีกทั้งขอขอบคุณ การสนับสนุนจากทุน “100 ปี จุฬาลงกรณ์มหาวิทยาลัย” สำหรับทุนอุดหนุนการศึกษาสำหรับนิสิตระดับปริญญาเอก

## Acknowledgement

This Research is funded by Chulalongkorn University and the National Research Council of Thailand (NRCT). I would like to thank my senior project advisees, Mr. Tatdanai Asavamongkolkul and Mr. Tianpichet Perngyai; my Master's thesis advisee, Mr. Miftahfarid Ibnu Abdulwahab; and my Doctoral thesis advisee, Mr. Arnon Khamkeaw for their assistances in research works. I also would like to acknowledge the 100<sup>th</sup> Anniversary Chulalongkorn University Fund for doctoral scholarship.

## บทคัดย่อ

แบคทีเรียเซลลูโลส (BC) ได้ถูกนำมาศึกษาเพื่อใช้เป็นวัสดุใหม่สำหรับการเตรียมถ่านกัมมันต์ โดยผ่านกระบวนการทำแห้ง และกระบวนการกระตุ้นทางเคมีด้วยการใช้สารละลายกรดฟอสฟอริก ( $H_3PO_4$ ) เป็นตัวกระตุ้น ที่อุณหภูมิ 400, 500 และ 600 องศาเซลเซียส สมบัติของถ่านกัมมันต์ ถูกวิเคราะห์ตรวจสอบ เช่น คุณสมบัติทางเคมี, โครงสร้าง และ ลักษณะรูพรุน คุณสมบัติทนความร้อน ด้วยเครื่อง Fourier transform infrared spectroscopy (FT-IR), X-ray diffraction (XRD),  $N_2$  -physisorption (BET), scanning electron microscopy (SEM), thermal gravimetric (TGA) จากการทดลองพบว่า ถ่านกัมมันต์จาก BC ที่ได้จากการถูกกระตุ้นที่ 500 องศาเซลเซียส (BC-AC500) มีพื้นที่ผิวที่วิเคราะห์โดย BET สูงสุดที่ 1,734 ตารางเมตร/กรัม โดยมีโครงสร้างรูพรุนขนาดกลาง มีขนาดรูพรุนโดยเฉลี่ยเท่ากับ 2.33 นาโนเมตร มีปริมาณความพรุนสูงถึง 1.01 ลูกบาศก์เมตร/กรัม สมบัติการดูดซับถูกประเมินโดยใช้เป็นตัวดูดซับเมทิลีนบลู (MB) โดยข้อมูลค่าดูดซับที่สมดุลถูกนำไปวิเคราะห์ด้วยแบบจำลองไอโซเทอมแบบ Langmuir, Freundlich, และ Redlich-Peterson โดยพบว่าข้อมูลการดูดซับที่สมดุลมีความสอดคล้องกับการอธิบายโดยแบบจำลองแบบ Redlich-Peterson มากที่สุด ที่ค่าสัมประสิทธิ์สหสัมพันธ์ (Correlation coefficient) ที่ค่า  $R^2 = 1.0$  มีค่าการดูดซับที่สมดุลสูงสุด ( $q_m$ ) ที่ 505.8 มิลลิกรัมต่อกรัม ผลจากการทดสอบชี้ให้เห็นว่า ถ่านกัมมันต์จาก BC มีศักยภาพในการนำมาใช้เป็นตัวดูดซับที่มีประสิทธิภาพสูง นอกจากนี้ BC และถ่านกัมมันต์ที่เตรียมจาก BC ได้ถูกพัฒนาต่อไปเป็นตัวรองรับตัวเร่งปฏิกิริยาตัวเร่งปฏิกิริยาแบบใหม่ Al/BC ถูกเตรียมโดยการแช่ BC บริสุทธิ์ในสถานะเจลบวมน้ำ (hydrogel) ในสารละลายอลูมิเนียมไนเตรตในน้ำ จากนั้นนำไปทำแห้งและเผาภายใต้อุณหภูมิสูง เมื่อนำตัวเร่งปฏิกิริยา Al/BC ไปใช้ในปฏิกิริยาการแยกน้ำออกจากเอทานอล (Ethanol dehydration) พบว่าให้ค่าผลได้ของไดเอทิลอีเทอร์จากเอทานอลสูงที่ประมาณ 42 เปอร์เซ็นต์ ที่อุณหภูมิ 200 องศาเซลเซียส โดยมีค่าการเลือกเกิด (selectivity) เกือบ 100 เปอร์เซ็นต์ อีกทางหนึ่งเมื่อนำ BC-AC500 ไปปรับปรุงสมบัติโดยการโหลดกรดฟอสฟอริก ( $H_3PO_4$ ) ที่ปริมาณต่างๆ และนำไปประยุกต์ใช้เป็นตัวเร่งปฏิกิริยาแบบกรด ในปฏิกิริยาการแยกน้ำออกจากเอทานอล (ethanol dehydration) ที่อุณหภูมิตั้งแต่ 200 ถึง 400 องศาเซลเซียส โดยการเพิ่มความเข้มข้นการโหลดกรดฟอสฟอริกตั้งแต่ 5 ถึง 40 เปอร์เซ็นต์ จะทำให้เพิ่มปริมาณตำแหน่งกรดอ่อนบนพื้นผิวตัวเร่งปฏิกิริยาซึ่งส่งผลให้การเปลี่ยนเอทานอลเป็นผลิตภัณฑ์ทำได้มากขึ้น ที่อุณหภูมิในการทำปฏิกิริยา 400 องศาเซลเซียส, BC-AC500 ที่มีกรดฟอสฟอริก 30-40 เปอร์เซ็นต์ (P/BC-AC) ให้ค่าการเปลี่ยนเอทานอลเป็นผลิตภัณฑ์ถึง 100 เปอร์เซ็นต์ โดยมีค่าการเลือกเกิดของเอทิลีนที่ 100 เปอร์เซ็นต์ ในขณะที่เมื่อใช้อุณหภูมิทำปฏิกิริยาที่ 200 องศาเซลเซียส จะได้ค่าการเปลี่ยนเอทานอลเป็นผลิตภัณฑ์ 49-51 เปอร์เซ็นต์และมีค่าการเลือกเกิดของไดเอทิลอีเทอร์ ที่ 66-68 เปอร์เซ็นต์ จากการทดสอบเสถียรภาพของระบบเป็นเวลา 12 ชั่วโมง ที่การดำเนินปฏิกิริยาที่ 200 และ 400 องศาเซลเซียส พบว่า ตัวเร่งปฏิกิริยา P/BC-AC มีความเสถียรภาพเชิงความร้อน และมีค่าการเร่งปฏิกิริยาที่คงที่ ดังนั้น P/BC-AC จึงเป็นตัวเร่งปฏิกิริยาที่มีประสิทธิภาพสูง มีราคาไม่แพงและเป็นมิตรต่อสิ่งแวดล้อม ในการนำมาใช้ในการผลิตเอทิลีนจากปฏิกิริยาการแยกน้ำออกจากเอทานอล

## Abstract

Bacterial cellulose (BC) was investigated as a novel material for preparing activated carbons. BC was dried by heating and it was carbonized with a chemical activation process using phosphoric acid ( $\text{H}_3\text{PO}_4$ ) as an activating agent at different temperatures (400, 500 and 600 °C). The properties of the activated carbons were characterized such as chemical property, structure, pore size, thermal property by Fourier transform infrared spectroscopy (FT-IR), X-ray diffraction (XRD),  $\text{N}_2$  -physisorption (BET), scanning electron microscopy (SEM), thermal gravimetric (TGA). The obtained BC activated carbons at carbonization temperature of 500 °C (BC-AC500) showed maximum BET surface area (1,734  $\text{m}^2/\text{g}$ ) with mesoporous structure (2.33 nm) and large pore volume (1.01  $\text{cm}^3/\text{g}$ ). The adsorption capacity was evaluated by using as adsorbent for the adsorption of methylene blue (MB). The equilibrium adsorption data were analyzed by the Langmuir, Freundlich, and Redlich-Peterson isotherm models. The results showed that the Redlich-Peterson model was found to be most fitted to the equilibrium data with correlation coefficient ( $R^2$ ) value of 1.000. The maximum adsorption capacity ( $q_m$ ) was 505.8 mg/g. The experimental results indicated that the BC activated carbon has the potential to be used as an effective adsorbent. A novel catalyst of Al/BC was developed by soaking purified BC hydrogel in aluminum nitrate aqueous solution, dehydration and calcination. The high yield of diethyl ether at ~ 42 % can be produced from ethanol at 200 °C with the selectivity of almost 100% by using Al/BC as catalyst in ethanol dehydration. On the other hand, BC activated carbon, BC-AC500 is modified with various loading of  $\text{H}_3\text{PO}_4$  and applied as acid catalyst in the ethanol dehydration reaction at the temperature from 200-400 °C. An increase in the  $\text{H}_3\text{PO}_4$  loading from 5% to 40% increased the number of weak acid sites on the catalyst surface, which consequently enhanced ethanol conversion. At a reaction temperature of 400 °C, the modified BC-AC500 with 30-40%  $\text{H}_3\text{PO}_4$  loading (P/BC-AC) gave ethanol conversion at 100%, with ethylene selectivity of 100%, whereas high selectivity for DEE at 66%-68%, at ethanol conversion of 49%-51% was obtained at 200 °C. Stability tests with a time-on-stream of 12 h, at reaction temperatures of 200 and 400 °C showed that the P/BC-AC catalyst had high thermal stability and stable catalytic activity. Therefore, P/BC-AC was found to be very effective as an inexpensive and environmentally friendly catalyst for ethylene production from ethanol dehydration.

## สารบัญเรื่อง (Table of Contents)

	หน้า
กิตติกรรมประกาศ	2
Acknowledgement	2
บทคัดย่อ	3
Abstract	4
สารบัญเรื่อง (Table of Contents)	5
สารบัญตาราง (List of Tables)	6
สารบัญภาพ (List of Illustration)	7
1. Introduction	8
1.1 Motivation	8
1.2 Specific objectives of the study	8
1.3 Theory and literature review	9
2. Materials and Methods	11
2.1 Materials	11
2.2 Methods	11
3. Results and discussions	13
3.1 Characterizations	13
3.2 Development of novel catalyst of Al/BC	17
3.3 Adsorption study	18
3.4 BC activated carbon as acid catalyst in the ethanol dehydration reaction	20
4. Conclusion	20
References	21
5. Output of the research	24
ภาคผนวก(Appendix) 1	25
ภาคผนวก(Appendix) 2	36
ภาคผนวก(Appendix) 3	37
ภาคผนวก(Appendix) 4	25
ภาคผนวก(Appendix) 5	36
ภาคผนวก(Appendix) 6	37
ประวัตินักวิจัยและคณะ พร้อมหน่วยงานสังกัด	67

## สารบัญตาราง (List of Tables)

	หน้า
Table 1 Porous properties of activated carbons derived from BC (BC-AC) at various carbonization temperatures and the comparison to those of activated carbons derived from other biomaterials.	15
Table 2 Catalytic activity of Al/BC catalyst as compared to other catalysts	17
Table 3 The maximum adsorption capacity for MB removal by BC-ACs as compared to those by ACs derived from other cellulosic materials.	18

## สารบัญภาพ (List of Illustration)

	หน้า
Figure 1. SEM images of BC activated carbons treated by $H_3PO_4$ .	9
Figure 2. SEM images of BC activated carbons treated by KOH.	10
Figure 3. The XRD patterns of activated carbons derived from BC (BC-AC).	13
Figure 4. The FT-IR patterns of activated carbon derived from bacterial cellulose at various carbonization temperatures.	14
Figure 5. SEM micrographs of activated carbon derived from bacterial cellulose at various carbonization temperatures.	16
Figure 6. Thermal gravimetric of BC-ACs at various carbonization temperatures;	16
Figure 7. Summarization of the procedure for the AI/BC preparation	17
Figure 8. Removal of MB at difference initial MB concentration	19

## 1. Introduction

### 1.1 Motivation

Activated carbon [1] is a form of carbon with high porosity, high surface area with physical and chemical stability, high adsorptive activity and high mechanical strength. Therefore, it is widely used in various applications in the industries such as an adsorbent in pressure swing adsorption [2], catalyst or catalyst support in chemical reactions [3], the removal of heavy metals from wastewaters [4], and gas separation process [5].

Activated carbon is usually derived from coal, wood or petroleum residues [6]. Biomass materials are considered as alternative raw materials which are inexpensive and renewable, such as hazelnut shell [7], coconut shell [8] and many agricultural wastes. Bacterial cellulose (BC) [9] is a cellulosic biomaterial with the formula  $(C_6H_{10}O_5)_n$  which is produced by bacteria, *Acetobacter xylinum*. BC has the unique properties including its high tensile strength, high water absorption capacity, high crystallinity and a nano-fiber network. Because of these characteristics, this research has been focusing on activated carbon derived from BC and the characteristics of BC activated carbon were studied.

BC was dried by heating and it was carbonized with a chemical activation process using phosphoric acid ( $H_3PO_4$ ) as an activating agent at different temperatures (400, 500 and 600 °C). The properties of the activated carbons were characterized by X-ray diffraction (XRD), scanning electron microscopy (SEM),  $N_2$ -physisorption, Fourier transform infrared spectroscopy (FT-IR) and thermal gravimetric (TGA). Adsorption capacity of BC activated carbon was investigated by using as adsorbent for the adsorption of methylene blue (MB). Novel catalysts using BC and activated carbon derived from BC were developed and characterized by using chemical activation ( $H_3PO_4$  as activated agent) at different activation temperatures such as 400, 500 and 600°C. The physical properties of samples were examined by means of XRD, SEM,  $N_2$ -physisorption, FTIR and TGA. In addition, BC activated carbons were used as catalyst support for acid catalysts in ethanol dehydration reaction at various temperatures in range 200 – 400°C.

### 1.2 Specific objectives of the study

1.2.1 To develop and characterize activated carbons derived from BC

1.2.2 To evaluate adsorption capacity of activated carbons derived from BC

1.2.3 To examine the catalytic activities of solid acid catalyst activity in the ethanol dehydration reaction such as selectivity and conversion.



### 1.3 Theory and literature review

**Activated carbon preparation:** There are two methods for activated carbon preparation; chemical and physical activation [1, 10-12]. Each of methods is responsible in different characteristics and structure of activated carbon.

- Physical activation: The process is divided into 2 steps. BC will be carbonized first at temperature range of 400-800°C to obtain charcoal and reduce volatile substance. Secondly, charcoal will be followed by activation step by oxygen or steam at temperature range 600-900°C.
- Chemical activation: BC is impregnated with an activating agent and then carbonized under an absence of atmosphere at lower temperature range of 450-600°C. The activating agent is typically acid or basis solution review such as ZnCl<sub>2</sub>, H<sub>3</sub>PO<sub>4</sub>, NaOH and KOH. The activating agent can partially dissolve the cellulosic components of the sample. This activation needs lower carbonization temperature, obtains higher yield, higher surface area, and better developed porosities compared to the physical activation.

#### 1.3.1 BC activated carbon by impregnation with H<sub>3</sub>PO<sub>4</sub> solution

Our preliminary works had studied on BC activated carbon using H<sub>3</sub>PO<sub>4</sub> and KOH solution as activating agents and then carbonized at different temperature. It was shown that activated carbons obtained by acid activation had mesoporous structure with higher surface area (1,000 -2,500 m<sup>2</sup>/g), whereas those from basic activation had more variance and larger porous structure with much less surface area (400-600 m<sup>2</sup>/g).

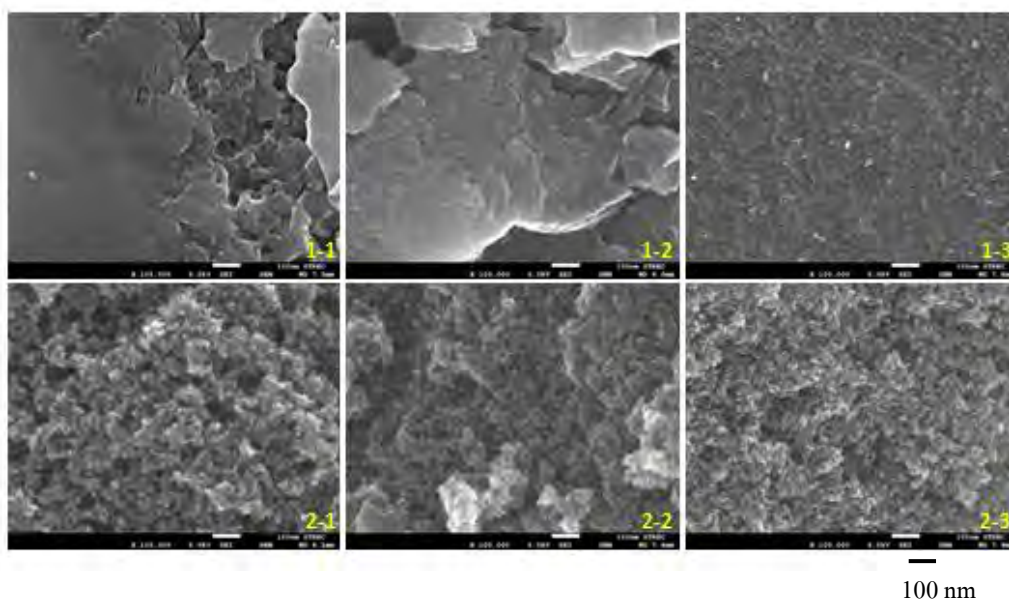


Figure 1. SEM images of BC activated carbons treated by H<sub>3</sub>PO<sub>4</sub>.

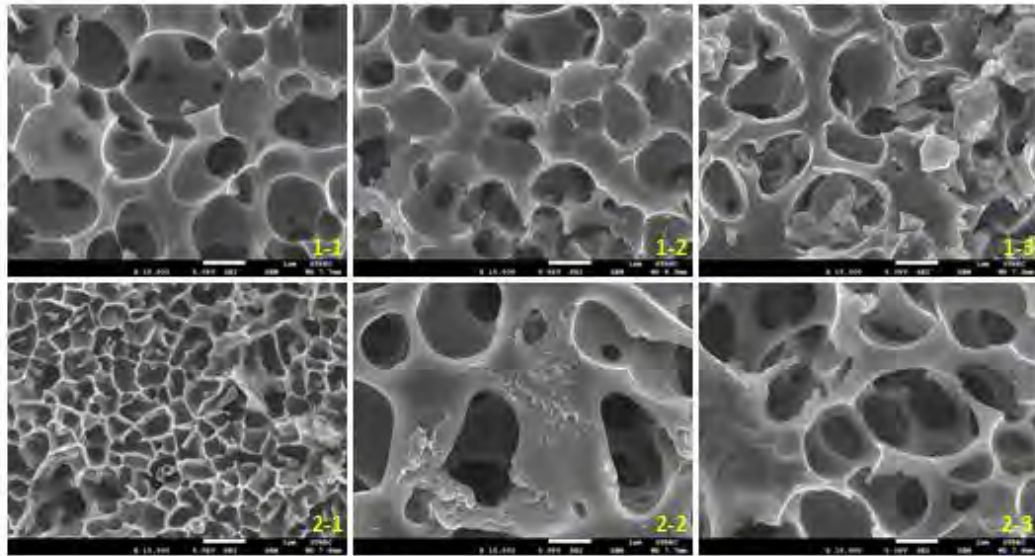
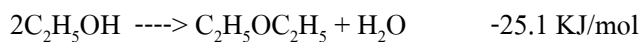
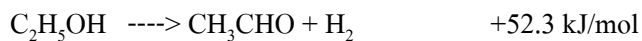
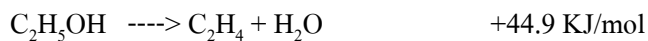


Figure 2. SEM images of BC activated carbons treated by KOH.

1  $\mu\text{m}$

### 1.3.2 Ethanol dehydration

Ethanol dehydration reaction [10, 12] is a removal of water from alcohol to produce ethylene and acetaldehyde as the main products followed byproduct including di-ethyl ether. This reaction is an endothermic reaction which requires acid catalyst such as phosphoric acid and sulfuric acid and requires a lower temperature than hydrocarbon cracking, leading to an energy cost reduction that is more environmental friendly. Recently, different catalysts such as zeolite, alumina and silica-alumina have been investigated as solid catalyst for this process. The reaction temperature is 180-500°C in gas phase. The chemical reactions are illustrated as below



### 1.3.3 Adsorption study

Adsorption technology [13] is a technique for removing micro pollutants from aqueous solutions such as organic and inorganic micro pollutants or colored and colorless organic pollutants. Adsorption process is considered as an important application for separation and purification in industrial processes using suitable adsorbents. The quality of adsorption depends on characteristics of the adsorbent including polarity, pore size and spacing. Adsorption experiments were conducted in liquid phase and the maximum adsorption capacity was determined. Experimental data were modeled using the Langmuir, Freundlich and Redlich–Peterson adsorption models to investigate the equilibrium isotherms, adsorption capacity and ability of the adsorbent to remove pollutants in aqueous solution.

## **2. Materials and Methods**

### **2.1 Materials**

Bacterial cellulose (BC) used in this project was supplied from the Institute of Research and Development of Food Product, Kasetsart University, Bangkok, Thailand. BC was synthesized by *A. xylinum* AGR 60. All the chemicals used in this project including sodium hydroxide (NaOH), potassium hydroxide (KOH), phosphoric acid (H<sub>3</sub>PO<sub>4</sub>), hydrochloric acid (HCl) and methylene blue (MB) were purchased from Sigma-Aldrich.

### **2.2 Methods**

#### **2.2.1 *Bacterial cellulose preparation***

BC hydrogel was treated with 1% w/v NaOH for 24 hours to remove bacterial cells, and then was rinsed with deionized (DI) water until pH was 7.0 and dried at 110°C for 24 hours.

#### **2.2.2 *Activated carbon preparation***

BC was first activated via 85% H<sub>3</sub>PO<sub>4</sub> with the ratio of 1:1 w/w and dried at 110°C for 24 hours. Then, it was carbonized in the furnace at the temperature of 400-600°C for 1 hour. The activated carbon (AC) was washed in stirred 1 molar HCl solution at 70°C for 4 hours and then washed with DI water until the pH of 7 was reached. Then, the AC was dried at 110°C for 24 hours.

#### **2.2.3 *Characterization***

The morphology of the BC-AC was detected by scanning electron microscope (SEM). SEM model was JEOL mode JSM-5900LV from the Scientific and Technological Research Equipment Center, Chulalongkorn University (STREC). The pore diameter, pore volume, and surface area were determined via N<sub>2</sub> adsorption at liquid nitrogen temperature of -196°C using a Micromeritics ASAP 2020 analyzer. The pore distribution, pore volume, and BET surface area were determined via the Brunauer-Emmett-Teller (BET) methods. Thermal gravimetric analysis (TGA) was performed at room temperature to 1000°C at the heating rate of 10°C per minute in N<sub>2</sub>. The TGA's model was the SDT analyzer Model Q600 from TA instrument, USA. The functional groups of BC-ACs were detected via FT-IR analysis (Nicolet 6700 FTIR spectrometer).

#### **2.2.4 Adsorption study**

Methylene blue (MB) solution of 40 mL was prepared at concentration of 600 mg/L in 100 mL Erlenmeyer flasks. Then, 0.02 g of different BC-AC was added into methylene blue solution in each flask and incubated in an orbital shaker at 30°C, 125 rpm for 6 hours. The samples were analyzed for MB concentration by UV-visible spectrophotometer (UV-2450; Shimadzu, Kyoto, Japan) at the wavelength of 664 nm. The samples were collected to analyze at 5, 10, 20, 30, 40, 50, 60, 90, 120, 180, 240, 300, and 360 minutes.

#### **2.2.5 Phosphoric acid catalyst preparation**

The phosphoric acid was loaded into BC-ACs. Then, the loaded BC-ACs were dried in oven at 110°C for 20 hours before cooling down. After that, the BC-ACs were washed in deionized water until the pH of 7 was reached. Lastly, the obtained catalysts were dehydrated at 110°C for 24 hours.

#### **2.2.6 Catalytic activity examination**

The catalytic activities of prepared BC-AC catalysts were examined via ethanol dehydration reaction at 200-400°C with a temperature increment of 50°C.

### 3. Results and discussions

#### 3.1 Characterization

**3.1.1 X-Ray Diffraction (XRD):** The bulk crystal structure of BC-ACs was identified by using XRD technique (Figure 3); XRD patterns of activated carbon by various carbonization temperatures were investigated. According to XRD result, activated carbons derived from BC have only a diffraction peak around  $2\theta = 22.50$ , which can be describe as amorphous carbon composted of aromatic carbon sheets [14].

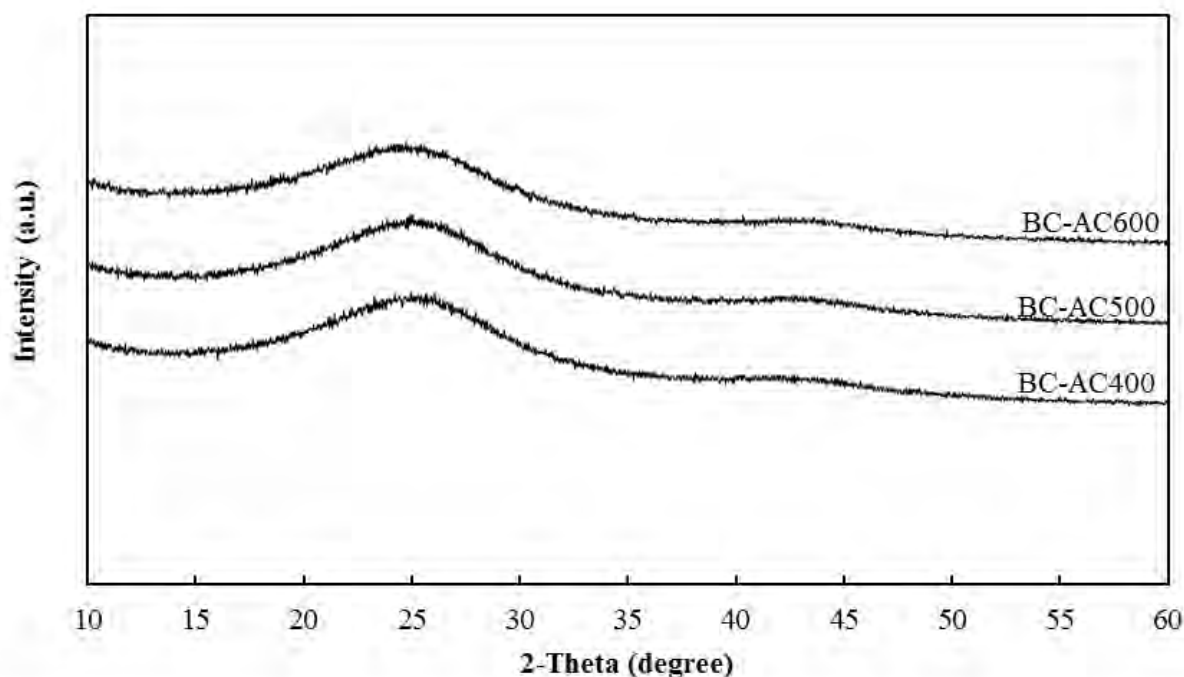


Figure 3. The XRD patterns of activated carbons derived from BC (BC-AC).

**3.1.2 Chemical structure:** The determination of functional group or chemical bonds existing in BC activated carbons (BC-AC) at various carbonization temperatures were measured in wave numbers by FT-IR spectra technique as shown in Figure 4. The broad band located around  $3200-3700\text{ cm}^{-1}$  is attributed to the O-H stretching vibration of the hydroxyl group. It was formed from the adsorption of water vapor in surrounding and moisture residue during carbonization process. The band at  $1600$  and  $1230\text{ cm}^{-1}$  are denoted as C=O and C-O stretching vibration of carbonyl groups, respectively due to the oxidative decomposition of organic species [15]. According to previous researchs [16-18], the broad bands are quite similar to activated carbons from difference biomass - based, which indicates the presence of the same functional groups. Other bands in the range of  $1000-1200\text{ cm}^{-1}$  are the characteristic of phosphorous and

phosphor carbonaceous compounds from phosphoric acid activation. The band at  $1100\text{ cm}^{-1}$  may be ascribed to the stretching vibration of hydrogen bonded P=O groups from phosphates or polyphosphates to O-C stretching vibrations in P-O-C (aromatic) linkage and to P=OOH [19]. The band that appears at  $1000\text{ cm}^{-1}$  ascribe to ionized linkage P-O- in acid phosphate esters and symmetrical vibration in a P-O-P chain [20]. The bands at 885 and 830 are assigned to C-H stretching of aromatic compounds [21].

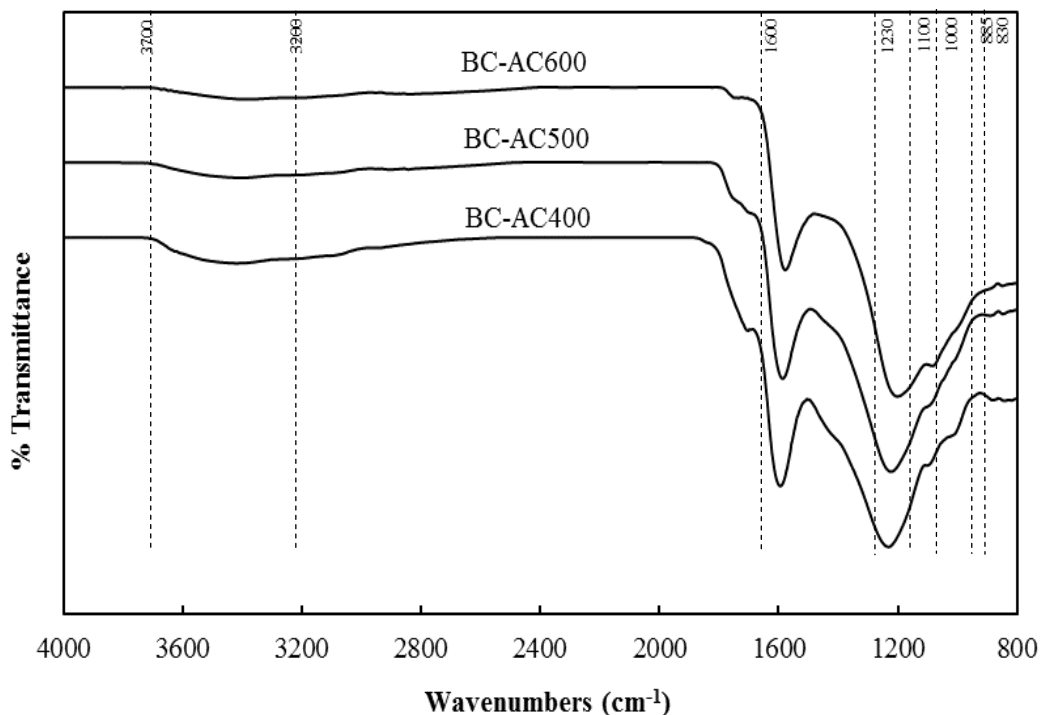


Figure 4 The FT-IR patterns of activated carbon derived from bacterial cellulose at various carbonization temperatures.

**3.1.3 Porous structure:** the structure of porosity; pore volume, pore size and specific surface area of activated carbon derived by BC (AC-BC) at various activation temperatures and drying method were determined by Nitrogen physisorption technique and compared to those of activated carbons derived from other biomaterials as shown in Table 1.

**Table 1** Porous properties of activated carbons derived from BC (BC-AC) at various carbonization temperatures and the comparison to those of activated carbons derived from other biomaterials.

Material	Activating agent	S <sub>BET</sub> (m <sup>2</sup> /g)	V <sub>t</sub> (cm <sup>3</sup> /g)	D <sub>p</sub> (nm)	Reference
BC-AC400	H <sub>3</sub> PO <sub>4</sub>	1,540	0.87	2.25	} This work
BC-AC500	H <sub>3</sub> PO <sub>4</sub>	1,734	1.01	2.33	
BC-AC600	H <sub>3</sub> PO <sub>4</sub>	1,702	1.01	2.37	
Cotton stalk	H <sub>3</sub> PO <sub>4</sub>	1,720	0.89	-	22
Coconut shell	CO <sub>2</sub>	1,700	1.14	2.70	23
Hazelnut bagasse	KOH	1,642	0.96	-	24
Bamboo	KOH	1,533	0.50	-	25
Deoiled rice bran residues	ZnCl <sub>2</sub>	1,385	0.68	1.98	26
Deoiled rice bran residues	H <sub>3</sub> PO <sub>4</sub>	1,187	0.61	2.22	26
Mangosteen	K <sub>2</sub> CO <sub>3</sub>	1,123	0.56	1.98	27
Almond treepruning	Steam	1,080	0.95	-	28
Durian shell	H <sub>3</sub> PO <sub>4</sub>	1,024	0.35	2.50	29
Rice husk	ZnCl <sub>2</sub>	927	0.56	0.80	30
Bagasse	ZnCl <sub>2</sub>	923	0.53	0.80	30
Coir pith	ZnCl <sub>2</sub>	910	0.36	1.60	31
Apricot stone	ZnCl <sub>2</sub>	814	0.43	34.7	32
Olivestone	Steam	813	0.55	-	28
Wood apple outer shell	ZnCl <sub>2</sub>	794	0.47	-	33
Walnutshell	Steam	792	0.52	-	28
Pistachio-nut shell	CO <sub>2</sub>	778	0.47	-	34
Hazelnut shell	ZnCl <sub>2</sub>	647	0.35	34.0	32
Cocoa podhusk	K <sub>2</sub> CO <sub>3</sub>	615	0.31	2.0	35
Almond shell	Steam	601	0.37	-	28
Sugarcane bagasse	Steam	320	0.17	2.10	36
Peanut hull	Steam	253	0.22	-	37
Palm kernel shell	KOH	217	0.12	-	38
Acacia mangim wood	KOH	5.25	0.015	11.79	39

Where: S<sub>BET</sub> = BET surface area; V<sub>total</sub> = Total pore volume; D<sub>p</sub> = Average pore diameter

**3.1.4. Surface morphology:** the surface morphologies of BC-ACs were observed by SEM as shown in Figure 5. In the comparison to surface morphology of BC, the surface morphology of all BC-ACs after carbonization by  $H_3PO_4$  activation was rougher, consisting of irregular small pores because of the evaporation of  $H_3PO_4$  and other volatiles during the carbonization.

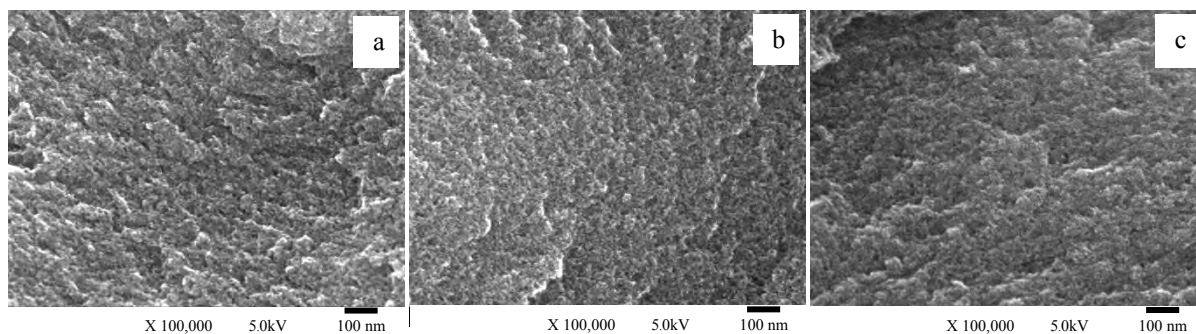


Figure 5. SEM micrographs of activated carbon derived from bacterial cellulose at various carbonization temperatures; BC-AC400 (a), BC-AC500 (b), and BC-AC600 (c).

**3.1.5. Thermal stability:** the mass loss during thermal gravimetric analysis of BC-AC at various carbonization temperatures is shown in Figure 6. The trends of TGA patterns of all BC-ACs are similar. The initial small mass loss at temperature around room temperature to  $100^{\circ}C$  could be attributed to moisture elimination. At 100 to  $500^{\circ}C$ , only small amount of carbon decomposition (less than 5 % of initial weight for BC-AC400 and BC-AC500; less than 2% of initial weight for BC-AC600) was detected, indicating that BC-ACs had high stability in the temperature range between 0 to  $500^{\circ}C$ .

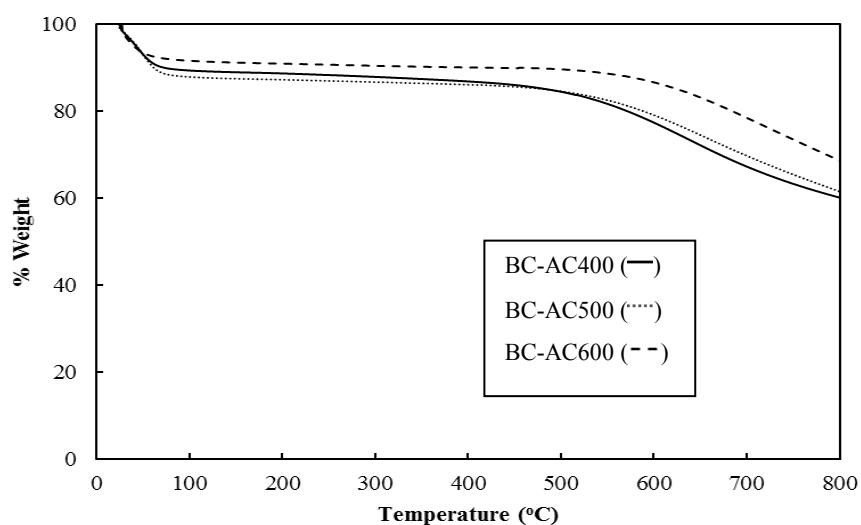


Figure 6. Thermal gravimetric of BC-ACs at various carbonization temperatures;



### 3.2 Development of novel catalyst of Al/BC (รายละเอียดเพิ่มเติมในภาคผนวก 1)

A novel catalyst of Al/BC was successfully developed by soaking purified bacterial cellulose (BC) hydrogel in aluminum nitrate aqueous solution, dehydration and calcination. Summarization of the procedure for the Al/BC preparation is shown in Figure 7. The Al/BC catalysts reveal interior meso–macro porous structures with average pore diameters in the range of 17–34 nm. The Al/BC catalyst has many promising properties, such as good metal dispersion, high chemical and thermal stabilities. The high yield of diethyl ether at ~ 42 % can be produced from ethanol at 200 °C with the selectivity of almost 100% by using Al/BC as catalyst in ethanol dehydration. The comparison of catalytic activity of Al/BC with others in ethanol dehydration is shown in Table 2.

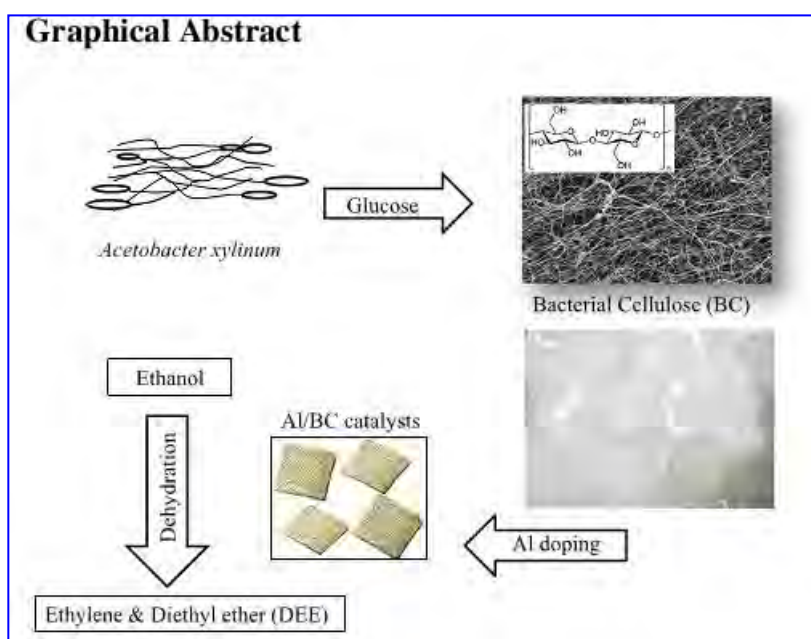


Figure 7. Summarization of the procedure for the Al/BC preparation [14].

**Table 2 Catalytic activity of Al/BC catalyst as compared to other catalysts [14]**

Catalysts	Surface area (m <sup>2</sup> /g)	Pore diameter (nm)	Reaction temperature (°C)	Ethanol conversion (%)	Ethylene yield (%)	DEE yield (%)
25Al/BC-TD	18	25.6	200–400	41.5–54.6	0.0–35.4	41.6–13.4
25Al/BC-FD	22	26.3	200–400	41.3–65.7	1.1–43.3	40.0–17.6
Al-com	137	3.9	200–400	0–95	0.0–71.3	0.0–0.0
Al-SG	152	3.5	200–400	15–98	6.8–78.4	7.0–0.0
Al-SV	215	9.3	200–400	10–100	2.5–100	7.5–0.0
Al-SSP	443.6	5.9	200–400	20–85	18.6–82.0	1.4–0.0
HBZ	522	2.2	200–400	7–100	0.0–99.4	7.1–0.0
Al-HBZ	306	3.4	200–400	9–92	0.0–90.2	9.5–1.8
M-Al	195	9.0	200–400	12–92	0.0–88.9	12.5–2.5

### 3.3 Adsorption study (รายละเอียดเพิ่มเติมในภาคผนวก 2 และ 3)

BC-AC600 and BC-AC500 had very high adsorption capacity with the maximum MB absorption of 507.5 and 504.4 mg/g, respectively, whereas BC-AC400 had relatively less adsorption capacity of 393.0 mg/g. The increasing of the surface area could encourage improved adsorption capacity due to more interaction between active sites of adsorbents and molecules of MB [40]. Considering the removal of MB, the percent removal of MB increased with the increase of the contact time, until the equilibrium was reached (Figure 8). The removal of MB of all BC-ACs at 100% could be achieved if the initial MB concentration was not greater than 100 mg/L. This is because the ratio of active site and MB molecule at low concentration is high, therefore all MB molecules could be adsorbed on active sites of the adsorbents [41]. BC-AC400, BC-AC500 and BC-AC600 showed the MB removal at 88.4, 99.8, and 99.8%, respectively, when the initial MB concentration was 200 mg/L. The removal of MB relatively decreased with the increase of the initial MB concentration from 200 to 600 mg/L. The results indicated that BC-ACs are effective adsorbents for the removal of MB from the solution, especially for the solutions with MB concentration  $\leq 200$  mg/L.

**Table 3** The maximum adsorption capacity for MB removal by BC-ACs as compared to those by ACs derived from other cellulosic materials.

Adsorbent	$q_m$ (mg/g)	Reference
BC-AC400	393.0	This work
BC-AC500	505.8	This work
BC-AC600	507.5	This work
Coconut husk-based AC	434.8	[42]
Peach stones-based AC	412.0	[43]
Date stone-based AC	398.2	[44]
Oil palm shell-based AC	303.0	[45]
Coconut shell-based AC	277.9	[46]
Oil palm fiber-based AC	277.8	[46]
Ground shell-based AC	164.9	[47]
Bamboo dust-based AC	143.2	[47]
Activated sewage char	120.0	[48]
Rice husk-based AC	60.1	[49]

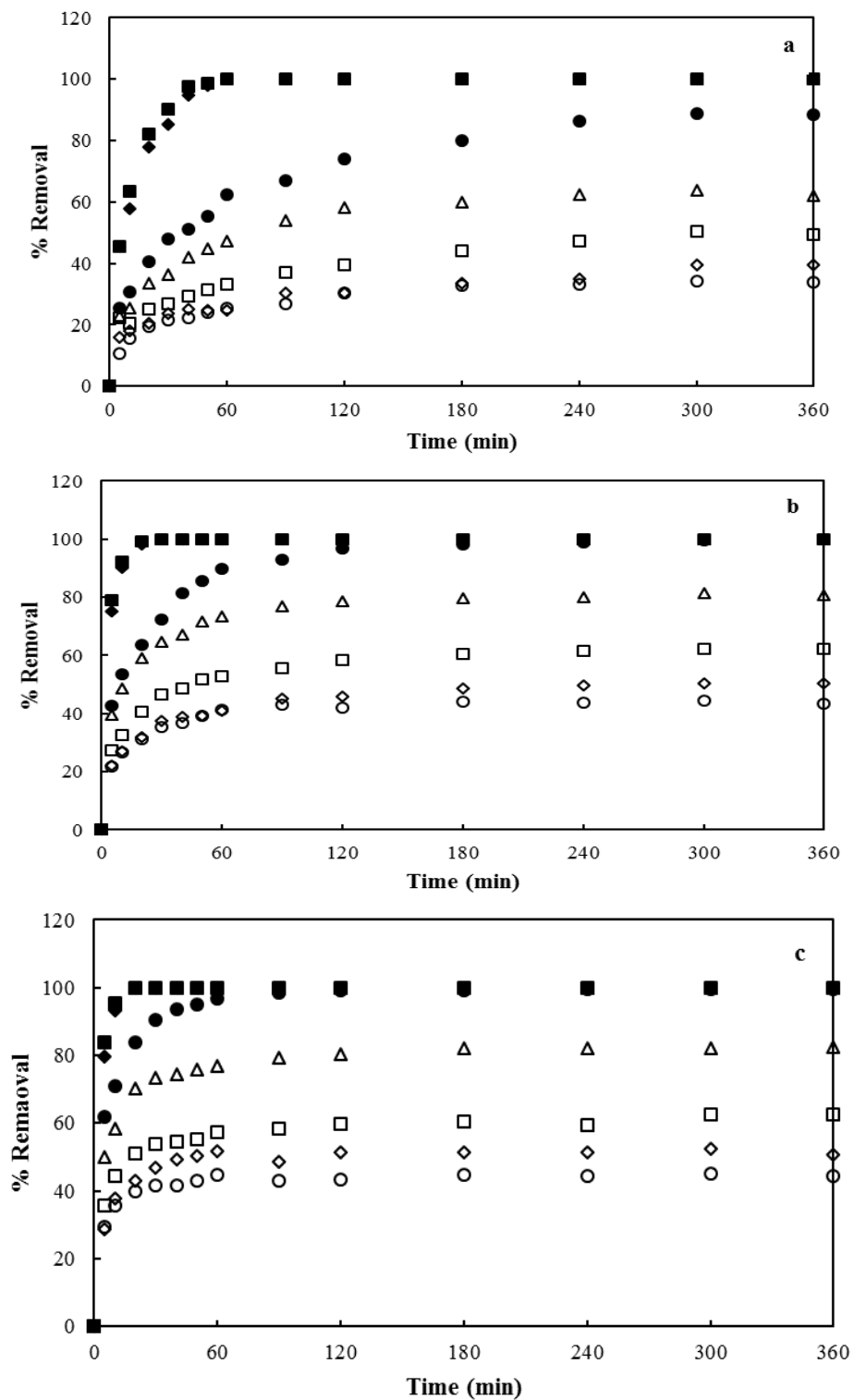


Figure 8 Removal of MB at difference initial MB concentration (■50, ◆100, ●200, △300, □400, ◇500, and ○600 mg/L) on difference BC-ACs; BC-AC400 (a), BC-AC500 (b), and BC-AC600 (c).

### 3.4 BC activated carbon as acid catalyst in the ethanol dehydration reaction (รายละเอียดเพิ่มเติมในภาคผนวก 4 และ 6)

Activated carbon derived from BC (BC-AC) with a highly uniform mesoporous structure was successfully prepared by one-step  $\text{H}_3\text{PO}_4$  activation at a carbonization temperature of  $500^\circ\text{C}$ . The BC-AC500 was modified with various loadings of  $\text{H}_3\text{PO}_4$ , namely P/BC-AC500 and was used as an inexpensive and environmentally friendly catalyst for ethanol dehydration. The results show that the P/BC-AC500 catalysts had larger numbers of weak acid sites than of moderate to strong acid sites, and the amount of weak acid sites increased with increasing  $\text{H}_3\text{PO}_4$  loading from 5% to 40%. The modified P/BC-AC catalyst was an efficient catalyst for the dehydration of ethanol to ethylene and DEE. The ethanol conversion of 98-100% and ethylene selectivity of 93-100% were obtained by using 30P/BC-AC500 and 40P/BC-AC500 catalysts at reaction temperature of  $300\text{-}400^\circ\text{C}$ , whereas the ethanol conversion at 42-50% with the selectivity of DEE at 65.7-68.4% was obtained at reaction temperature of  $200^\circ\text{C}$ . Under the stability test for 12 h, 30P/BC-AC500 was shown to act as an effective catalyst with high thermal stability to achieve complete conversion of ethanol with 100% ethylene yield at  $400^\circ\text{C}$ . Activated carbon developed from BC was found considerably more effective than those of commercial activated carbons. Unique physicochemical properties of highly pure nanocellulose fiber network structure with high surface area and uniform pore distribution are considered to be beneficial for BC to be used as a source of effective activated carbon catalysts.

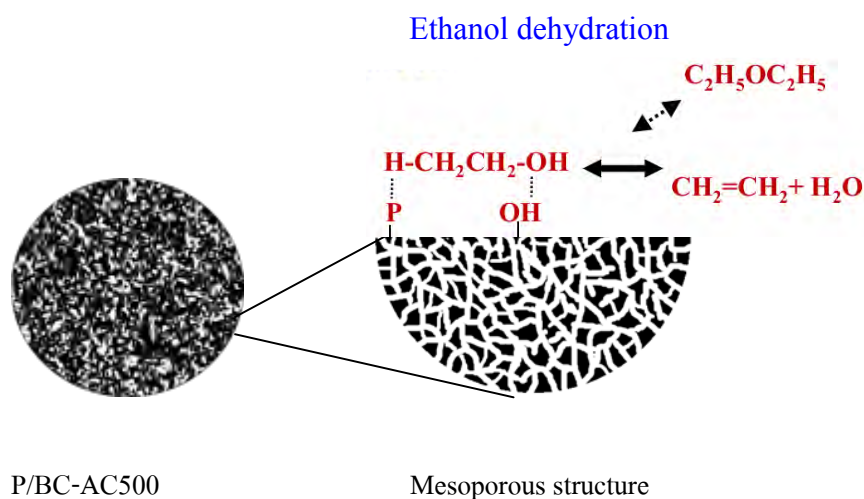
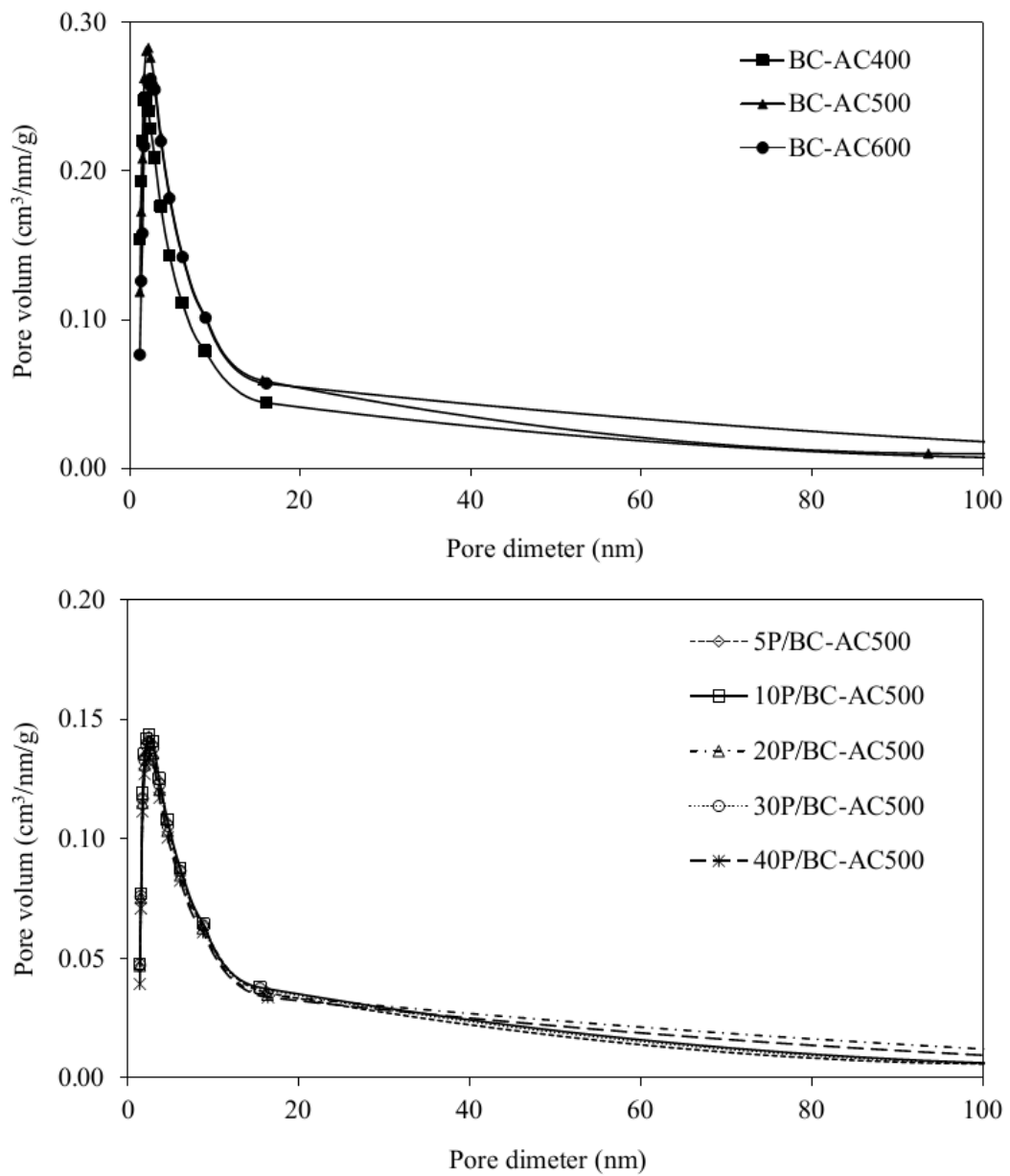


Figure 9 High surface area mesoporous activated carbon of P/BC-AC500 and its application in ethanol dehydration



**Figure 3** BJH pore size distribution of BC-AC (top) and P/BC-AC500 (bottom) catalysts

**Table 2** Surface elemental composition of catalysts obtained from EDX.

Catalysts	% weight			% Atom		
	C	P	O	C	P	O
BC-AC400	76.4	19.4	4.3	82.5	1.8	15.7
BC-AC500	80.0	10.0	10.0	87.5	4.3	8.2
BC-AC600	73.9	11.2	14.9	82.6	4.9	12.5
5P/BC-AC500	70.5	15.5	14.0	81.0	7.0	12.0
10P/BC-AC500	61.8	17.6	20.6	73.5	8.1	18.4
20P/BC-AC500	51.5	23.3	25.2	64.8	11.4	23.8
30P/BC-AC500	44.9	24.9	30.2	58.2	12.5	29.3
40P/BC-AC500	40.7	37.5	21.8	56.8	20.3	22.9

**Table 3** Acidity of catalysts

Catalysts	Acid site ( $\mu\text{mol NH}_3/\text{g catalyst}$ )*		
	Weak	Moderate to strong	Total
BC-AC400	162.9	109.4	272.3
BC-AC500	206.0	75.5	281.5
BC-AC600	200.0	73.6	273.6
5P/BC-AC500	215.4	98.9	311.4
10P/BC-AC500	239.1	114.1	353.2
20P/BC-AC500	434.6	146.4	581.0
30P/BC-AC500	1140.6	294.3	1434.8
40P/BC-AC500	1249.0	649.7	1898.7

\*Quantities of acid site of catalysts were determined using  $\text{NH}_3$ -TPD with Fityk program calculation.

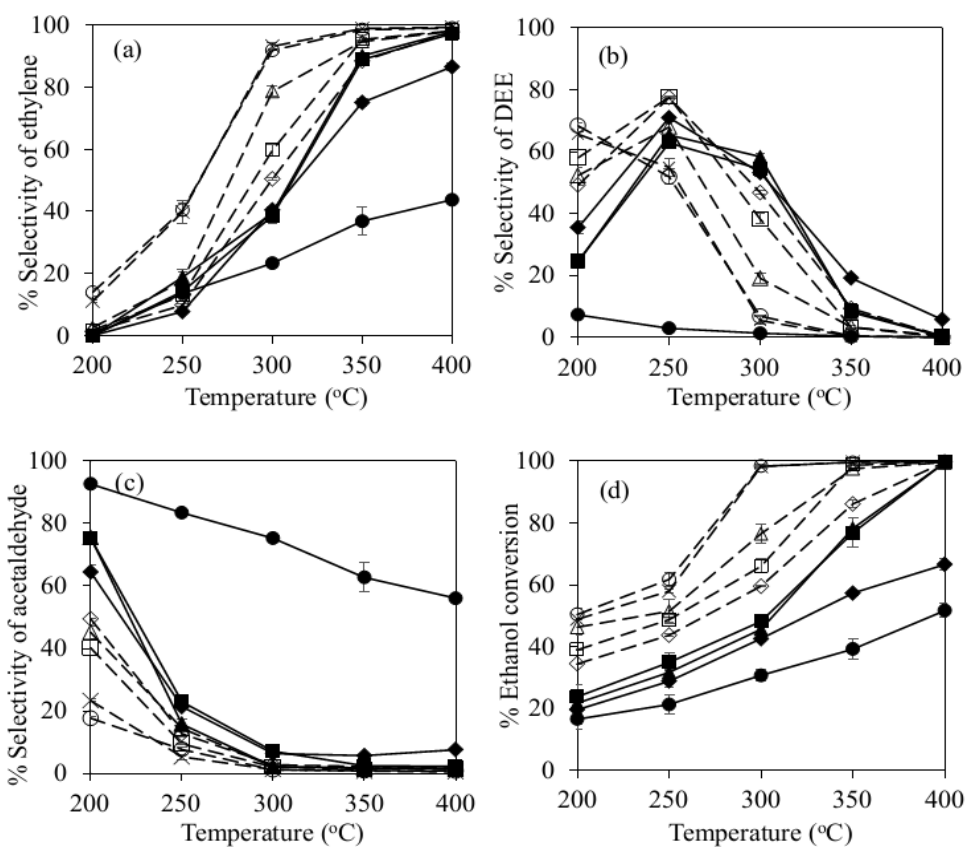


**Figure 8** Selectivity of ethylene (a), selectivity of DEE (b), and selectivity of acetaldehyde (c), and ethanol conversion (d) in ethanol dehydration at reaction temperatures of 200-400°C using the BC-AC, ACC, and P/BC-AC500 catalysts; BC-AC400 (◆), BC-AC500 (■), BC-AC600 (▲), ACC (●), 5P/BC-AC500 (◇), 10P/BC-AC500(□), 20P/BC-AC500 (Δ), 30P/BC-AC500 (○), and 40P/BC-AC500 (×)

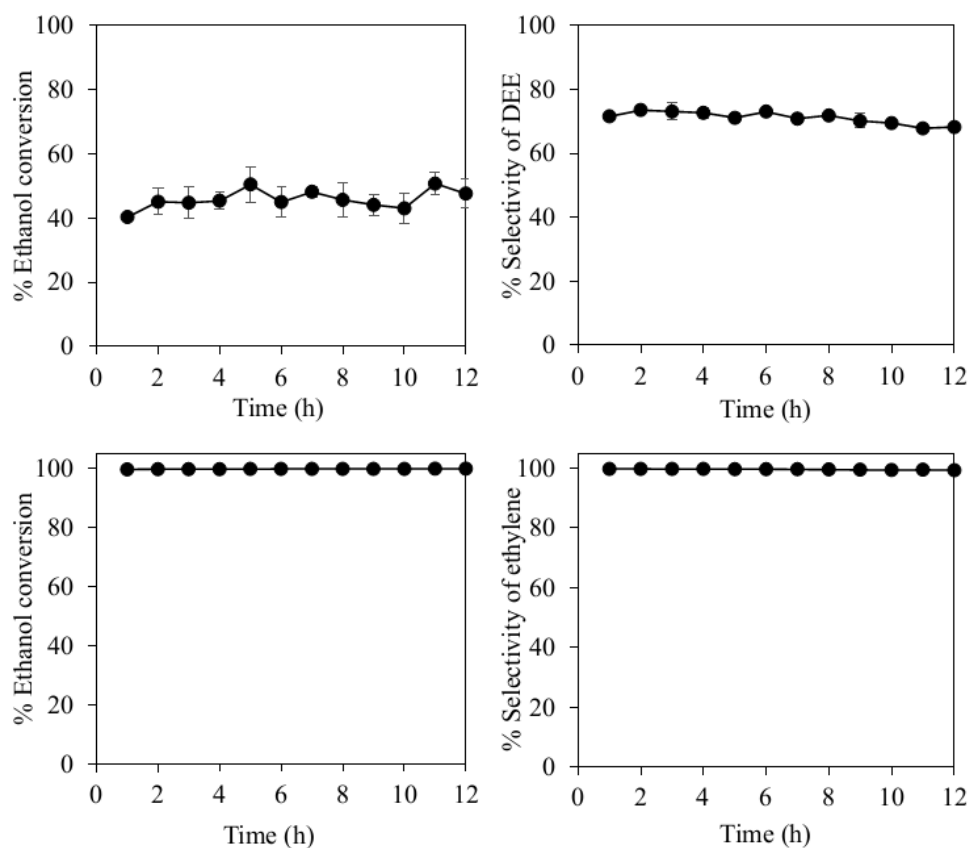


**Figure 9** Stability test with TOS for 30P/BC-AC500 catalyst at reaction temperature of 200 (top), and 400°C (bottom)

**Table 4** Yield of ethylene, diethyl ether (DEE), and acetaldehyde (MeCHO) from ethanol dehydration at 200, 300, and 400°C

Catalysts	200°C			300°C			400°C		
	Ethylene	DEE	MeCHO	Ethylene	DEE	MeCHO	Ethylene	DEE	MeCHO
ACC	0.0	0.8	15.3	7.3	0.4	23.0	22.6	0.1	29.0
BC-AC400	0.1	7.0	12.5	17.2	22.6	2.7	57.7	3.7	4.7
BC-AC500	0.0	6.0	17.8	18.9	25.9	3.3	97.0	0.3	2.3
BC-AC600	0.0	5.3	16.4	18.0	26.7	1.0	97.5	0.3	1.74
5P/BC-AC500	0.4	17.0	17.1	30.1	27.8	1.6	97.7	0.5	1.6
10P/BC-AC500	0.7	22.7	0.7	39.6	25.1	1.3	98.0	0.2	1.5
20P/BC-AC500	1.2	24.2	1.1	60.3	14.6	1.6	97.8	0.5	1.3
30P/BC-AC500	7.1	34.5	2.5	90.5	6.8	1.1	100.0	0.0	0.0
40P/BC-AC500	5.4	32.1	2.6	91.7	5.4	1.2	100.0	0.0	0.0



#### 4. Conclusion

The production of high surface area activated carbon from biomass has attracted attentions due to its wide range of applications. In this research, bacterial cellulose (BC) is used as carbon source for activated carbon preparation due to its highly nanoporous structure and eco-friendliness. BC was carbonized with a chemical activation process using phosphoric acid ( $H_3PO_4$ ) as an activating agent at different temperatures (400, 500 and 600 °C). The carbonization temperature significantly affected the porous structure of BC-AC. The carbonization temperature at 500°C exhibits the highest surface area of 1,734.2  $m^2/g$  with the total pore volume of 1.011  $cm^3/g$ . BC-ACs had mesoporous structure with the average pore diameter of 2.2-2.4 nm. BC-ACs had high stability in the temperature between 100 to 500°C.

By using BC-AC500 or BC-AC600 for MB removal, the equilibrium could be reached within 10 min for the system with low MB concentration (50-100 mg/L) and 240 min with high MB concentration (200-600 mg/L). The removal of MB from the solution with the initial MB concentration not greater than 200 mg/L was almost 100%. From the experimental study, the maximum MB adsorption capacity of BC-AC400, BC-AC500, and BC-AC600 were 393.0, 505.8, and 507.5 mg/g, respectively, which were very close to the values of maximum adsorption capacity ( $q_m$ ) estimated from Langmuir model. The Redlich-Peterson was shown to be the best-fitting model with  $R^2$  value of 1.000 for all BC-ACs. BC-AC was found very effective for using as an adsorbent to remove MB from water.

A novel catalyst of Al/BC was developed by soaking purified BC hydrogel in aluminum nitrate aqueous solution, dehydration and calcination. The Al/BC catalyst has many promising properties as catalyst in ethanol dehydration, such as good metal dispersion, high chemical and thermal stabilities. The high yield of diethyl ether at ~ 42 % can be produced from ethanol at 200 °C with the selectivity of almost 100% by using Al/BC as catalyst in ethanol dehydration.

BC-AC500 were modified by  $H_3PO_4$  loading and characterized. The physical properties of samples were examined by means of XRD, SEM, N<sub>2</sub>-physisorption, FTIR and TGA. It was applied as an acid catalyst in ethanol dehydration reaction at various temperatures in range 200 – 400°C. An increase in the  $H_3PO_4$  loading from 5% to 40% increased the number of weak acid sites on the catalyst surface, which consequently enhanced ethanol conversion. At a reaction temperature of 400 °C, the modified BC-AC500 with 30-40%  $H_3PO_4$  loading (P/BC-AC) gave ethanol conversion at 100%, with ethylene selectivity of 100%, whereas high selectivity for DEE at 66%-68%, at ethanol conversion of 49%-51% was obtained at 200 °C. Stability tests with a time-on-stream of 12 h, at reaction temperatures of 200 and 400 °C showed

that the P/BC-AC catalyst had high thermal stability and stable catalytic activity. Therefore, P/BC-AC was found to be very effective as an inexpensive and environmentally friendly catalyst for ethylene production from ethanol dehydration. For future work, Modification of the porous structure for improved mass transfer rate and enhanced product selectivity will be carried out. Experimental studies will be performed in order to develop a simple and effective method for producing effective solid catalysts from BC-AC as an alternative eco-friendly catalyst.

## References

- [1] Adib Yahya, Mohd; Al-Qodah, Z.; and Zanariah Ngah, C.W. Agricultural bio-waste materials as potential sustainable precursors used for activated carbon production: A review. *Renewable and Sustainable Energy Reviews* 46 (2015): 218–235
- [2] Siriwardane, V. R.; Shen S. M.; Fisher P. E.; and Poston, A. J. Adsorption of CO<sub>2</sub> on Molecular Sieves and Activated Carbon. *Energy Fuels* 15 2(2001): 279-284.
- [3] Wu, X.; Zhu, F.; Qi, J.; and Zhao, L. Biodiesel production from sewage sludge by using alkali catalyst catalyze. *Procedia Environmental Sciences* 31 (2016): 26–30.
- [4] Kadirvelu, K.; Thamaraiselvi, K.; and Namasivayam, C. Removal of heavy metals from industrial wastewaters by adsorption onto activated carbon prepared from an agricultural solid waste. *Bioresource Technology* 761 (2001): 63-65.
- [5] Sircar, S.; Golden, C. T.; Rao, B. M. Activated carbon for gas separation and storage. *Carbon* 34, (1996): 1-12.
- [6] Altenor, S.; Carene, B.; Emmanuel, E.; Lambert, J.; Ehrhardt, JJ.; and Gaspard, S. Adsorption studies of methylene blue and phenol onto vetiver roots activated carbon prepared by chemical activation. *J Hazard Mater* 169 (2009): 1029–1039.
- [7] Orkun, Y.; Karatepe, N.; and Yavuz, R. Influence of temperature and impregnation ratio of H<sub>3</sub>PO<sub>4</sub> on the production of activated carbon from hazelnut shell. *Acta Phys Pol A* 121 (2012): 277–280.
- [8] Olafadehan, OA.; Jinadu, OW.; Salami, L.; and Popoola, OT. Treatment of brewery waste water effluent using activated carbon prepared from coconut shell. *Int J Appl Sci Technol* 2 (2012): 165–178.
- [9] Kirdponpattara, S. Properties and application of bacterial cellulose-alginate composite sponges. Doctoral's Thesis, Department of Chemical Engineering, Faculty of Engineering, Chulalongkorn University, 2012.
- [10] Phanthang, L. Characteristics of activated carbon derived from bacterial cellulose and its application as a catalyst support. Master's Thesis, Department of Chemical Engineering, Faculty of Engineering, Chulalongkorn University, 2013.

- [11] Boongate, C.; and Phisalaphong, M. Activated carbons from bacterial cellulose by chemical activation with potassium hydroxide. International conference on science and technology, Bangkok: RMUTT, 2015.
- [12] Chatchawanrat, S. Dehydrogenation of ethanol to acetaldehyde over activated carbon catalyst. Master's Thesis, Department of Chemical Engineering, Faculty of Engineering, Chulalongkorn University, 2013.
- [13] Emad N. El Qada; Allen, J. S.; and Walker, M. G. Adsorption of Methylene Blue onto activated carbon produced from steam activated bituminous coal: A study of equilibrium adsorption isotherm. *Chemical Engineering Journal* 124 (2006): 103–110.
- [14] Ibnu Abdulwahab, M.; Khamkeaw, A.; Jongsomjit, B.; and Phisalaphong, M. Bacterial Cellulose Supported Alumina Catalyst for Ethanol Dehydration. *Catalysis Letters* 147(2017): 2462-2472.
- [15] Finocchio, E.; Cristiani, C.; Dotelli, G.; Stampino, P.G.; Zampori, L. Thermal evolution of PEG-based and BRIJ-based hybrid organo-inorganic materials. FT-IR studies, *Vib. Spectrosc.* 71 (2014): 47-56.
- [16] Chen, Y.; Huang, B.; Huang, M.; Cai, B. On the preparation and characterization of activated carbon from mangosteen shell, *J. Taiwan Inst. Chem. E.* 42 (2011): 837-842.
- [17] Oliveira, L.C.A.; Pereira, E.; Guimaraes, I.R.; Vallone, A.; Pereira, M.; Mesquita, J.P.; Sapag, K. Preparation of activated carbons from coffee husks utilizing  $\text{FeCl}_3$  and  $\text{ZnCl}_2$  as activating agents, *J. Hazard. Mater.* 165 (2009): 87-94.
- [18] Shi, Q.; Zhang, J.; Zhang, C.; Li, C.; Zhang, B.; Hu, W.; Xu, J.; Zhao, R. Preparation of activated carbon from cattail and its application for dyes removal, *J. Environ. Sci.* 22 (2010): 91-97.
- [19] Yorgun, S.; Yıldız, D. Preparation and characterization of activated carbons from Paulownia wood by chemical activation with  $\text{H}_3\text{PO}_4$ , *J. Taiwan Inst. Chem. E.* 53 (2015): 122-131.
- [20] Yakout, S.M.; Sharaf El-Deen, G. Characterization of activated carbon prepared by phosphoric acid activation of olive stones, *Arab. J. Chem.* 9 (2016): S1155-S1162.
- [21] Pereira, R.G.; Veloso, C.M.; Silva, N.M.; Sousa, L.F.; Bonomo, R.C.F.; Souza, A.O.; Souza, M.O; Fontan, R. Preparation of activated carbons from cocoa shells and siriguela seeds using  $\text{H}_3\text{PO}_4$  and  $\text{ZnCl}_2$  as activating agents for BSA and  $\alpha$ -lactalbumin adsorption, *Fuel Process. Technol.* 126 (2014): 476-486.
- [22] Nahil, MA., et al., Pore characteristics of activated carbons from the phosphoric acid chemical activation of cottons talks. *Biomass Bioenergy* 37 (2012): 142–9.
- [23] Guo, S., et al., Effects of  $\text{CO}_2$  activation on porous structures of coconut shell-based activated carbons. *Appl Surf Sci*, 255 (2009): 8443–8449.
- [24] Demiral, H., et al., Pore structure of activated carbon prepared from hazelnut bagasse by chemical activation. *Surf Interface Anal* 40 (2008): 616–619.
- [25] Hirunpraditkoon, S., et al., Adsorption capacities of activated carbons prepared from bamboo by KOH activation. *World Acad Sci Eng Technol*, 78 (2011): 711–715.

- [26] Niticharoenwong, B., et al., Characteristics of activated carbons derived from deoiled rice bran residues. *Chemical Engineering Communications*, 200 (2013): 1309-1321.
- [27] Chen, Y., et al., On the preparation and characterization of activated carbon from mangosteen shell. *Journal of the Taiwan Institute of Chemical Engineers*, 42(2011): 837-842.
- [28] Gonzalez, J.F., et al., Pyrolysis of various biomass residues and char utilization for the production of activated carbons. *J Anal Appl Pyrol*, 85(2009): 134–141.
- [29] Jun, T.Y., et al., Effect of activation temperature and heating duration on physical characteristics of activated carbon prepared from agriculture waste. *Environ Asia*, 3 (2010): 143–148.
- [30] Boonpoke, A., et al., Synthesis of activated carbon and MCM-41 from bagasse and rice husk and their carbon dioxide adsorption capacity. *J Sustain Energy Environ*, 2(2011): 77–81.
- [31] Subha, R., et al., Zinc chloride activated coir pith carbon as low cost adsorbent for removal of 2,4-dichlorophenol: equilibrium and kinetics studies. *Indian J Chem Technol*, 14(2009): 471–479.
- [32] Ozcimen, D., et al., Adsorption of copper(II) ions on hazelnut shell and apricot stone activated carbons. *Adsorp Sci Technol*, 28(2010): 327–41.
- [33] Bhadusha, N., et al., Adsorptive removal of methylene blue onto ZnCl<sub>2</sub> activated carbon from wood apple outer shell: kinetics and equilibrium studies. *E-JChem*, 8(2011): 1696–1707.
- [34] Lua, A.C., et al., Effect of pyrolysis conditions on the properties of activated carbon prepared from pistachio-nutshells. *J Anal Appl Pyrol*, 72 (2004): 279–287.
- [35] Cruz, G., et al., Production of activated carbon from Cocoa (*Theobroma cacao*) pod husk. *Civ Environ Eng*, 2(2012): 1–6.
- [36] Devnarain, P.B., et al., Production of activated carbon from South African sugar cane bagasse. *Proc SAfr Sug Tech Ass*, 76(2002): 477–489.
- [37] Girgis, B.S., et al., Characteristics of activated carbon from peanut hulls in relation to conditions of preparation. *Mater Lett*, 57 (2002): 164–172.
- [38] Abechi, S.E., et al., Preparation and characterization of activated carbon from Palm Kernel shell by chemical activation. *Res J Chem Sci*, 3(2013): 54–61.
- [39] Danish, M., et al., Characterization of Acacia mangium wood based activated carbons prepared in the presence of basic activating agents. *Bioresources*, 6(2011): 3019–3033.
- [40] Aguayo-Villarreal, I.A.; Bonilla-Petriciolet, A.; Muñiz-Valencia, R. Preparation of activated carbons from pecan nutshell and their application in the antagonistic adsorption of heavy metal ions, *J. Mol. Liq.* 230 (2017): 686-695.
- [41] Geçgel, Ü.; Özcan, G.; Gürpınar, G.Ç. Removal of methylene blue from aqueous solution by activated carbon prepared from pea shells (*Pisum sativum*), *J. Chem-Ny.* 2013 (2013): 9.

- [42] Tan, I.A.W.; Ahmad, A.L.; Hameed, B.H. Adsorption of basic dye on high-surface-area activated carbon prepared from coconut husk: Equilibrium, kinetic and thermodynamic studies, *J. Hazard. Mater.* 154 (2008): 337-346.
- [43] Attia, A.A.; Girgis, B.S.; Fathy, N.A. Removal of methylene blue by carbons derived from peach stones by H<sub>3</sub>PO<sub>4</sub> activation: Batch and column studies, *Dyes Pigments* 76 (2008): 282-289.
- [44] Ahmed, M.J.; Dhedan, S.K. Equilibrium isotherms and kinetics modeling of methylene blue adsorption on agricultural wastes-based activated carbons, *Fluid Phase Equilibr.* 317 (2012): 9-14.
- [45] Tan, I.A.W.; Ahmad, A.L.; Hameed, B.H. Enhancement of basic dye adsorption uptake from aqueous solutions using chemically modified oil palm shell activated carbon, *Colloid. Surface A.* 318 (2008): 88-96.
- [46] Tan, I.A.W.; Hameed, B.H.; Ahmad, A.L. Equilibrium and kinetic studies on basic dye adsorption by oil palm fibre activated carbon, *Chem. Eng. J.* 127 (2007): 111-119.
- [47] Kannan, N.; Sundaram, M.M. Kinetics and mechanism of removal of methylene blue by adsorption on various carbons—a comparative study, *Dyes Pigment* 51 (2001): 25-40.
- [48] Sainz-Diaz, C.I.; Griffiths, A.J. Activated carbon from solid wastes using a pilot-scale batch flaming pyrolyser, *Fuel* 79 (2000): 1863-1871.
- [49] El-Halwany, M.M. Study of adsorption isotherms and kinetic models for Methylene Blue adsorption on activated carbon developed from Egyptian rice hull (Part II), *Desalination* 250 (2010): 208-213.

## **5. Output of the research** (international journal publication / international conference / patent)

### 5.1 Bacterial Cellulose Supported Alumina Catalyst for Ethanol Dehydration,

International journal publication, *Catalysis Letters*: 147:2462–2472, 2017 (IF in 2017= 2.911),

(Appendix 1)

5.2 Characteristics of Activated Carbon Derived from Bacterial Cellulose and Its Application as an Adsorbent, Oral presentation in the 3<sup>th</sup> Symposium on Bacterial NanoCellulose, Fukuoka, Japan (16-17 Oct, 2017) (Appendix 2)

5.3 Activated Carbon from Bacterial Cellulose as an Effective Adsorbent for Removing Dye from Aqueous Solution, International journal publication, *Separation Science and Technology* (Published online: 04 Dec 2018) (IF in 2017= 1.200) (Appendix 3)

5.4 Activated carbon derived from bacterial cellulose and its application as an adsorbent and catalyst support material, Poster presentation in *Chemeca 2018*, 30 September - 3 October 2018, New Zealand (Appendix 4)

5.5 ดำเนินการจดอนุสิทธิบัตรสิ่งประดิษฐ์และกรรมวิธีการผลิต เรื่องถ่านกัมมันต์จากแบคทีเรียเซลลูโลสด้วยกระบวนการกระตุ้นทางเคมี และกรรมวิธีการผลิต ผ่านสถาบันทรัพย์สินทางปัญญา จุฬาลงกรณ์มหาวิทยาลัย (Appendix 5)

5.6 Activated carbon derived from bacterial cellulose and its use as a catalyst for ethanol dehydration, International journal publication, submitted to Catalysis communications (2019)(IF in 2017= 3.463), (Appendix 6)

## Bacterial Cellulose Supported Alumina Catalyst for Ethanol Dehydration

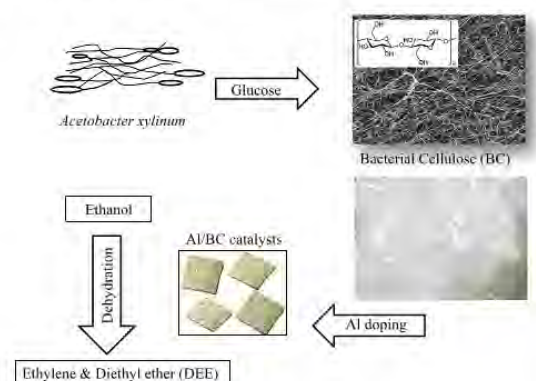
M. Ibnu Abdulwahab<sup>1,2</sup> · A. Khamkeaw<sup>1,2</sup> · B. Jongsomjit<sup>2</sup> · M. Phisalaphong<sup>1</sup>

Received: 28 March 2017 / Accepted: 9 July 2017 / Published online: 20 July 2017  
© Springer Science+Business Media, LLC 2017

**Abstract** An ultrafine three-dimensional nanofiber network structure of a very high porosity endows bacterial cellulose (BC) to function as support for heterogeneous catalysis. A novel catalyst of BC supported alumina ( $\text{Al}_2\text{O}_3$ ) was developed by soaking purified BC hydrogel in aluminum nitrate ( $\text{Al}(\text{NO}_3)_3$ ) aqueous solution, dehydration (hot air drying and freeze-drying) and calcination. The Al/BC catalysts reveal interior meso–macro porous structures with average pore diameters in the range of 17–34 nm. The catalytic activities were examined through an ethanol dehydration reaction in the gas phase at atmospheric pressure in the range of 200–400 °C. The effects of acidic metal loading and dehydration methods were investigated. Increasing Al loading from 12 to 50% resulted in a decreased surface area but an increase in pore size. At the same Al loading, the catalysts with a dehydration process by hot air drying presented higher Al concentrations on the outer surface compared with those by freeze-drying. At high temperature of 400 °C, Al/BC catalysts with 25 wt% Al loading and dehydrated by freeze drying (25Al/BC FD) and 50 wt% Al loading, dehydrated by hot air drying (50Al/BC TD) exhibited the highest ethanol conversions of 65.7–66.4% and ethylene yields of 43.26–44.24%, respectively, whereas at low temperature of 200 °C, Al/BC catalysts with 25 wt% Al

loading with either dehydration method exhibited the highest diethyl ether yields of 40.02–41.60%.

### Graphical Abstract



**Keywords** Catalyst support · Composites · Reaction · Bacterial cellulose · Alumina · Ethanol dehydration

### 1 Introduction

Carbon materials show several advantages as supports in heterogeneous catalysis, including highly porous structure, high stabilities at high temperatures in non-oxidizing atmospheres, renewable resources, low-cost and environmental friendly materials [1–4]. Cellulose is the most abundant carbon source, mainly obtained from plant-based materials. Very few species of bacteria can also produce cellulose. Plant-based cellulose generally contains impurities such as lignin and hemicellulose, whereas bacterial cellulose (BC) is nearly pure cellulose [5]. BC can be

✉ M. Phisalaphong  
Muenduen.p@chula.ac.th

<sup>1</sup> Chemical Engineering Research Unit for Value Adding of Bioresources, Department of Chemical Engineering, Faculty of Engineering, Chulalongkorn University, Bangkok 10330, Thailand

<sup>2</sup> Center of Excellence on Catalysis and Catalytic Reaction Engineering, Department of Chemical Engineering, Faculty of Engineering, Chulalongkorn University, Bangkok 10330, Thailand

extracellularly synthesized into nanosized fibrils by the bacteria *Acetobacter xylinum*, and glucose is used as a common substrate. Plant-derived cellulose and BC have the same chemical structure; however, BC displays superior physical and chemical properties to plant-derived cellulose, including ultrafine nanofiber network structure, extensive surface area, high mechanical strength, high crystallinity, high chemical stability and high hydrophilicity [5, 6]. Those advantageous properties could endow BC to function as excellent matrix or support for heterogeneous catalysis. Recently, CdS nanoparticles/BC hybrid nanofibers was successful developed for photocatalysis application by deposition of CdS nanoparticles onto the substrate of hydrated BC nanofibers (BCF) [7]. However, up till now, there has been very little information available on the utilization of BC for the application as catalyst supports.

Ethanol production from renewable carbohydrate materials has attracted worldwide interest in its use as a carbon source for chemical and fuel production. Ethylene and diethyl ether (DEE) are the main products of ethanol dehydration reaction. Ethylene can be used as a polymerization raw material to produce a variety of important organic chemical products such as polyethylene, polyvinyl chloride, and polystyrene. Ethylene is also used as the precursor for synthesizing ethylene oxide, ethylene dichloride, ethylene glycol, and ethylbenzene [8–11]. DEE is widely used as a solvent for waxes, fats, oils, perfumes, alkaloids, and gums. DEE is also used as a fuel additive for biodiesel or diesel fuels to improve engine performance and emission properties. Dehydration of ethanol over solid acid catalysts to produce ethylene and DEE requires a lower temperature than hydrocarbon cracking, leading to an energy cost reduction that is more ecofriendly. Recently, different catalysts such as zeolite [12, 13], alumina [14, 15], silica [16], and silica–alumina [17] have been investigated to increase ethanol conversion and lower reaction temperature [9]. Among them, alumina is an efficient catalyst because of its excellent thermal stability and lower acid strength [18–20]. Moreover, alumina is cheap and readily available; it is suitable for industrial applications. However, the reaction temperature for the use of pure alumina or modified alumina catalysts is relatively high (usually more than 350 °C), thus the production consumes high amount of energy [9, 11]. By using zeolite catalysts, the operating temperature could be reduced; however its stability is poor and easily deactivated through carbon deposition [11]. In addition, the porous structure of those catalysts should be improved to prevent internal mass transport limitation.

BC displays excellent physical and chemical properties, such as ultrafine nanofiber network structure, high porosity and high mechanical strength. Therefore, in order to modify the pore structure of alumina catalyst, aluminum was loaded into a BC nanofiber and its application was explored

for the catalysis of ethanol dehydration to ethylene and diethyl ether (DEE). Important factors that influence the reaction rate and selectivity including temperature, acidity, and porous structure of the catalysts were investigated [18, 21]. The influences of acidic metal loading and dehydration methods are examined to optimize the catalyst preparation method for ethanol dehydration.

## 2 Materials and Methods

### 2.1 Materials

BC was synthesized by *A. xylinum* AGR 60. The stock culture was kindly provided by Pramote Thammarad, The Institute of Research and Development of Food Product, Kasetsart University, Bangkok, Thailand. BC hydrogel was treated with 1% w/v NaOH to remove bacterial cells and was neutralized with 1% w/v acetic acid. The cleaned BC was rinsed with deionized water until pH was 7.0.

### 2.2 BC-Supported Alumina Catalyst Preparation

The purified wet BC hydrogel ( $\approx 1 \times 1 \times 1 \text{ cm}^3$ ) of 200 g was soaked in 200 ml  $\text{Al}(\text{NO}_3)_3$  aqueous solution of various concentrations of 3, 7, and 14% w/v, producing approximately 12, 25, and 50 wt% Al after drying, respectively. The mixtures were stirred continuously for 12 h at room temperature to fully distribute Al into the BC matrix. The obtained BC/Al products were separated into two groups. One was dehydrated by hot air drying at 110 °C for 24 h and calcined in air at 200 °C for 4 h. The other one was freeze-dried under vacuum pressure ( $\approx 100 \text{ mTorr}$ ) for 24 h, dehydrated at 110 °C for 12 h and calcined in air at 200 °C for 4 h. All of the prepared catalysts were stored in plastic films at room temperature.

### 2.3 Catalyst Characterization

The surface area, pore volume, and pore diameter of catalysts were determined by nitrogen gas adsorption at liquid nitrogen temperature ( $-196 \text{ }^\circ\text{C}$ ) using Micromeritics Chemisorb 2750 Pulse instrument (Norcross, GA, USA). Before characterization, the sample was thermally treated at 150 °C for 1 h.

XRD patterns of the catalysts were determined by Siemens D5000 X-ray diffractometer (Aubrey, TX, USA) using  $\text{CuK}_\alpha$  radiation with a Ni filter in the  $2\theta$  range of  $10^\circ$ – $80^\circ$  with a resolution of  $0.04^\circ$ .

Scanning electron microscopy (JEOL JSM-5800LV, Tokyo, Japan) and energy dispersive X-ray spectroscopy were used to determine the surface morphology and elemental distribution of the catalyst particles. The energy dispersive X-ray spectroscopy was performed using a Link Isis Series 300



program at the Scientific and Technological Research Equipment Center, Chulalongkorn University, Bangkok, Thailand. Before analyzing the morphology, the samples were sputtered with platinum and photographed. The coated specimens were kept in a dry place before examination.

The functional groups of catalyst chemical structure were determined by Fourier transform infrared analysis using a Nicolet 6700 FTIR spectrometer (Thermo Scientific, Waltham, MA, USA).

The total acidic proton ( $H^+$ ) upon the dissolution of the catalysts was determined using standard acid–base back titration. Approximately 0.1 g of catalyst sample was placed in an 250 ml-Erlenmeyer flask containing 60 ml of 0.008 M NaOH, and stirred at room temperature for 1 h. The excessive amount of NaOH was neutralized using 0.02 M HCl as the titrant.

The acid properties of catalysts were investigated by temperature-programmed desorption of ammonia ( $NH_3$ -TPD) using Micromeritics Chemisorb 2750 pulse chemisorption system.  $NH_3$ -TPD tests of the catalyst samples (0.2 g) were carried out under a helium gas flow of 30 cm/min. After chemisorption step, a helium gas was flown over catalyst to remove any adsorbed molecules from catalyst active site from temperature of 40–500°C, at heating rate 10°/min. The spectrum of  $NH_3$ -TPD was deconvoluted by using a peak-fitting program, Fityk.

## 2.4 Catalytic Performance

Ethanol dehydration was performed in a glass fixed-bed continuous flow reactor with an inner diameter and length of 0.7 and 33 cm, respectively [18, 21]. The reactor was placed into a temperature-programmed tubular furnace. In each experiment, 0.01 g of a packed quartz wool and 0.05 g of catalyst were packed in the reactor, and the catalyst was then pre-treated in argon (50 ml/min) at 200°C for 1 h under atmospheric pressure. A feed consisting of 99.95% ethanol was fed into the reactor, and the reaction was performed under the controlled temperatures of 200, 250, 300, 350 and 400°C, at atmospheric pressure. The effluent products were collected and analyzed by a Shimadzu GC8A gas chromatograph with a flame ionization detector using a capillary column (DB-5) at 150°C.

Ethanol conversion (%)

$$= \frac{(\text{moles of ethanol in feed} - \text{moles of ethanol in product}) \times 100}{\text{moles of ethanol in feed}}$$

$$\text{Selectivity (\%)} = \frac{\text{moles of desired product formed} \times 100}{\text{moles of total products formed}}$$

$$\text{Yield (\%)} = \frac{\text{selectivity} \times \text{ethanol conversion}}{100}$$

## 3 Results and Discussion

### 3.1 Catalyst Characterization

#### 3.1.1 Surface Morphology and Al Distribution

The purified wet BC hydrogel was soaked in aluminum nitrate ( $Al(NO_3)_3$ ) aqueous solution producing approximately 12, 25, and 50 wt% of Al loadings after drying. The BC/Al products were dehydrated by hot air drying or freeze-drying. The sample names are xAl/BC-TD, where x is the wt% of Al loading after drying; i.e., 50Al/BC-TD refers to a BC-supported alumina catalyst with a 50 wt% Al loading (after drying), dehydrated by hot air drying. In a similar way, 50Al/BC-FD refers to a BC-supported alumina catalyst with a 50 wt% Al loading, dehydrated by freeze-drying.

Scanning electron microscopy images in Fig. 1 illustrate the surface morphologies of dried BC, Al/BC-TD, and Al/BC-FD catalysts. The catalyst particles showed an average width of 10–30  $\mu\text{m}$  with a thickness of  $\approx 10 \mu\text{m}$ . A rough surface with small clusters of Al particles on the surface was observed for the Al/BC catalysts. Higher-magnification views of surface morphology and cross section of the sample of Al/BC catalyst were shown in Fig. 2, in which the networks of carbon fibers on the catalyst surface and interior meso–macro porous structure were observed. It was shown that the average pore size of the Al/BC catalyst dehydrated by freeze-drying was relatively higher than that of the catalyst dehydrated hot air-drying. Energy dispersive X-ray spectroscopy was used to map the elemental distribution and percentage on the support surface. The maps for Al distribution of catalysts dehydrated by hot air drying and freeze-drying are shown in Fig. 3. All of the Al/BC catalysts exhibited a good dispersion of Al on the surface of BC supports. As shown in Table 1, Al percentages on the surface of Al/BC catalysts increased with the loading content of Al. At the same loading contents of Al, Al/BC-TD presented a higher concentration of Al on the surface than those of the Al/BC-FD catalysts. During the dehydration by hot air drying, the high shrinkage in carbon structure created a more dense structure with less porosity, resulting in a higher percentage of alumina on the surface. Dehydration via freeze-drying produced catalysts with a significantly higher porosity than Al/BC-TD catalysts.

#### 3.1.2 Acidity

Standard acid–base back titrations were used to examine the total acidic proton ( $H^+$ ) upon the dissolution of the catalysts, and the result are shown in Table 1. The total  $H^+$  of Al/BC catalysts were in the order: 50Al/

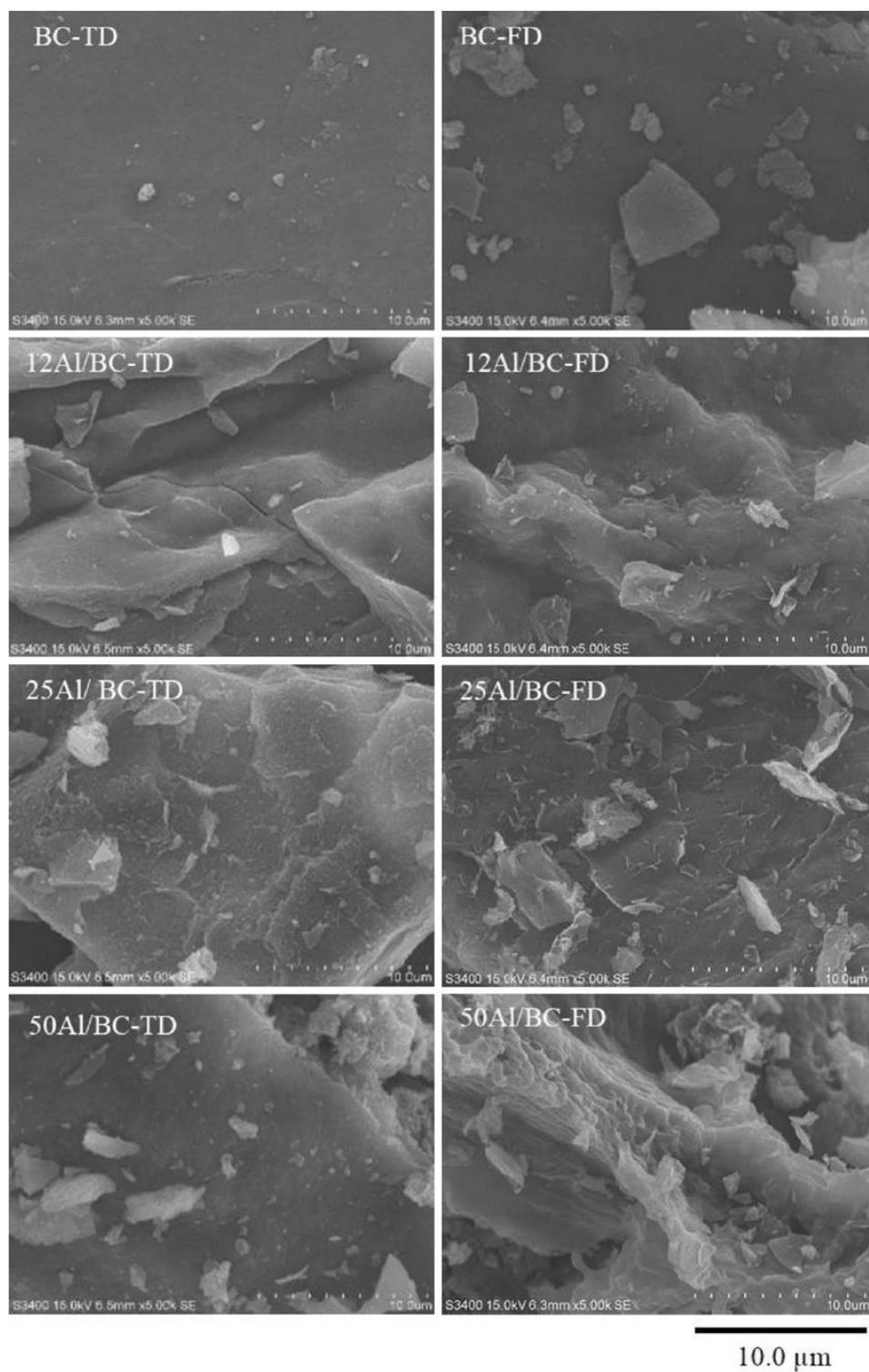


**Fig. 1** SEM micrograph of surface morphology of BC and Al/BC catalysts dehydrated by hot air-drying (*left*) and by freeze-drying (*right*)

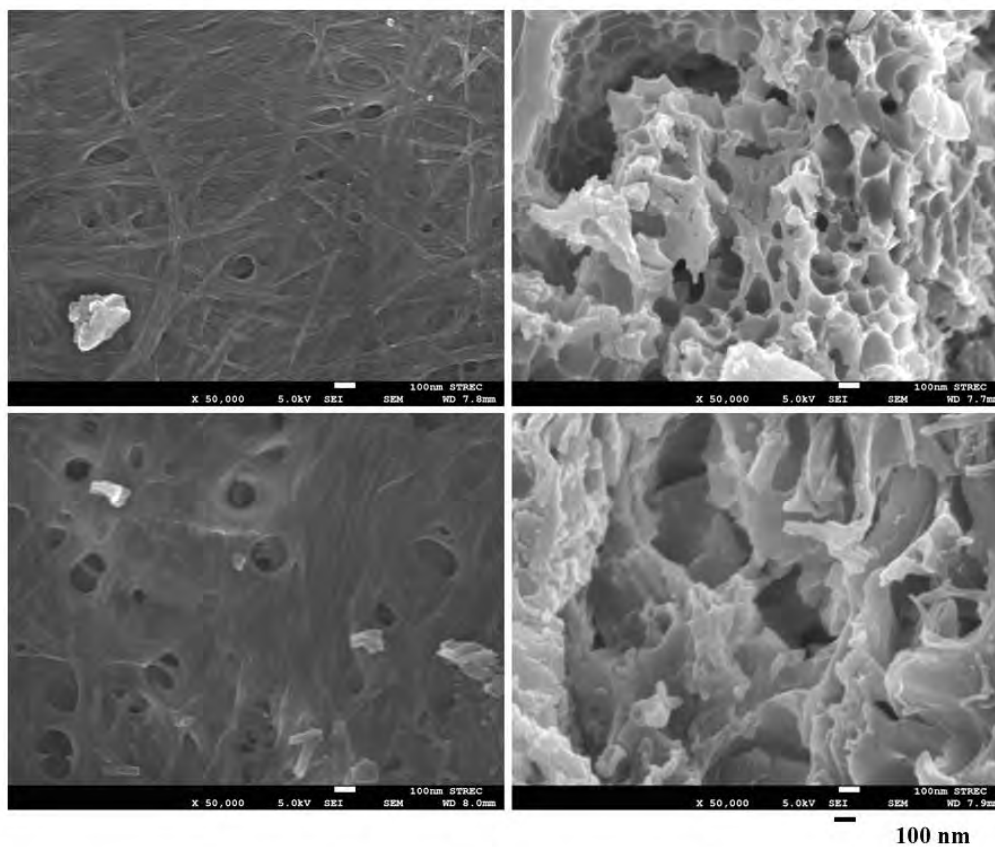
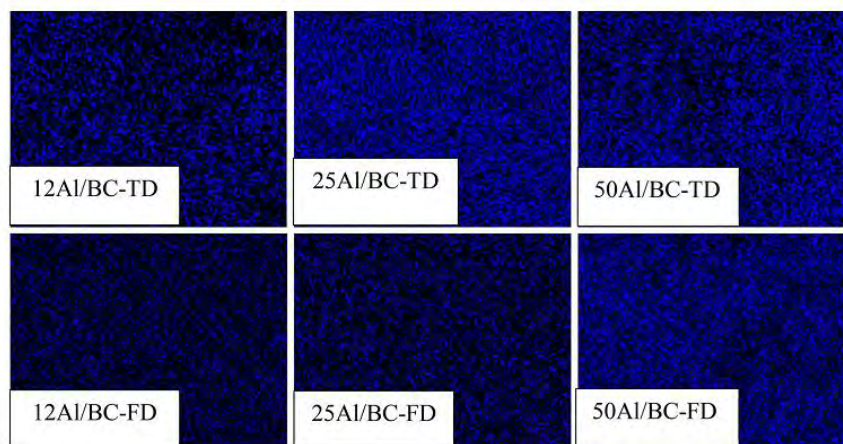


**Fig. 2** Higher-magnification views of surface morphology (*left*) and cross section (*right*) of 25 Al/BC catalysts dehydrated by hot air-drying (*top*) and by freeze-drying (*bottom*)

**Fig. 3** EDX mapping for Al distribution on surface of Al/BC catalysts dehydrated by hot air-drying (*top*) and by freeze-drying (*bottom*)



BC > 25Al/BC > 12Al/BC, for both dehydration methods. The catalyst of 50Al/BC-TD displayed the highest total  $H^+$  of 2158  $\mu\text{mol/g}$  cat. Overall, Al/BC catalysts

dehydrated by hot air drying showed slightly higher total  $H^+$  densities than those by of freeze-drying at the same Al loading.

**Table 1** Surface elemental composition obtained from energy dispersive X-ray spectroscopy and acidity of Al/BC catalysts

Catalysts	% Weight			% Atom			Total H <sup>+</sup> ( $\mu\text{mol/g}$ cat) <sup>*</sup>	Acid sites ( $\mu\text{mol NH}_3/\text{g}$ catalyst) <sup>**</sup>		
	C	Al	O	C	Al	O		Weak	Moderate to strong	Total
12Al/BC-TD	8.8	50.4	40.8	14.2	36.3	49.5	956	781.8	2671.6	3453.3
25Al/BC-TD	5.5	50.5	44.1	8.9	36.8	54.2	1621	567.1	2438.6	3005.7
50Al/BC-TD	6.2	60.4	33.5	10.6	46.2	43.2	2158	248.0	5342.9	5591.0
12Al/BC-FD	31.5	19.5	49.0	40.9	11.3	47.8	848	NA	NA	NA
25Al/BC-FD	23.9	36.2	39.9	34.2	23.0	42.8	1417	568.6	883.4	1452.0
50Al/BC-FD	8.0	55.7	36.4	13.2	41.3	45.5	1825	418.6	2970.1	3388.7

<sup>\*</sup>Total H<sup>+</sup> upon the dissolution of the catalysts was determined using standard acid–base back titration

<sup>\*\*</sup>Quantities of acid sites of catalysts were determined using Ammonia (NH<sub>3</sub>) TPD with Fityk program calculation

The quantities of acid sites with different strength were determined by using NH<sub>3</sub> TPD (Table 1). The first peak observed at lower temperature (<230 °C) was due to the desorption of ammonia chemisorbed at the weak acid sites, while the higher temperature peak observed at 250–400 °C was related to moderate to strong acid sites (Figure not shown). It was revealed that the amounts of moderate to strong acid sites were higher and the amount of weak acid sites was lower with the increased loading of Al from 12 to 50%.

### 3.1.3 X-ray Diffraction

X-ray diffraction (XRD) was used to identify the bulk structure of the catalysts. Figure 4 shows XRD patterns of dried BC, Al/BC-TD catalysts, and Al/BC-FD catalysts. The XRD pattern of BC shows the peaks observed at 14.4°, 16.6°, and 22.4°, which are the expected peaks of BC cultured in static conditions [6, 22]. There were no regular sharp peaks of BC in the XRD patterns of all Al/BC catalysts, and the percentage of crystallinity was close to zero. Only the 12Al/BC-FD catalyst showed a broad diffraction peak around 2 $\theta$  at 22.5, representing amorphous carbon composed of aromatic carbon sheets [23]. These results indicate that the highly crystalline structure of BC was totally disrupted after being soaked in aluminum nitrate solution, dehydrated, and calcined. The remaining carbons from the calcination were covered by an amorphous Al coating. From the XRD analysis, all BC-supported alumina catalyst samples were fully amorphous, which is expected for alumina catalysts calcined at a low temperature.

### 3.1.4 Pore Structure and Surface Area

The N<sub>2</sub> adsorption–desorption isotherms of BC and Al/BC catalysts with various Al loadings in both dehydration processes are shown in Fig. 5. According to the International Union of Pure and Applied Chemistry classification of physisorption isotherms, the isotherms of all Al/BC catalysts

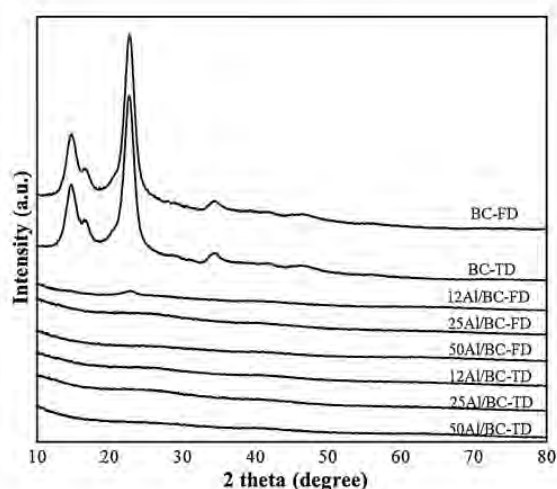


**Fig. 4** XRD patterns of BC and Al/BC catalysts

were type IV, which appear as hysteresis loops at a high pressure. All the catalysts display a mesoporous structure. The Al loading content and dehydration method affected the porous structure in terms of surface area, pore volume, and pore diameter. The Brunauer–Emmett–Teller surface areas, pore volumes, and pore size diameters of dried BC, Al/BC-TD catalysts, and Al/BC-FD catalysts are summarized in Table 2. Pore size distributions of BC and Al/BC catalysts from both dehydration methods are shown in Fig. 6. The total pore volume and Brunauer–Emmett–Teller surface area decreased with increasing Al loading. The surface area decreased from 19.21 to 10.50 m<sup>2</sup>/g and from 63.82 to 15.96 m<sup>2</sup>/g with increasing amount of Al loading from 0 to 50 wt% on Al/BC catalysts dehydrated by hot air drying and freeze-drying, respectively. The mean pore diameters were to some extent influenced by the different dehydration methods. Al/BC catalysts dehydrated by the hot air drying method showed lower surface areas and smaller pore diameters than those of the freeze-drying

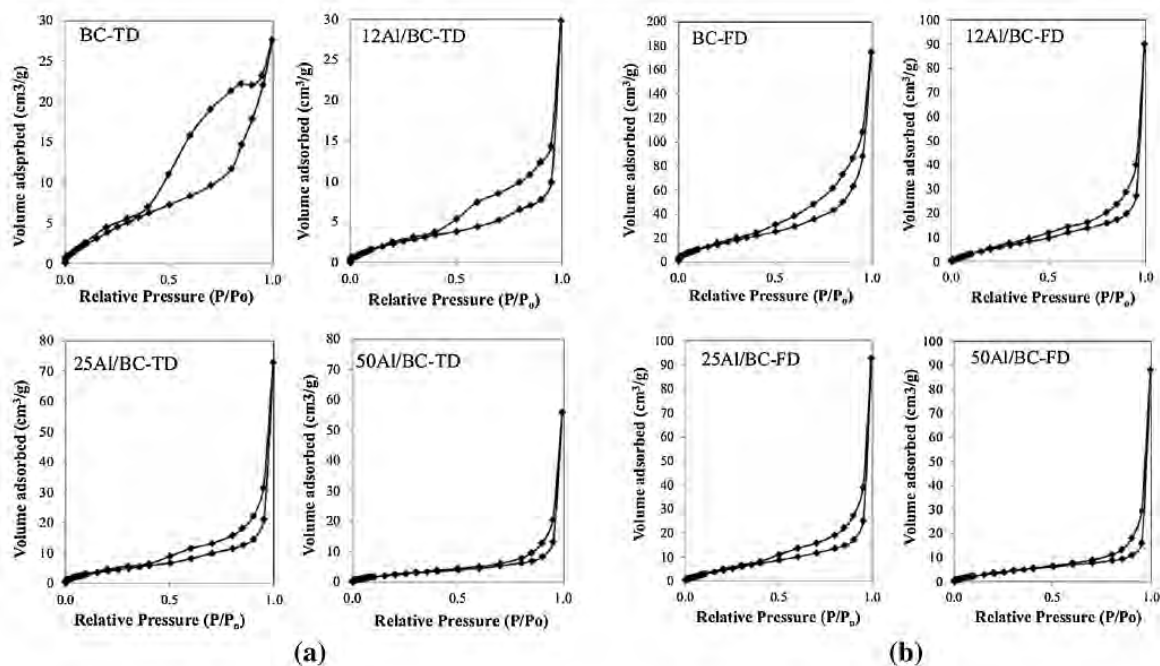


**Fig. 5** The N<sub>2</sub> adsorption–desorption isotherms of BC and Al/BC catalysts dehydrated by hot air-drying (a) and freeze-drying (b)

**Table 2** Surface area, pore volume, and average pore diameter of calcined BC particles and Al/BC catalysts determined by nitrogen adsorption and desorption (BET)

Catalysts	Surface area (m <sup>2</sup> /g)	Total pore volume (cm <sup>3</sup> /g)	Average pore diameter (nm)
BC-TD	19.21	0.043	8.92
12Al/BC-TD	10.47	0.046	17.67
25Al/BC-TD	17.67	0.093	25.57
50Al/BC-TD	10.50	0.087	33.01
BC-FD	63.82	0.271	16.97
12Al/BC-FD	20.07	0.140	20.62
25Al/BC-FD	21.92	0.144	26.26
50Al/BC-FD	15.96	0.137	34.25

method. In addition, significantly higher total pore volumes were obtained by dehydration via freeze-drying. All Al/BC catalysts showed average pore diameters of 17–34 nm, which were larger than that of BC without Al loading. A few micro and macro pores were also detected (Figs. 2, 6). The average pore diameter was increased with an increase of Al loading content, which was in the order: 50Al/BC > 25Al/BC > 12Al/BC > BC, for either the catalysts dehydrated by hot air drying or freeze-drying. The result indicated that the partial hydrolysis of BC might occur during the processes of soaking in the acid solution of Al(NO<sub>3</sub>)<sub>3</sub> and calcination, resulting in increased pore

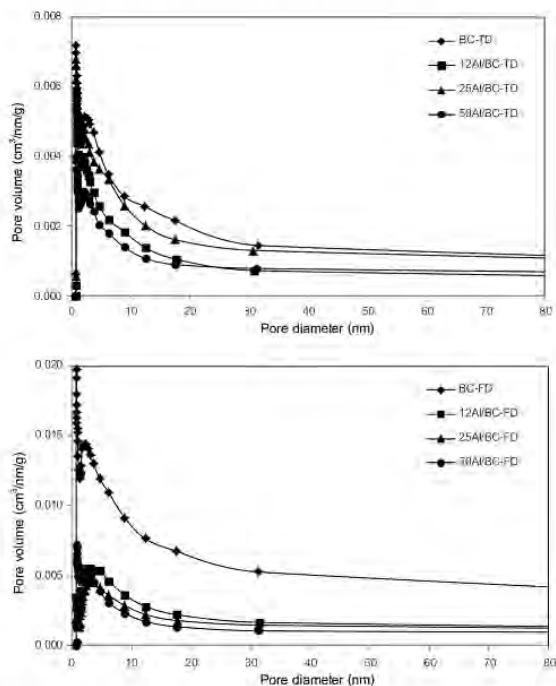


**Fig. 6** BJH pore size distribution of BC and Al/BC catalysts dehydrated by hot air-drying (top) and freeze-drying (bottom)

diameters. The destruction of small pores or combination of small pores into larger pores during doping and calcination processes was previously reported [24].

### 3.1.5 Fourier Transform Infrared Spectroscopy

Fourier transforms infrared spectroscopy is often used to determine functional groups or chemical bonds in a material [25]. Figure 7 shows the infrared spectra of Al/BC-TD and Al/BC-FD catalysts with various Al loadings. The spectra of all catalyst samples were detected at wavenumbers ranging 4000–500  $\text{cm}^{-1}$ . The infrared patterns of Al/BC-TD catalysts were similar to those of Al/BC-FD for the same concentrations of Al ( $\text{NO}_3$ )<sub>3</sub> soaking solution. The broad band located around 3380  $\text{cm}^{-1}$  is attributed to the O–H stretching vibration of hydroxyl groups. The band at 2962  $\text{cm}^{-1}$  is attributed to C–H interaction at the carbon surface. The sharp bands located at 2362 and 2161  $\text{cm}^{-1}$  are attributed to the C $\equiv$ C stretching vibrations of alkyne groups. However, those bands were unclear in 50Al/BC-TD and 50Al/BC-FD. The band at around 1690  $\text{cm}^{-1}$  can be denoted as stretching C=O carbonyl groups. Moreover, the band at around 1670–1587  $\text{cm}^{-1}$  is attributed to the C–C stretching vibration of aromatic rings and/or C=O of carboxylic groups and the bands in the region at around 1413–1300  $\text{cm}^{-1}$  are attributed to C–O stretching

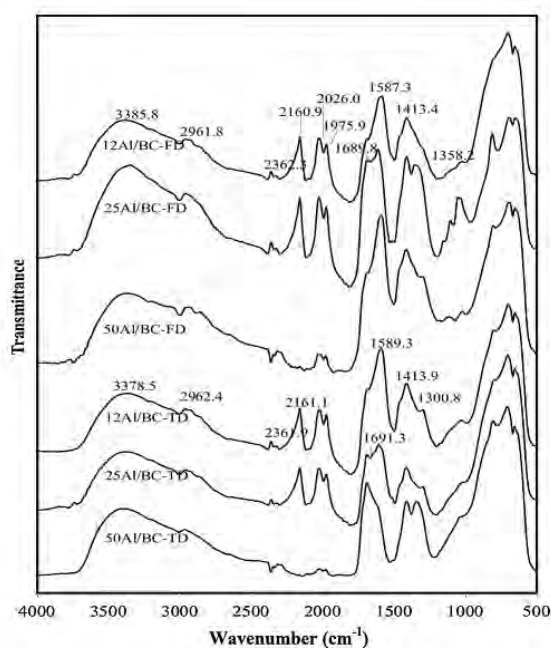


**Fig. 7** The FT-IR spectra of Al/BC catalysts in wavenumber ranging from 500 to 4000  $\text{cm}^{-1}$

vibrations. The presence of oxygen surface functional groups can be associated with the total acidity, which indicated that Al/BC catalysts were acid carbon catalysts. The results are consistent with the values of total acidity obtained by acid–base back titration (Table 1).

### 3.2 Catalytic Activity for Ethanol Dehydration

The catalytic activity of Al/BC catalysts with various Al loadings was examined in an ethanol dehydration reaction under non-oxidizing atmospheres at atmospheric pressure in the range of 200–400 °C. The dehydration products were ethylene, DEE and acetaldehyde. The ethanol conversion and selectivity for ethanol dehydration depend on the reaction temperature [26, 27]. The selectivities of ethylene and DEE, and ethanol conversion of all Al/BC catalysts are shown in Fig. 8a–c, respectively. As an endothermic reaction, the ethylene production favors high temperature. The catalysts exhibited the highest selectivity of ethylene for the reaction temperatures of 350–400 °C. The selectivity of acetaldehyde was also increased with increasing reaction temperature in a similar way as ethylene selectivity, however the concentration of acetaldehyde was much lower (figure not shown). Conversely, the selectivity of DEE was increased with decreasing reaction temperature because it is an exothermic reaction product. The highest selectivity of DEE was obtained at the reaction temperature of 200 °C. The similar effects of temperature on activity and selectivity of acid carbon catalysts for the ethanol dehydration reaction have been previously reported [18, 21, 28, 29].

Overall, the selectivity of ethylene in ethanol dehydration by Al/BC-TD catalysts was higher than that of Al/BC-FD catalysts. The results at the reaction temperatures of 250–350 °C show that the selectivity of ethylene decreased with an increase of Al loading content, which was in the order of 12Al/BC-TD > 25Al/BC-TD > 25Al/BC-FD > 50Al/BC-TD  $\approx$  50Al/BC-FD. The results agree with the general observation that the ethanol conversion to ethylene occurs on weak acid sites, while the strong acid centers can easily lead to ethylene polymerization [11, 18, 28]. However, by increasing the reaction temperature to 400 °C, all the Al/BC catalysts showed similar selectivity for ethylene at about 65–70% except for 12Al/BC-FD, which showed the low ethylene selectivity at  $\approx$ 18% due to its very low Al concentration on the outer surface. Because of the more open pore structure on the surface of Al/BC-FD catalysts, the concentration of Al on the outer surface of 12Al/BC-FD was much lower than the other catalysts (Table 1). 12Al/BC-TD exhibited the highest selectivity of ethylene of approximately 73.0% at 350 °C. In opposition to the ethylene selectivity, the selectivity of DEE decreased with increasing reaction temperature. At the reaction temperatures of

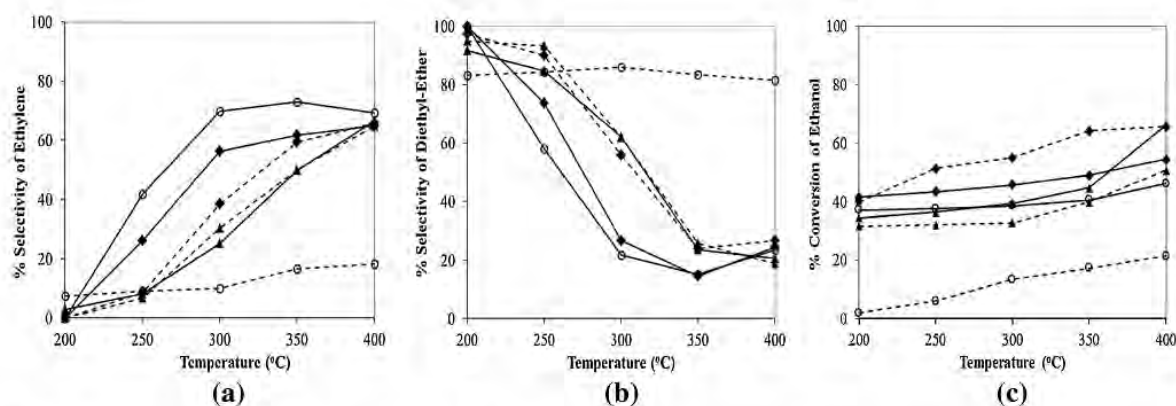


**Fig. 8** Selectivity of ethylene (a), selectivity of diethyl-ether (DEE) (b) and conversion of ethanol (c) in ethanol dehydration at temperatures of 200–400 °C by Al/BC catalysts dehydrated by air drying (solid line) and freeze-drying (dash line) at Al loadings of 12 (open circle), 25 (closed diamond) and 50 (closed triangle) wt%

250 °C, the selectivity of DEE by Al/BC-FD catalysts was higher than that of Al/BC-TD catalysts and the selectivity of DEE increased with an increase of Al loading content. At 200 °C, the selectivity of all Al/BC-TD catalysts increased to 92–100%, except for the 12Al/BC-FD catalyst in which the selectivity of DEE was consistent of around 82–85% for all reaction temperatures from 200 to 400 °C. According to the selectivities of ethylene and DEE as shown in Fig. 8a, b, the reaction for ethylene production tended to occur more on the outer surface, whereas the reaction for DEE production might occur more on the inner surface of the catalysts.

Ethanol conversion by Al/BC catalysts is shown in Fig. 8c, and the catalytic performance in term of yields of ethylene, DEE, and acetaldehyde is shown in Table 3. Ethanol conversion increased with increasing reaction temperature from 200 to 400 °C. At the reaction temperature of 400 °C, the conversion of ethanol was in the order of 50Al/BC > 25Al/BC > 12Al/BC. The similar effects of temperature and the acidity of catalysts on the conversion of ethanol were previously reported [29]. The highest ethanol conversion at 66.4%, with ethylene, DEE, and acetaldehyde selectivity of 66.6, 20.7, and 12.7%, respectively, was

obtained from the use of 50Al/BC-TD catalyst at 400 °C. The Al/BC catalyst with 25 wt% of Al loading and dehydration by freeze-drying (25Al/BC-FD) exhibited the highest surface area and pore volume, which were 21.92 m<sup>2</sup>/g and 0.144 cm<sup>3</sup>/g, respectively. At high operating temperatures (400 °C), the 25Al/BC-FD catalyst provided a similar conversion of ethanol and ethylene yield to those of the 50Al/BC-TD catalyst. However, 25Al/BC-FD catalyst showed a much higher ethanol conversion than 50Al/BC-TD catalyst at lower temperatures (200–350 °C). In addition, at low temperature of 200 °C, the catalyst of 25Al/BC-FD provided a high ethanol conversion of 40.1% with the selectivity of DEE of 97.3%. Among all Al/BC catalysts, the catalysts of 25Al/BC-FD and 50Al/BC-TD exhibited the highest ethylene yields of 43.26–44.24% at 400 °C, whereas 25Al/BC-TD and 25Al/BC-FD catalysts exhibited the highest DEE yields of 40.02–41.60% at 200 °C. Consequently, 25Al/BC-FD is considered as the promising catalyst for ethanol dehydration for both ethylene and DEE production, which could be owing to a more open porous structure with a uniform distribution of Al in the 25Al/BC-FD catalyst. The concentration of Al on the surfaces plays an important role in ethanol conversion and selectivity. Al doping at

**Table 3** Yields of ethylene, diethyl ether (DEE), and acetaldehyde (MeCHO) from the dehydration of ethanol at 200, 300, and 400 °C

Catalysts	200 °C			300 °C			400 °C		
	Ethylene	DEE	MeCHO	Ethylene	DEE	MeCHO	Ethylene	DEE	MeCHO
12Al/BC-TD	0.00	37.17	0.00	27.51	8.56	3.15	32.02	10.90	3.32
25Al/BC-TD	0.00	41.60	0.00	25.77	12.31	7.76	35.36	13.36	5.82
50Al/BC-TD	0.00	31.77	1.71	9.98	24.45	4.94	44.24	13.77	8.42
12Al/BC-FD	0.16	1.78	0.19	1.37	11.64	0.52	3.96	17.66	0.00
25Al/BC-FD	1.13	40.02	1.09	21.24	30.85	3.01	43.26	17.62	4.82
50Al/BC-FD	0.00	30.18	1.57	10.01	20.35	2.46	32.94	9.57	8.22

too low concentration, especially on a highly porous support (12Al/BC-FD) caused a slow reaction, resulting in low ethanol conversion and low selectivity of ethylene. On the other hand, Al doping at very high concentration could lead to a lower overall surface area, resulting in a reduction of ethanol conversion.

In comparison with differently modified Al-based solid acid catalysts using other supports [18, 21, 28] in the same operating condition (Table 4), at high temperature operation (400 °C) the Al/BC catalysts show a lower ethanol conversion and lower ethylene yield, which could be due to the difference in form and species of alumina and its lower surface area. However, at low temperature operation (200 °C), a significantly higher ethanol conversion and higher DEE yield (DEE selectivity  $\approx$  100%) were obtained using 25Al/BC-TD and 25Al/BC-FD catalysts as compared with those using other Al-based solid acid catalysts [18, 21, 28]. This should be due to the interior meso–macro porous structure of the Al/BC catalyst. Due to the higher molecular size of DEE (MW of DEE = 74 or about 2.64 times of ethylene), the use of catalysts with small pores could limit the diffusion of DEE out of the catalyst particles. Consequently, the accumulation of DEE within the catalyst particles could limit the formation of DEE. Therefore, the porous structure of the catalyst could be one of important factors affecting the yield and selectivity of the products. In consideration of the stability of the catalysts, under a non-oxidative environment, carbon as a catalyst support can be resistant to high temperature. The structure carbon support in catalytic applications is stable at high temperatures under nonoxidative conditions (even above 726 °C) [30]. Alumina-based catalyst is also generally accepted for good stability at high temperature [29]. The 25 Al/BC catalysts showed good stability (no significant loss in conversion) during 8 h time on stream (data not shown). However, for the study of the life time of the catalysts, further work for long-term stability test should be carried out.

DEE is an excellent compression ignition fuel with higher energy density and is recently reported for the potential use as a low-emission, high-quality diesel fuel replacement. The main reaction to produce DEE from ethanol is exothermic, reversible and limited by equilibrium. With the use of Al/BC catalyst, DEE can be produced from ethanol at low temperature (200 °C) with the DEE selectivity of almost 100%. The reaction for DEE production requires much less energy than ethylene production. Therefore, for an alternative use of ethanol as a feedstock, this process would potentially provide economic and environmental benefits to the industry. Additionally, the performance of Al/BC catalyst can be further improved by optimizing the operating conditions, modifying Al/BC catalyst in terms of porous structure to enhance the surface area or improving catalytic activity by loading with more appropriate type and form of catalysts and/or adding promoters. In view of a simple, low cost, and low energy preparation method, the Al/BC catalysts are attractive for further development as an environmentally friendly catalyst for ethanol dehydration, especially for DEE production.

#### 4 Conclusions

The supported alumina catalyst derived from BC was prepared by soaking purified BC hydrogel in  $\text{Al}(\text{NO}_3)_3$  aqueous solution with various concentrations, dehydrated by hot air drying or freeze-drying and calcination in air at 200 °C for 4 h. The Al/BC catalysts reveal interior meso–macro porous structures with average pore diameters in the range of 17–34 nm. The distribution of Al on the outer surface of BC support was uniform. The increase in Al loading content from 12 to 50% increased moderate to strong acid sites, but decreased weak acid site. The Al/BC catalysts dehydrated by the freeze-drying method show higher surface area and pore volume than those by hot air drying. Increasing Al loading on BC/Al catalysts caused an increase in

**Table 4** Comparison of catalysts for ethanol dehydration and their catalytic ability

Catalysts	Surface area (m <sup>2</sup> /g)	Pore diameter (nm)	Reaction temperature (°C)	Ethanol conversion (%)	Ethylene yield (%)	DEE yield (%)	Refs
25Al/BC-TD	18	25.6	200–400	41.5–54.6	0.0–35.4	41.6–13.4	This work
25Al/BC-FD	22	26.3	200–400	41.3–65.7	1.1–43.3	40.0–17.6	This work
Al-com	137	3.9	200–400	0–95	0.0–71.3	0.0–0.0	[18]
Al-SG	152	3.5	200–400	15–98	6.8–78.4	7.0–0.0	[18]
Al-SV	215	9.3	200–400	10–100	2.5–100	7.5–0.0	[18]
Al-SSP	443.6	5.9	200–400	20–85	18.6–82.0	1.4–0.0	[28]
HBZ	522	2.2	200–400	7–100	0.0–99.4	7.1–0.0	[21]
Al-HBZ	306	3.4	200–400	9–92	0.0–90.2	9.5–1.8	[21]
M-Al	195	9.0	200–400	12–92	0.0–88.9	12.5–2.5	[21]



the pore size and a decrease in the surface area. The Al/BC catalysts show efficient dehydration of ethanol to ethylene and DEE. The highest ethanol conversion of 65.7–66.4% and ethylene yield of 43.26–44.24% were obtained by using 25Al/BC-FD or 50Al/BC-TD catalysts at a reaction temperature of 400 °C, whereas the highest DEE yield of 40.02–41.60% was obtained using 25Al/BC-FD or 25Al/BC-TD catalysts at 200 °C. It can be concluded that the acidic properties, distribution and pore structure of catalysts significantly affect the conversion of ethanol dehydration and selectivity of the reaction. The results demonstrate that BC supported Al catalyst has many promising properties, such as good metal dispersion, high chemical and thermal stabilities. In the viewpoint of eco-friendly and sustainable green chemistry, it is interesting to explore the applicability of BC-supported catalyst in various types of heterogeneous catalysis.

**Acknowledgements** The authors thank the Grant for International Research Integration: Chula Research Scholar, Ratchadaphiseksomphot Endowment Fund, and the National Research Council of Thailand (NRCT) for their financial support of this project.

## References

- Bailón-García E, Maldonado-Hódar FJ, Pérez-Cadenas AF, Carrasco-Marín F (2013) *Catalysts* 3:853
- Zhang T, Zhao J, Xu J, Xu J, Di X, Li X (2016) *Chin J Chem Eng* 24:484
- Klemm D, Heublein B, Fink HP, Bohn A (2005) *Angew Chem Int Ed* 44:3358
- Xu Y, Zhang L, Cu Y (2008) *J Appl Polym Sci* 110:2996
- Kanjanamosit N, Muangnapoh C, Phisalaphong M (2010) *J Appl Polym Sci* 115:1581
- Phomrak S, Phisalaphong M (2017) *J Nanomater*. doi:10.1155/2017/4739793
- Yang JZ, Yu J, Fan J, Sun DP, Tang WH, Yang X (2011) *J Hazard Mater* 189:377
- Bedia J, Barrionuevo R, Rodriguez-Mirasol J, Cordero T (2011) *Appl Catal B* 103:302
- Fan D, Dai D-J, Wu H-S (2013) *Materials* 6:101
- Huang L-D (2005) *China Chlor-Alkali* 5:1
- Zhang M, Yu Y (2013) *Ind Eng Chem Res* 52:9505
- Bi J, Guo X, Liu M, Wang X (2010) *Catal Today* 149:143
- Han Y, Lu C, Xu D, Zhang Y, Hu Y, Huang H (2011) *Appl Catal A* 396:8
- El-Katatny EA, Halawy SA, Mohamed MA, Zaki MI (2000) *Appl Catal A* 199:83
- Liu D, Yao C, Zhang J, Fang D, Chen D (2011) *Fuel* 90:1738
- Matsumura Y, Hashimoto K, Yoshida S (1989) *J Catal* 117:135
- Takahashi R, Sato S, Sodesawa T, Arai K, Yabuki M (2005) *J Catal* 229:24
- Wannaborworn M, Praserttham P, Jongsomjit B (2015) *J Nanomater* 2015:1
- Knözinger H (1968) *Angew Chem Int Ed* 7:791
- Daniell W, Schubert U, Glockler R, Meyer A, Noweck K, Knozinger H (2000) *Appl Catal A* 196:247
- Kamsuwan T, Jongsomjit B (2016) *Eng J* 20:63
- Phisalaphong M, Suwanmajo T, Sangtherapitkul P (2008) *J Appl Polym Sci* 107:292
- Kitano M, Arai K, Kodama T, Kousaka T, Nakajima K, Hayashi S, Hara M (2014) *Catal Lett* 131:242
- Xiang Q, Lee YY, Pettersson PO, Torget R (2003) *Appl Biochem Biotechnol* 105–108:505
- Lee YM, Kim SH, Kim SJ (1994) *Polymer* 37:5897
- Lu J, Liu Y, Li N (2011) *J Nat Gas Chem* 20:423
- Ouyang J, Kong F, Su G, Hu Y, Song Q (2009) *Catal Lett* 132:64
- Chanchuey T, Authanit C, Jongsomjit B (2016) *J Chem* 2016:96730
- Chen G, Li S, Jiao F, Yuan Q (2007) *Catal Today* 125:111
- Lam E, Luong JHT (2014) *ACS Catal* 4:3393

## Characteristics of activated carbon derived from bacterial cellulose and its application as a adsorbent for methylene blue adsorption

Arnon Khamkeaw and Muenduen Phisalaphong\*

Chemical Engineering Research Unit for Value Adding of Bioresources, Department of Chemical Engineering, Faculty of Engineering, Chulalongkorn University, Phayathai Rd., Patumwan, Bangkok, 10330, Thailand.

\*E-mail: [muenduen.p@chula.ac.th](mailto:muenduen.p@chula.ac.th)

### Abstract

Bacterial cellulose (BC) was investigated as a novel material for preparing activated carbons. BC was dried by heating and it was carbonized with a chemical activation process using phosphoric acid ( $H_3PO_4$ ) as an activating agent at different temperatures (400, 500 and 600 °C). The properties of the activated carbons were characterized by X-ray diffraction (XRD), scanning electron microscopy (SEM),  $N_2$ -physisorption, Fourier transform infrared spectroscopy (FT-IR) and thermal gravimetric (TGA). The obtained BC activated carbons at carbonization temperature of 500°C (BC-AC500) showed maximum BET surface area (1,734  $m^2/g$ ) with mesoporous structure (2.33 nm) and large pore volume (1.01  $cm^3/g$ ). In addition, the BC-AC500 was used as adsorbent for the adsorption of methylene blue (MB). The equilibrium adsorption data were analyzed by the Langmuir, Freundlich, and Redlich-Peterson isotherm models. The results showed that the Redlich-Peterson model was found to be most fitted to the equilibrium data with correlation coefficient ( $R^2$ ) value of 1. The maximum adsorption capacity ( $q_m$ ) was 505.8 mg/g. The experimental results indicated that the BC activated carbon has the potential to be used as an effective adsorbent.

**Keywords:** activated carbon, bacterial cellulose, chemical activated carbon, adsorption, methylene blue.



## Activated carbon from bacterial cellulose as an effective adsorbent for removing dye from aqueous solution

Arnon Khamkeaw<sup>a</sup>, Bunjerd Jongsomjit<sup>b</sup>, Jonah Robison<sup>a,c</sup>, and Muenduen Phisalaphong<sup>a</sup>

<sup>a</sup>Biochemical Engineering Research Unit, Department of Chemical Engineering, Faculty of Engineering, Chulalongkorn University, Patumwan, Bangkok, Thailand; <sup>b</sup>Center of Excellence on Catalysis and Catalytic Reaction Engineering, Department of Chemical Engineering, Faculty of Engineering, Chulalongkorn University, Patumwan, Bangkok, Thailand; <sup>c</sup>Department of Bioengineering, Clemson University, Clemson, SC, USA

### ABSTRACT

Novel activated carbon (AC) derived from bacterial cellulose (BC-AC) was produced by phosphoric acid activation at a carbonization temperature of 500 °C. BC-AC possesses mesoporous structures of 2.3 nm in diameter, porosity of 1.0 cm<sup>3</sup>/g and surface area of 1734 m<sup>2</sup>/g with high thermal stability between 100 and 500 °C. BC-AC could be used as an effective adsorbent for removing methylene blue (MB) from aqueous solutions with the maximum adsorption capacity of 505.8 mg/g. BC-AC presented physisorption and the adsorption of MB was most likely to be a monolayer adsorption. The Redlich–Peterson model displayed the best fit with the experimental data.

### ARTICLE HISTORY

Received 23 November 2017  
Accepted 25 October 2018

### KEYWORDS

Activated carbon; bacterial cellulose; adsorption; methylene blue

### Introduction

Bacterial cellulose (BC) produced by *Acetobacter xylinum* has received much attention in recent years as a renewable material with desirable properties. *Acetobacter xylinum* is a non-photosynthetic organism that can convert c-sources, such as glucose, sugar and glycerol, into pure nanocellulose.<sup>[1]</sup> BC has the same chemical structure as plant cellulose, but has a uniform nanofiber network structure and unique properties including high crystallinity, porosity and surface area for adsorption, water holding capacity, tensile strength and resistance to organic solvents.<sup>[2–4]</sup> BC has been used in a wide range of applications, including raw material in food industries, a reinforcing agent for paper and biocompatible material for biomedical applications.<sup>[5,6]</sup> Because of its advantageous properties, BC should have great potential to be used as a source material for highly efficient activated carbon (AC) adsorbents. Previously, BC has been pyrolyzed at 950 °C and physically activated with carbon dioxide to produce active nanosized carbon for electric double-layer capacitors.<sup>[7]</sup> Recently, BC was modified with AC, amino groups, and ferrihydrous oxide covered by silica to develop an adsorbent for lead ions and methyl orange from aqueous solution.<sup>[8]</sup> However, there have been very few studies conducted on the development,

characterization and evaluation of AC adsorbents derived from BC to date.

Generally, AC is prepared by either a physical or chemical process. The physical activation process involves two steps, carbonization and activation, which require a high temperature. Chemical activation has advantages over physical activation. The required temperature is lower, it produces a higher yield of AC with a higher surface and usually involves only one step.<sup>[9]</sup> Either a strong acid or strong base can be used for chemical activation. Chemicals used for activation can lead to final materials with different porous structures based on the results from dehydration and degradation of the carbon substances. Phosphoric acid (H<sub>3</sub>PO<sub>4</sub>) is a non-toxic acid commonly used as an activating agent.<sup>[9]</sup> The use of H<sub>3</sub>PO<sub>4</sub> can provide high AC yield, surface area and pore volume.

Methylene blue (MB) was initially used as a dye in the textile industry. However, MB can lead to water pollution, burn the eyes of humans and animals and cause long-term health problems. On inhalation, MB can lead to difficulty breathing for a short period of time. Upon ingestion, MB can cause nausea, sweating, vomiting and mental confusion.<sup>[10]</sup> Adsorption is the most common process used to treat dye-containing wastewater<sup>[11]</sup> and AC is one of the most important materials used in adsorption processes. Generally, AC is produced from

CONTACT Muenduen Phisalaphong  Muenduen.p@chula.ac.th  Department of Chemical Engineering, Chulalongkorn University, Patumwan, Bangkok, Thailand.

Color versions of one or more of the figures in the article can be found online at [www.tandfonline.com/lsst](http://www.tandfonline.com/lsst).

© 2018 Taylor & Francis

carbonaceous materials such as coconut shells, rice husks and rice bran. The physical and chemical properties of AC can depend on the materials it is derived from.

This study focuses on the development of nanoporous AC adsorbents derived from BC (denoted BC-AC) by  $H_3PO_4$  activation at different carbonization temperatures. The produced BC-AC samples are then used as adsorbents for MB. The adsorption characteristics of the BC-AC samples were evaluated by the Langmuir, Freundlich and Redlich–Peterson isotherm models.

## Materials and methods

### Materials

BC (Fig. 1) was used as the raw material to prepare AC. BC was synthesized by *A. xylinum* AGR 60 from mature coconut juice. In many tropical countries (such as Thailand, Indonesia, Philippine and Malaysia), mature coconut juice had been mostly discarded as a waste from many coconut-based industries.<sup>[12]</sup> In addition, by-product streams from the biodiesel industry, waste streams from confectionery industries<sup>[13]</sup> and waste fiber sludge<sup>[14]</sup> have reportedly been used as carbon sources for the production of BC with similar properties. Therefore, the cost of carbon source for BC

production can be very low. MB used as an adsorbate was purchased from Ajax Finechem Pty. Ltd., Australia. MB has the chemical formula  $C_{16}H_{18}N_3S^+Cl^-$  and a molecular weight of 319.86 g/mol. The chemical structure of MB is shown in Fig. 2.

### Preparation of BC-ACs

The dried BC was impregnated with  $H_3PO_4$  by an incipient wetness technique. The incipient wetness impregnation method refers to impregnation using a solution with a volume that can properly fill all pores of a porous material. The activation of BC was conducted as follows. Dried BC was mixed with  $H_3PO_4$  at a ratio of 1:1 (w/w) and then was dried in a general electric oven (SNOL 67/350 LSP01, SNOL, Lithuania) at 110 °C for 24 h. The dried products were placed in a furnace (CWF 1100, Carbolite, UK) and carbonized at a temperature of 400, 500, or 600 °C without gas purging for 1 h before cooling. The obtained ACs were washed sequentially with 1 M HCl solution under mild stirring (120 rpm) at 70 °C for 4 h to remove residual chemicals in the porous structure of AC, before being rinsed with distilled water several times (until the pH was 7.0). The samples were then dehydrated at 110 °C for 24 h. The BC-AC products obtained from the

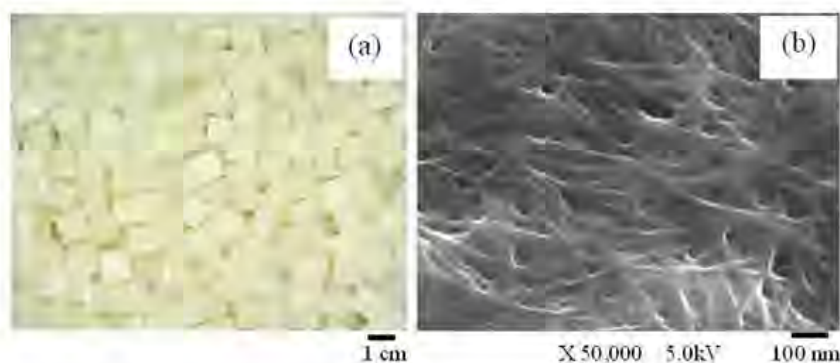


Figure 1. Image of BC (a) and SEM surface morphology of BC (b).

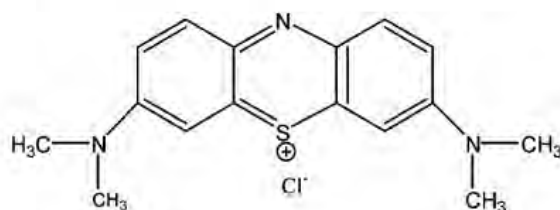


Figure 2. Structure of methylene blue dye (MB).<sup>[12]</sup>

carbonization at 400, 500 and 600 °C were denoted as BC-AC400, BC-AC500 and BC-AC600, respectively. The yield of AC was calculated using Eq. (1):

$$\% \text{Yield} = \frac{W_f}{W_0} \times 100 \quad (1)$$

where  $W_f$  (g) and  $W_0$  (g) are the weights of final BC-AC product and dried BC, respectively.

### Characterizations of BC-ACs

The characterizations of BC-ACs were performed by several techniques as follows. X-ray diffraction (XRD) (SIEMENS D5000 X-ray diffractometer, Aubrey, USA) was performed to determine the bulk crystal structure of BC-ACs using  $\text{CuK}\alpha$  radiation with Ni filter in the  $2\theta$  range of  $10^\circ$ – $70^\circ$  with a resolution of  $0.02^\circ$  and the crystallite size was calculated from Scherrer's equation. CHN Analyzer (628 Series, LECO, Germany) was used to determine the composition of C, H and N of BC-ACs. Fourier transform infrared (FT-IR) spectroscopy (Nicolet 6700 FTIR spectrometer, Thermo Scientific, USA) was used to identify functional groups in BC-AC samples. The surface area, pore volume and pore diameter of BC-ACs were determined by nitrogen ( $\text{N}_2$ ) physisorption-desorption at liquid  $\text{N}_2$  temperature of  $-196^\circ\text{C}$  using a Micromeritics Chemisorb 2750 Pulse instrument (Norcross, GA, USA). Field Emission Scanning Electron Microscope and Energy Dispersive X-Ray (FESEM-EDS) Spectrometer (Model of JSM-7610F and X-MaxN 20, JEOL, USA) was used to determine the morphology of BC-ACs.

The pH at the potential of zero point charge ( $\text{pH}_{zpc}$ ) of the ACs was determined using solid content adding method.<sup>[15]</sup> The solution of 0.1 M NaCl at 50 mL was transferred into a 125 mL Erlenmeyer flask. The initial pH of NaCl solution was adjusted from 1.0 to 11.0 by the addition of 0.1 M NaOH or 0.1 M HCl solution. The initial pH value of each solution was measured by a pH meter (S20, Mettler, USA). AC of 0.05 g was added into each flask and the flask was then sealed with parafilm. The experiment was conducted at a constant temperature of  $30^\circ\text{C}$  and 125 rpm for 24 h in an incubator shaker (Innova 4330, New Brunswick Scientific, USA). The final pH values of the solutions at the equilibrium were determined.

### Adsorption studies

#### Adsorption capacity

BC-AC was used as an adsorbent for removing MB from aqueous solutions. MB is the cationic dye. At

the beginning, the pH values of the MB solutions of 50, 100, 200, 300, 400, 500 and 600 mg/L were 6.05, 5.90, 5.97, 5.82, 5.90, 5.79 and 5.68, respectively. The initial pH of each MB solution was then adjusted to pH 7.0 by adding 0.1 M NaOH. Subsequently, BC-AC (0.02 g) was added into the MB solution (40 mL) in a 100-mL Erlenmeyer flask. Each MB adsorption experiment was conducted at  $30^\circ\text{C}$  and 125 rpm using an incubator shaker (Innova 4330, New Brunswick Scientific, USA). For the kinetics and equilibrium study of MB adsorption, the solution of 0.1 mL of each flask was taken every 10 min for 1 h and every 60 min for 6 h, until the system had reached equilibrium. The samples were centrifuged for 10 min at 3000 rpm by a centrifuge (U-320, Boeco, Germany). The concentrations of MB in the solutions were analyzed by a UV-visible spectrophotometer (UV-2450, Shimadzu, Japan) at a wavelength of 664 nm. A constructed calibration curve was used to relate the optical density measurements to MB concentrations in the solutions. The percentage removal of MB from the solution was calculated. The amount of MB adsorbed per gram of adsorbent at any given time,  $q_t$  (mg/g) and the amount of MB adsorbed per gram of adsorbent after the equilibrium,  $q_e$  (mg/g) were determined.

#### Adsorption isotherm modeling

The interaction between an adsorbate and adsorbent can be described by adsorption isotherms. The equilibrium data for MB adsorption on the BC-AC samples were analyzed by the Langmuir, Freundlich and Redlich-Peterson models.

#### Langmuir model

The Langmuir isotherm model<sup>[16]</sup> was developed from the assumption that adsorption occurs on a specific homogeneous surface containing sites with equal energy. This model has been successfully applied to monolayer adsorption. The Langmuir model is expressed by Eq. (2):

$$q_e = \frac{q_m K_L C_e}{1 + K_L C_e} \quad (2)$$

where  $C_0$  and  $C_e$  (mg/L) are the concentrations of MB in the solution at the initial time ( $t = 0$ ) and after reaching equilibrium, respectively;  $q_m$  (mg/g) is the maximum adsorption capacity per unit mass of BC-AC and  $K_L$  (L/mg) is the Langmuir adsorption constant. The essential characteristics of a Langmuir isotherm can be expressed by a dimensionless constant called the equilibrium parameter  $R_L$ ,<sup>[17]</sup> as shown in Eq. (3):

$$R_L = \frac{1}{1 + K_L C_0} \quad (3)$$

The value of  $R_L$  indicates whether the adsorption is irreversible ( $R_L = 0$ ), favorable equilibrium ( $0 < R_L < 1$ ), linear ( $R_L = 1$ ), or unfavorable equilibrium ( $R_L > 1$ ).<sup>[17]</sup>

#### Freundlich model

The Freundlich model<sup>[18]</sup> was developed from the assumption that adsorption occurs at specific heterogeneous surface energies. Therefore, this model is appropriate to describe multilayer adsorption with interaction between adsorbed molecules. The Freundlich model is summarized in Eq. (4):

$$q_e = K_F C_e^{1/n_F} \quad (4)$$

where  $K_F$  ((mg/g)(L/mg)<sup>1/n<sub>F</sub></sup>) and  $n_F$  are the Freundlich constant and heterogeneity factor, respectively. The type of adsorption is linear for  $n_F = 1$ , a favorable chemical process for  $n_F < 1$  and a favorable physical process for  $n_F > 1$ .<sup>[18]</sup> Meanwhile, the value of  $1/n_F < 1$  indicates a normal Langmuir isotherm and  $1/n_F > 1$  indicates cooperative adsorption.

#### Redlich–Peterson model

The Redlich–Peterson model was developed to improve the curve fitting between Langmuir and Freundlich equations. It can be used to represent adsorption equilibrium over a wide concentration range, and can be applied to either homogeneous or heterogeneous systems. The Redlich–Peterson model is shown in Eq. (5):<sup>[19]</sup>

$$q_e = \frac{K_R C_e}{1 + a_R C_e^\beta} \quad (5)$$

where  $K_R$  (L/g) is the Redlich–Peterson constant, and  $a_R$  (L/mg) and  $\beta$  ( $0 < \beta < 1$ ) are constants. For  $\beta = 1$ , the Redlich–Peterson equation transforms to Langmuir form. When  $K_R$  and  $a_R$  are much greater than unity, the equation can transform into Freundlich form.<sup>[19]</sup>

## Results and discussion

### Activated carbon characterization

Chemical activation basically involves a relatively low temperature range from 300 to 700 °C<sup>[20]</sup> or 400 to

600 °C<sup>[21]</sup> and depends on the action of an additive to degrade and dehydrate the cellulosic materials. The surface area and pore volume of the AC from the chemical activation process increased with an increase in the activation temperature up to around 600 °C and decreased with an increased activation temperature over 600 °C.<sup>[22–24]</sup> This is due to the shrinkage and/or partial collapse of carbon structure, which could lead to a reduction of surface area and pore volume of the AC at high activation temperature.<sup>[23,24]</sup> The effect of temperature on the structure of AC might also depend on the structure of cellulose material. Therefore, an activation temperature of 400–600 °C was selected for the study of the effect of activation temperature on properties of AC in this work. The yields and elemental analyses of BC-AC samples obtained at different carbonization temperatures are shown in Table 1. The yield of AC decreased considerably with rising carbonization temperatures from 400 to 600 °C due to the more efficient removal of volatile species.<sup>[25]</sup> Because a gaseous fraction from the carbonization of biomass is usually rich in hydrogen and light hydrocarbon and also contains biomass tar (mostly in form of aromatic hydrocarbons), the carbon content in a solid fraction increases with the carbonization temperature. The amount of carbon in all BC-AC samples exceeded 70% with a yield of BC at 26–40%, indicating that BC is a suitable raw material to produce ACs in the carbonization temperature range of 400–600 °C.

The bulk crystal structure of BC-AC was determined by XRD, as shown in Fig. 3. The XRD patterns of BC cultured under static conditions commonly show three main peaks at 14°–15°, 16°–17° and 22°–23° originating from the (110), (110) and (200) planes, respectively (data not shown), which can be identified as the reflection planes of cellulose I.<sup>[2,26,27]</sup> The crystallinity of BC is usually between 75% and 90%.<sup>[2,26]</sup> After carbonization, the highly crystalline structure of BC was disrupted. The XRD patterns of all BC-AC samples were consistent with that of amorphous carbon derived from cellulose.<sup>[28]</sup> The XRD profiles of BC-AC samples produced at various carbonization temperatures were similar. All the BC-AC samples only displayed a diffraction peak at around 25°, which was ascribed to amorphous carbon composed of aromatic carbon sheets.<sup>[29]</sup>

Table 1. Yields and elemental analysis of activated carbons (AC) derived from bacterial cellulose (BC) at various carbonization temperatures.

BC-AC	Yield (%)	Carbon (%)	Oxygen (%)	Hydrogen (%)	Nitrogen (%)
BC-AC400	40.20	70.93	25.27	2.89	0.91
BC-AC500	33.40	72.48	23.93	2.44	1.15
BC-AC600	26.36	73.67	21.95	3.55	0.83

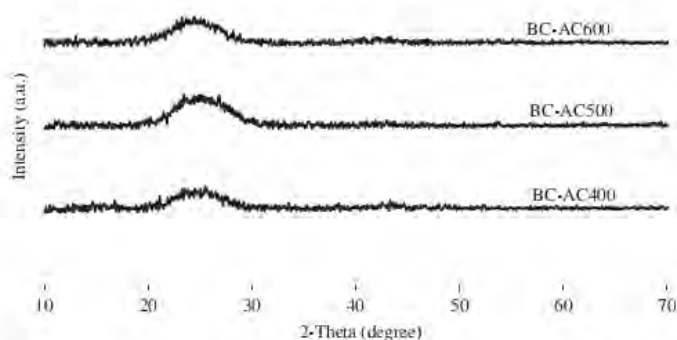


Figure 3. The XRD patterns of BC-ACs carbonized at temperatures of 400 °C (BC-AC400), 500 °C (BC-AC500) and 600 °C (BC-AC600).

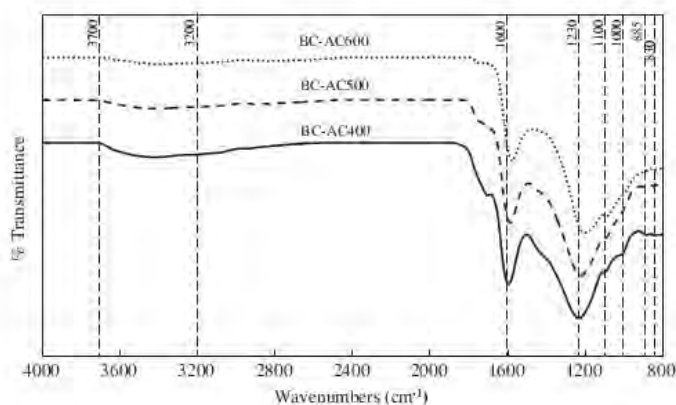


Figure 4. The FT-IR patterns of BC-ACs carbonized at temperatures of 400 °C (BC-AC400), 500 °C (BC-AC500) and 600 °C (BC-AC600).

The chemical structures of the BC-AC samples produced at various carbonization temperatures were determined by FT-IR spectroscopy; the spectra are shown in Fig. 4. The broad band located around 3200–3700  $\text{cm}^{-1}$  is attributed to the O-H stretching vibration of the hydroxyl group, which originated from the adsorption of water vapor from the surroundings and moisture residue during the carbonization process. The bands at 1600 and 1230  $\text{cm}^{-1}$  are ascribed to the C = O and C-O stretching vibrations of carbonyl groups, respectively, originating from the oxidative decomposition of organic species.<sup>[30]</sup> Comparison with previous reports<sup>[31–33]</sup> indicated that the broad bands are quite similar to ACs derived from many different biomass sources with the presence of the same functional groups. The bands in the range of 1000–1200  $\text{cm}^{-1}$  are characteristic of phosphorous and phosphor carbonaceous compounds originating from the phosphoric acid activation step. The band at 1100  $\text{cm}^{-1}$  is ascribed to the stretching vibration of

hydrogen-bonded P = O groups from phosphates or polyphosphates, O-C stretching vibrations in P-O-C (aromatic) linkages and P = OOH.<sup>[34]</sup> The band that appears at 1000  $\text{cm}^{-1}$  is ascribed to the ionized linkage P<sup>+</sup>-O<sup>-</sup> in acid phosphate esters and symmetrical vibration in a P-O-P chain.<sup>[35]</sup> The bands at 885 and 830  $\text{cm}^{-1}$  are assigned to C-H stretching of aromatic compounds.<sup>[36]</sup>

The porosity, pore volume, pore size and specific surface area of the BC-AC samples produced at various carbonization temperatures determined by the N<sub>2</sub> physisorption technique are presented in Table 2. Pore size distributions of the prepared BC-ACs are shown in Fig. 5. The BC-AC samples had mesoporous structures with average pore diameters in the range of 2.2–2.4 nm, which is similar to those of other ACs derived from cellulosic materials using phosphoric acid as an activating agent.<sup>[37,38]</sup> The BET surface area and total pore volume of BC-AC increased with carbonization temperatures from 400 to 500 °C. In contrast, the BET surface area and total pore volume

Table 2. Porous properties of BC-ACs carbonized at temperatures of 400 °C (BC-AC400), 500 °C (BC-AC500) and 600 °C (BC-AC600).

BC-AC	BET surface area (m <sup>2</sup> /g)	Total pore volume (cm <sup>3</sup> /g)	Average pore diameter (nm)
BC-AC400	1540.1	0.87	2.25
BC-AC500	1734.2	1.01	2.33
BC-AC600	1701.5	1.01	2.37

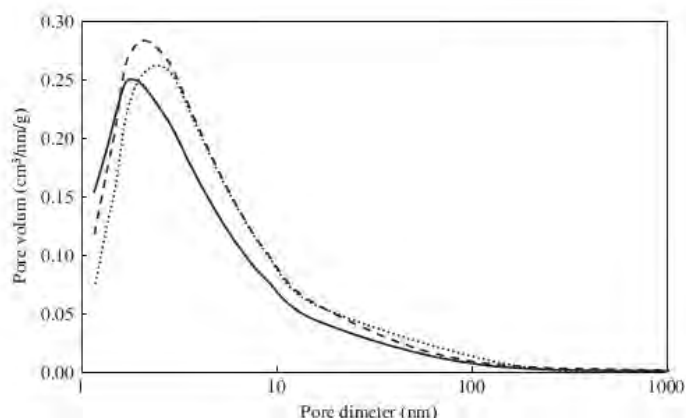


Figure 5. Pore size distribution of BC-ACs: BC-AC400 (—), BC-AC500 (---), and BC-AC600 (· · ·).

decreased slightly with rising carbonization temperatures from 500 to 600 °C. It was previously reported that if the carbonization temperature is too high, shrinkage and/or partial collapse of the carbon structure could occur and lead to decreases of the surface area and pore volume of AC products.<sup>[23,24]</sup> BC-AC500 had the maximum BET surface area of 1734.2 m<sup>2</sup>/g with an average pore diameter of 2.33 nm and a total pore volume of 1.01 cm<sup>3</sup>/g. The BC-AC samples demonstrated higher relative BET surface area and total pore volume than those of ACs derived from cotton stalk,<sup>[30]</sup> deoiled rice bran residue,<sup>[37]</sup> durian shell<sup>[38]</sup> and coconut shell.<sup>[39,39]</sup> The surface area and total pore volume of BC-AC500 were comparable to those of high surface area AC obtained from *Elaeagnus angustifolia* seeds by one-stage chemical activation using ZnCl<sub>2</sub> in N<sub>2</sub>;<sup>[40]</sup> however, the average pore size of BC-AC500 was relatively higher. According to a previous report on the preparation

of AC from deoiled rice bran residue, ZnCl<sub>2</sub> activation produced AC with a higher surface area and total pore volume but slightly smaller pore diameter than those from H<sub>3</sub>PO<sub>4</sub> activation.<sup>[37]</sup> However, when considering safety issues, H<sub>3</sub>PO<sub>4</sub> activation is widely preferred over ZnCl<sub>2</sub> activation.

The surface morphologies of the BC-AC samples were observed by FESEM, as depicted in Fig. 6. The BC-AC samples exhibit rough surfaces, which are associated with the presence of very small pores originating from the evaporation of H<sub>3</sub>PO<sub>4</sub> and other volatile matter during carbonization.<sup>[41]</sup>

The mass loss during thermogravimetric analysis (TGA) of BC-AC at various carbonization temperatures is shown in Fig. 7. The TGA patterns of all BC-ACs are similar. The initial small mass loss from around room temperature (30 °C) to 100 °C was attributed to

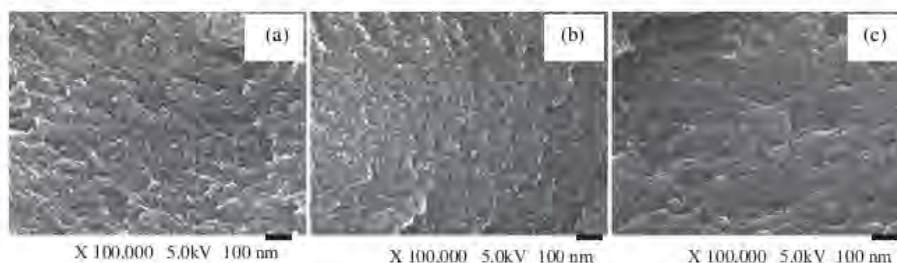


Figure 6. FESEM micrographs of BC-ACs: BC-AC400 (a), BC-AC500 (b) and BC-AC600 (c).



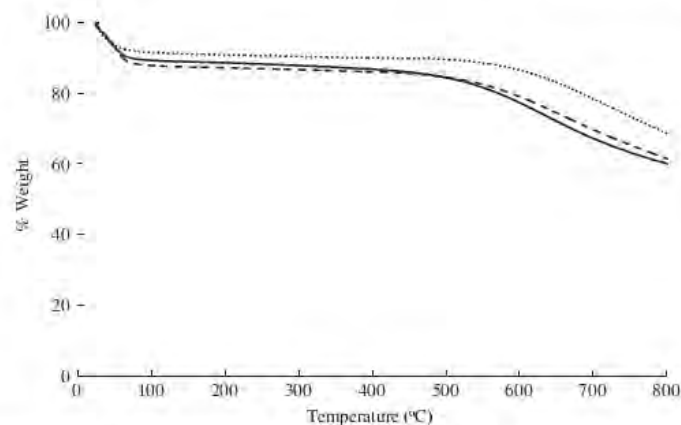


Figure 7. Thermal gravimetric of BC-ACs:BC-AC400 (—○—), BC-AC500 (—□—), and BC-AC600 (---△---).

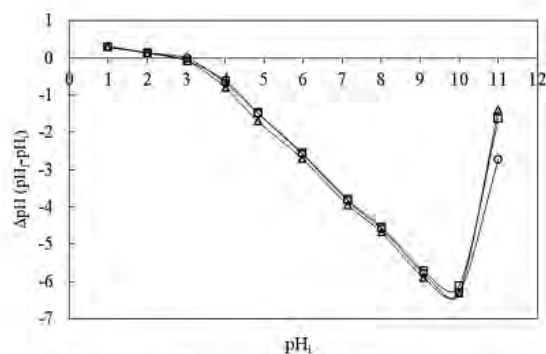


Figure 8. The pH at the potential of zero point charge ( $pH_{zpc}$ ) of BC-AC at various carbonization temperatures; BC-AC400 (○), BC-AC500 (□) and BC-AC600 (△).

moisture elimination. From 100 to 500 °C, only a small amount of carbon decomposition (less than 5% of the initial weight for BC-AC400 and BC-AC500; less than 2% of the initial weight for BC-AC600) was detected, indicating that the BC-AC samples exhibited high stability between 0 and 500 °C.

The  $pH_{zpc}$  values of different ACs used for the adsorption experiment were determined by the pH drift method.<sup>[15]</sup> The difference between the initial and final pH ( $pH_f - pH_i$ ) was plotted against the initial pH ( $pH_i$ ), as shown in Fig. 8. The junction point of the resulting curve and  $pH_i$  axis gives the  $pH_{zpc}$  (whereas, the  $pH_{zpc}$  of BC-AC400, BC-AC500 and BC-AC600 are 3.02, 2.74 and 2.76, respectively). At  $pH_{zpc}$  values above pH of solution, the surface is positively charged, while at  $pH_{zpc}$  values below pH of solution, the surface is negatively charged. As compared to pH of the solution (7.0), the  $pH_{zpc}$  was below pH of the solution. Therefore, the surface of all ACs was

negatively charged, which was suitable for the removal of cationic dyes such as MB due to the increase of electrostatic force of attraction.

#### Adsorption capacity: effects of contact time and initial MB concentration

Figure 9 shows the effects of contact time and initial MB concentration on the adsorption capacity of the BC-AC samples. Under the controlled conditions (see section on "Adsorption Capacity"), all samples initially showed rapid adsorption rates (0–15 min) and then the adsorption rates gradually decreased until the equilibrium was reached. The equilibrium of MB adsorption by BC-AC400 was achieved within 20 min for the systems with low MB concentration (50 and 100 mg/L) and within 300 min for those with high MB concentration (200–600 mg/L). For BC-AC500 and BC-AC600, the time required to reach

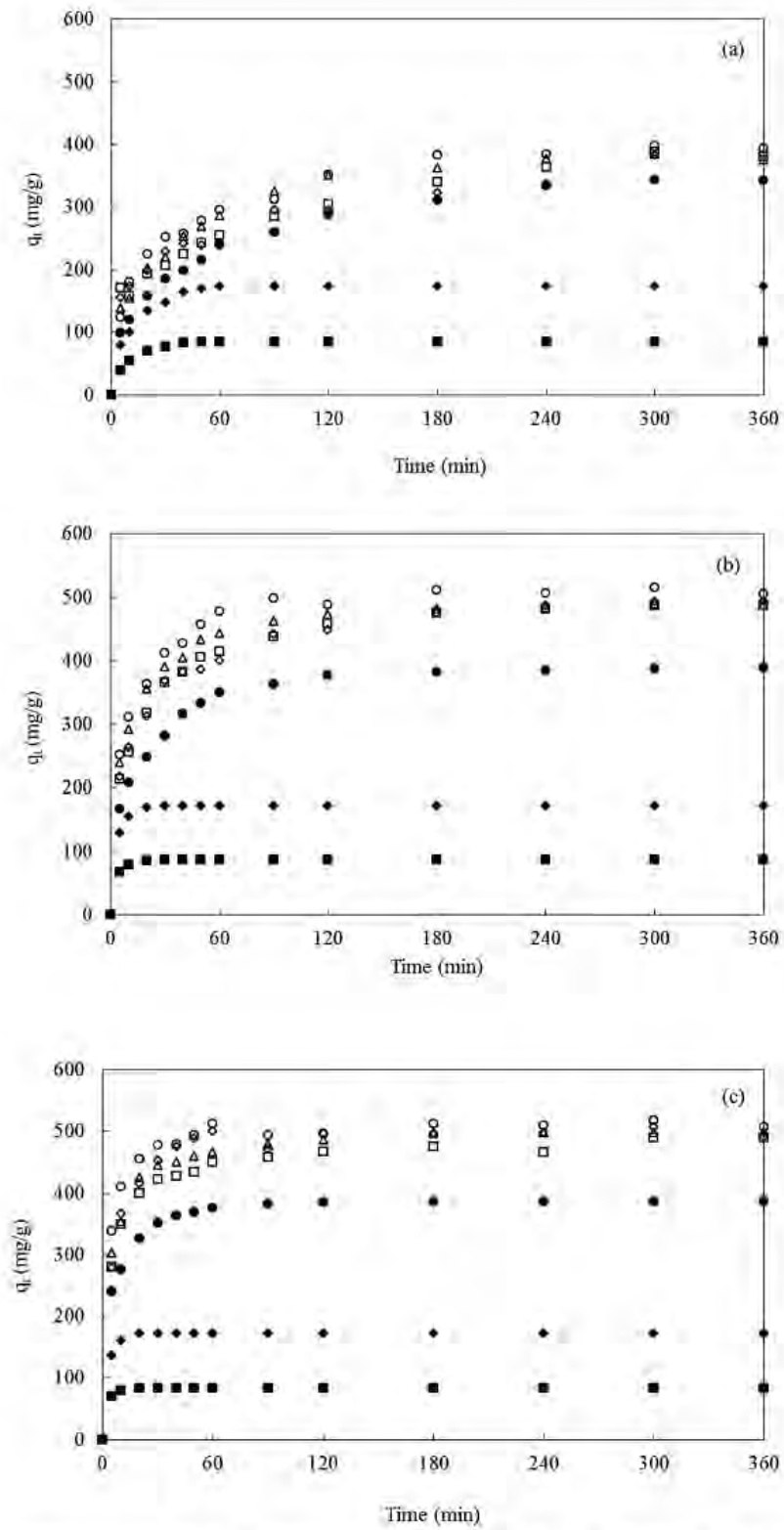


Figure 9. Effects of contact time and initial MB concentration (■50, ◆100, ●200, △300, □400, ◇500, and ○600 mg/L) on the adsorption capacity of BC-AC400 (a), BC-AC500 (b) and BC-AC600 (c).

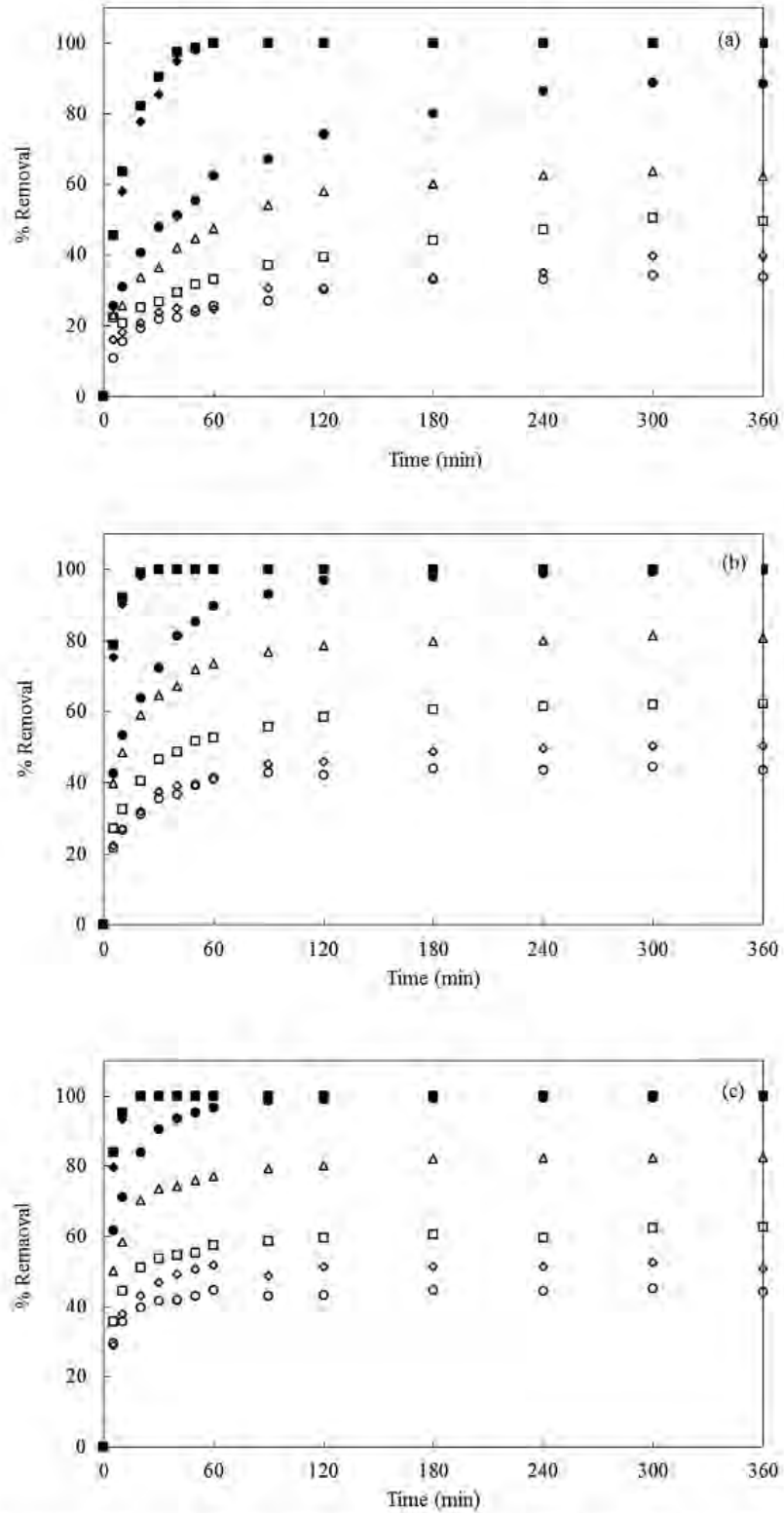


Figure 10. Effects of contact time and initial MB concentration (■ 50, ◆ 100, ● 200, □ 300, ◻ 400, ◊ 500, and ○ 600 mg/L) on the removal of MB of BC-AC400 (a), BC-AC500 (b) and BC-AC600 (c).

equilibrium was shorter compared with that for BC-AC 400 (10 min for the systems with low MB concentration and 240 min for those with high MB concentration). The higher pore volume and surface area of BC-AC500 and BC-AC600 (as compared to those of BC-AC400) could promote the diffusion of MB molecules from the bulk solution into the interior of the adsorbents. In addition, in the systems with low MB concentration, the adsorbent had a high content of available vacant active sites; thus, the adsorption equilibrium could be reached faster compared with the cases of high MB concentration.<sup>[10]</sup>

The maximum MB adsorption was attained using the MB solution with the highest initial MB concentration (600 mg/L), but this system also gave the lowest percent removal of MB from the solution (Fig. 10). BC-AC600 and BC-AC500 had very high adsorption capacities for MB with maximum values of 507.5 and 505.8 mg/g, respectively, whereas BC-AC400 had a lower adsorption capacity of 393.0 mg/g. The increase of the surface area of adsorbents could raise adsorption capacity by allowing more interaction between active sites and MB molecules.<sup>[42]</sup> The percent removal of MB increased with contact time until the equilibrium was reached (Fig. 10). Using the BC-AC samples, complete MB removal could be achieved if the initial MB concentration did not exceed 100 mg/L. Because the concentration ratio of active sites and MB in the systems with low MB concentration was high, all MB molecules could be adsorbed on active sites of the adsorbent.<sup>[43]</sup> In addition, BC-AC 400, BC-AC500 and BC-AC600 showed MB removal of 88.4%, 99.8% and 99.8%, respectively, when the initial MB concentration was 200 mg/L. The removal of MB decreased with the increasing of initial MB concentration from 200 to 600 mg/L. Table 3 compares the maximum capacity ( $q_m$ ) for MB adsorption by the BC-AC samples with those achieved by other AC adsorbents. The  $q_m$  values of BC-AC500 and BC-AC600 for MB adsorption are higher than those of ACs derived from other cellulosic materials ( $q_m \sim 90\text{--}435$  mg/g), which is likely because the BC-AC samples possess nanoporous structures with high porosity and surface area. The results indicated that the BC-AC samples are effective adsorbents for the removal of MB from aqueous solutions.

#### Adsorption isotherms

Figure 11 illustrates the non-linear fittings of the Langmuir, Freundlich and Redlich–Peterson

isotherm models for the three adsorbents, while Table 4 summarizes the corresponding isotherm parameters and their correlation coefficients ( $R^2$ ) for each fitting. The  $q_m$  values for BC-AC400, BC-AC500 and BC-AC600 obtained by fitting the Langmuir isotherm model to the equilibrium data are 383.2, 500.0 and 500.0 mg/g, respectively, which are very close to the experimental values (393.0, 505.8 and 507.5 mg/g, respectively; see Fig. 9). The  $K_L$  for the samples was 0.7–10.0 L/mg, indicating that the adsorption strength was strong.<sup>[51]</sup> Meanwhile, the value of  $R_L$  could indicate the nature of the isotherm. As illustrated in Fig. 11, for the initial MB concentrations of 200–600 mg/L,  $R_L$  decreased with the increasing of initial MB concentration and was in the range of  $2 \times 10^{-4}$  to  $7 \times 10^{-3}$ , which indicates that the adsorption of MB by the BC-AC samples was favorable.<sup>[17,52]</sup>

The  $n_F$  parameter of the Freundlich isotherm of all BC-ACs in this research presented a favorable physical adsorption process, while  $1/n_F$  was consistent with favorable normal Langmuir isotherms.<sup>[18]</sup> Comparison of the  $R^2$  values for all BC-AC samples between the Langmuir and Freundlich isotherms indicated that the Langmuir model fitted the experimental data better than the Freundlich model. Therefore, MB tended to be adsorbed as a monolayer by the BC-AC samples.<sup>[16]</sup> The Redlich–Peterson isotherm model was found to give the best fit of the experimental data, with an  $R^2$  value of 1.000. The Redlich–Peterson isotherm model was combined with the Langmuir and Freundlich isotherm models. Generally, the Langmuir isotherm model is good for predicting low adsorbate concentration, whereas the Freundlich model might better describe the adsorption at high adsorbate concentration.<sup>[19]</sup> The limitation of adsorbate concentration of the Langmuir and Freundlich isotherm model could be improved by the Redlich–Peterson isotherm model, which can be used to predict a wide range of adsorbate concentrations.<sup>[19]</sup> The  $\beta$  values for all BC-AC samples were close to 1.0, which indicates that the Langmuir isotherm model (describing monolayer adsorption) is more appropriate than the Freundlich (for describing multilayer adsorption). Overall, it can be concluded that the adsorption of MB by the BC-AC samples is mostly monolayer adsorption. Comparison of  $R^2$  values (Table 4) indicated that the order of the models that best fit the experimental data was Redlich–Peterson > Langmuir > Freundlich. It was previously reported that the Redlich–Peterson isotherm model showed the best fit for MB adsorption onto an AC produced from steam-activated bituminous coal over the Langmuir and Freundlich models.<sup>[53]</sup>

Table 3. The maximum adsorption capacity for MB removal by BC-ACs in this work as compared to those by ACs derived from other cellulosic materials.

Adsorbent	$q_m$ (mg/g)	Reference
BC-AC400	393.0	This work
BC-AC500	505.8	This work
BC-AC600	507.5	This work
Coconut husk-based AC	434.8	[44]
Peach stones-based AC	412.0	[45]
Date stone-based AC	398.2	[46]
Oil palm shell-based AC	303.0	[45]
Coconut shell-based AC	277.9	[47]
Oil palm fiber-based AC	277.8	[48]
Ground shell-based AC	164.9	[49]
Bamboo dust-based AC	150.0	[47]
Activated sewage char	120.0	[48]
Oil palm wood-based AC	90.0	[50]

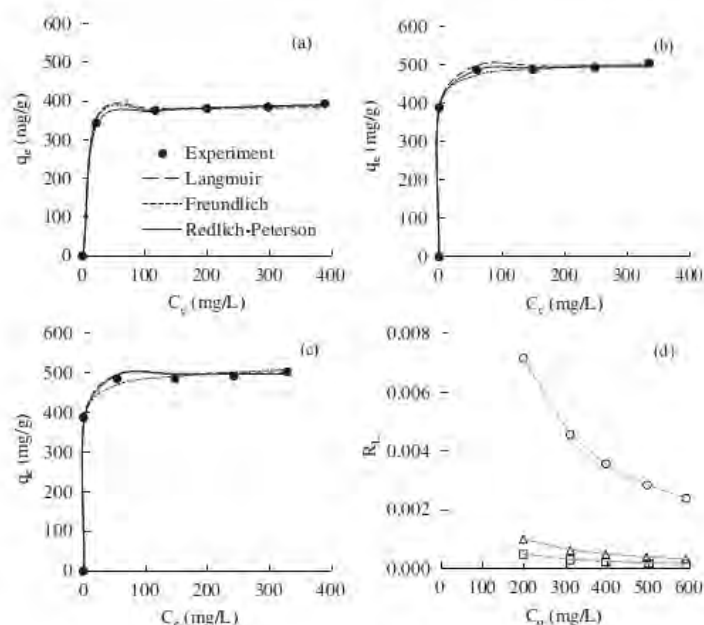


Figure 11. Equilibrium adsorption data of MB on different BC-ACs; BC-AC400 (a), BC-AC500 (b), BC-AC600 (c), analyzed by the Langmuir (—), Freundlich (---) and Redlich-Peterson  $\cdot$  isotherms and the equilibrium parameter  $R_L$  by the Langmuir model (d) for BC-AC400 (O), BC-AC500 ( $\square$ ) and BC-AC600 ( $\Delta$ ).

## Conclusion

Novel AC derived from BC was found to be effective as an adsorbent to remove MB from water. The carbonization temperature markedly affected the porous structure of the BC-AC samples. A carbonization temperature of 500 °C gave the sample that possessed the highest surface area of 1734.2 m<sup>2</sup>/g with a total pore volume of 1.011 cm<sup>3</sup>/g. The BC-AC samples had a mesoporous structure with an average pore diameter of 2.2–2.4 nm and high thermal stability between 100 and 500 °C. By using BC-AC500

or BC-AC600 at 0.02 g in 40 mL MB solution for MB removal, adsorption equilibria could be reached within 10 min for systems with low MB concentration (50–100 mg/L) and 240 min for those with high MB concentration (200–600 mg/L). The removal of MB from solutions with an initial MB concentration not exceeding 200 mg/L was almost 100% effective. The maximum MB adsorption capacities of BC-AC400, BC-AC500 and BC-AC600 were 393.0, 505.8 and 507.5 mg/g, respectively, which were very close to the  $q_m$  values estimated from the Langmuir model. The analysis results indicated that

Table 4. Isotherm parameters and  $R^2$  for MB adsorption on BC-ACs analyzed by the Langmuir, Freundlich and Redlich-Peterson isotherm models.

Activated carbon	Parameters of isotherms		
	Langmuir	Freundlich	Redlich-Peterson
BC-AC400	$q_m = 384.6 \text{ mg/g}$ $K_L = 0.7 \text{ L/mg}$ $R_L = 2 \times 10^{-3} - 7 \times 10^{-3}$ $R^2 = 0.985$	$K_F = 325.3 \text{ (mg/g)(L/mg)}^{1/n_F}$ $n_F = 32.57$ $1/n_F = 0.031$ $R^2 = 0.976$	$K_R = 326.9 \text{ L/g}$ $a_R = 1.000 \text{ L/mg}$ $\beta = 0.970$ $R^2 = 1.000$
BC-AC500	$q_m = 500.0 \text{ mg/g}$ $K_L = 10.0 \text{ L/mg}$ $R_L = 2 \times 10^{-4} - 5 \times 10^{-4}$ $R^2 = 0.984$	$K_F = 410.4 \text{ (mg/g)(L/mg)}^{1/n_F}$ $n_F = 28.33$ $1/n_F = 0.035$ $R^2 = 0.976$	$K_R = 6753.0 \text{ L/g}$ $a_R = 14.53 \text{ L/mg}$ $\beta = 0.988$ $R^2 = 1.000$
BC-AC600	$q_m = 500.0 \text{ mg/g}$ $K_L = 5.0 \text{ L/mg}$ $R_L = 3 \times 10^{-4} - 10 \times 10^{-4}$ $R^2 = 0.994$	$K_F = 398.5 \text{ (mg/g)(L/mg)}^{1/n_F}$ $n_F = 23.64$ $1/n_F = 0.042$ $R^2 = 0.923$	$K_R = 2280.0 \text{ L/g}$ $a_R = 4.577 \text{ L/mg}$ $\beta = 1.000$ $R^2 = 1.000$

all BC-ACs presented favorable physisorption and the adsorption of MB was most likely to be a monolayer adsorption. The Redlich-Peterson model displayed the best fit with the experimental data of the models considered, with  $R^2$  values of 1.000 for all BC-AC samples. With its very high adsorption capacities and rate, BC-AC has great potential to be used as an effective adsorbent for water treatment systems.

### Funding

The authors thank the Grant for International Research Integration: Chula Research Scholar, Ratchadaphiseksomphot Endowment Fund, Chulalongkorn University and the National Research Council of Thailand (NRCT) for their financial support of this project. The authors also acknowledge the 100th Anniversary Chulalongkorn University Fund for Doctoral Scholarship and the 90th Anniversary Chulalongkorn University Fund (Ratchadaphiseksomphot Endowment Fund).

### References

- [1] Hestrin, S.; Schramm, M. (1954) Synthesis of cellulose by *Acetobacter xylinum*. II. Preparation of freeze-dried cells capable of polymerizing glucose to cellulose. *The Biochemical Journal*, 58 (2): 345-352.
- [2] Taokaew, S.; Seetabhwang, S.; Siripong, P.; Phisalaphong, M. (2013) Biosynthesis and characterization of nanocellulose-gelatin films. *Carbohydrate Polymers*, 6 (3): 782-794.
- [3] Luddee, M.; Pivsa-Art, S.; Sirisansaneeyakul, S.; Pechyen, C. (2014) Particle size of ground bacterial cellulose affecting mechanical, thermal, and moisture barrier properties of PLA/BC biocomposites. *Energy Procedures*, 56: 211-218. doi: 10.1016/j.egypro.2014.07.151
- [4] Çakar, F.; Özer, I.; Aytikin, A.Ö.; Şahin, F. (2014) Improvement production of bacterial cellulose by semi-continuous process in molasses medium. *Carbohydrate Polymers*, 106: 7-13. doi: 10.1016/j.carbpol.2014.01.103
- [5] Kirdponpattara, S.; Khamkeaw, A.; Sanchavanakit, N.; Pavasant, P.; Phisalaphong, M. (2015) Structural modification and characterization of bacterial cellulose-alginate composite scaffolds for tissue engineering. *Carbohydrate Polymers*, 132: 146-155. doi: 10.1016/j.carbpol.2015.06.059
- [6] Klemm, D.; Schumann, D.; Udhardt, U.; Marsch, S. (2001) Bacterial synthesized cellulose - artificial blood vessels for microsurgery. *Progress Polym Sciences*, 26 (9): 1561-1603. doi:10.1016/S0079-6700(01)00021-1
- [7] Lee, K.-Y.; Qian, H.; Tay, F.H.; Blaker, J.J.; Kazarian, S. G.; Bismarck, A. (2013) Bacterial cellulose as source for activated nanosized carbon for electric double layer capacitors. *Journal of Materials Science*, 48 (1): 367-376. doi:10.1007/s10853-012-6754-y
- [8] Huang, X.; Zhan, X.; Wen, C.; Xu, F.; Luo, L. (2018) Amino-functionalized magnetic bacterial cellulose/activated carbon composite for  $Pb^{2+}$  and methyl orange sorption from aqueous solution. *Journal Materials Sciences Technological*, 34 (5): 855-863. doi:10.1016/j.jmst.2017.03.013
- [9] Yahya, M.A.; Al-Qodah, Z.; Ngah, C.W.Z. (2015) Agricultural bio-waste materials as potential sustainable precursors used for activated carbon production: a review. *Renew Sustainable Energy Reviews*, 46: 218-235. doi: 10.1016/j.rser.2015.02.051
- [10] Ahmed, M.J.; Dhedan, S.K. (2012) Equilibrium isotherms and kinetics modeling of methylene blue adsorption on agricultural wastes-based activated carbons. *Fluid Phase Equilibria*, 317: 9-14. doi: 10.1016/j.fluid.2011.12.026
- [11] Nagarajan, K.; Renganathan, T.; Krishnaiah, K. (2016) Dye removal in steady-state continuous countercurrent liquid-solid adsorber. *Separations Sciences and Technological*, 51 (12): 1955-1961. doi:10.1080/01496395.2016.1196220
- [12] Kongruang, S.; (2008) Bacterial cellulose production by *Acetobacter xylinum* strains from agricultural waste products. *Applied Biochemistry and Biotechnology*, 148 (1-3): 245-256. doi:10.1007/s12010-007-8119-6
- [13] Tsouko, E.; Kourmentza, C.; Ladakis, D.; Kopsahelis, N.; Mandala, I.; Papanikolaou, S.; Paloukis, F.; Alves, V.; Koutinas, A. (2015) Bacterial cellulose production from industrial waste and

- by-product streams. *International Journal Molecular Sciences*, 16 (7): 14832–14849. doi:10.3390/ijms160714832
- [14] Cavka, A.; Guo, X.; Tang, S.; Winestrand, S.; Jönsson, L.J.; Hong, F. (2013) Production of bacterial cellulose and enzyme from waste fiber sludge. *Biotechnology Biofuels*, 6: 25. doi: 10.1186/1754-6834-6-25
- [15] Eslami, A.; Borgheti, S.M.; Rashidi, A.; Takdastan, A. (2018) Preparation of activated carbon dots from sugarcane bagasse for naphthalene removal from aqueous solutions. *Separation Sciences Technological*. Published online 18 Apr 2018. doi:10.1080/01496395.2018.1462832
- [16] Langmuir, I. (1917) The constitution and fundamental properties of solids and liquids. *Journal Frankl Institute*, 183 (1): 102–105. doi:10.1016/S0016-0032(17)90938-X
- [17] Hall, K.; Eagleton, L.C.; Acrivos, A.; Vermeulen, T. (1966) Pore and solid diffusion kinetics in fixed-bed adsorption under constant-pattern. *Industrial Engineering Chemical Fundamentals*, 5: 212–223. doi: 10.1021/i160018a011
- [18] Bhatt, A.S.; Sakaria, P.L.; Vasudevan, M.; Pawar, R.R.; Sudheesh, N.; Bajaj, H.C.; Mody, H.M. (2012) Adsorption of an anionic dye from aqueous medium by organoclays: equilibrium modeling, kinetic and thermodynamic exploration. *RSC Advances*, 2: 8663–8671. doi: 10.1039/c2ra20347b
- [19] Omar, H.A.; (2013) Adsorption of <sup>60</sup>Co on natural and dithizone-modified Chitin. *Radiochemistry*, 55 (1): 101–107. doi:10.1134/S1066362213010207
- [20] Giraldo, S.; Moreno-Pirajan, J.C. (2012) Synthesis of activated carbon mesoporous from coffee waste and its application in adsorption zinc and mercury ions from aqueous solution. *E-Journal of Chemical*, 9 (2): 938–948. doi:10.1155/2012/120763
- [21] Gamal, O.E.S.; Mohamed, M.Y.; Amany, A.A. (2014) Assessment of activated carbon prepared from corncob by chemical activation with phosphoric acid. *Water Resources Industrial*, 7–8: 66–75. doi: 10.1016/j.wri.2014.10.001
- [22] Allwar, A.; Noor, M.; Naw, M.A.M. (2008) Textural characteristics of activated carbons prepared from oil palm shells activated with ZnCl<sub>2</sub> and pyrolysis under nitrogen and carbon dioxide. *Journal Physical Sciences*, 19 (2): 93–104.
- [23] Armandi, M.; Bonelli, B.; Geobaldo, F.; Garrone, E. (2010) Nanoporous carbon materials obtained by sucrose carbonization in the presence of KOH. *Microporous Mesoporous Mater*, 132 (3): 414–420. doi:10.1016/j.micromeso.2010.03.021
- [24] Chen, J.; Zhang, L.; Yang, G.; Wang, Q.; Li, R.; Lucia, L. A. (2017) Preparation and characterization of activated carbon from hydrochar by phosphoric acid activation and its adsorption performance in prehydrolysis liquor. *Biological Research*, 12 (3): 5928–5941.
- [25] Bedia, J.; Barrionuevo, R.; Rodríguez-Mirasol, J.; Cordero, T. (2011) Ethanol dehydration to ethylene on acid carbon catalysts. *Applications Catal B-Environmental*, 103 (3): 302–310. doi:10.1016/j.apcatb.2011.01.032
- [26] Phisalaphong, M.; Jatupaiboon, N. (2008) Biosynthesis and characterization of bacteria cellulose–chitosan film. *Carbohydrate Polymers*, 74 (3): 482–488. doi:10.1016/j.carbpol.2008.04.004
- [27] Ibnu Abdulwahab, M.; Khamkeaw, A.; Jongsomjit, B.; Phisalaphong, M. (2017) Bacterial cellulose supported alumina catalyst for ethanol dehydration. *Catal Letters*, 147 (9): 2462–2472. doi:10.1007/s10562-017-2145-y
- [28] Winter, C.; Caetano, J.N.; Araújo, A.B.C.; Chaves, A.R.; Ostroski, I.C.; Vaz, B.G.; Pérez, C.N.; Alonso, C.G. (2016) Activated carbons for chalcone production: Claisen-Schmidt condensation reaction. *Chemical Engineering Journal*, 303: 604–610. doi: 10.1016/j.cej.2016.06.058
- [29] Djilani, C.; Zaghdoudi, R.; Modarressi, A.; Rogalski, M.; Djazi, F.; Lallam, A. (2012) Elimination of organic micropollutants by adsorption on activated carbon prepared from agricultural waste. *Chemical Engineering Journal*, 189: 203–212. doi: 10.1016/j.cej.2012.02.059
- [30] Finocchio, E.; Cristiani, C.; Dotelli, G.; Stampino, P.G.; Zampori, L. (2014) Thermal evolution of PEG-based and BRIJ-based hybrid organo-inorganic materials. FT-IR studies. *Vibrational Spectroscopy*, 71: 47–56. doi: 10.1016/j.vibspec.2013.12.010
- [31] Chen, Y.; Huang, B.; Huang, M.; Cai, B. (2011) On the preparation and characterization of activated carbon from mangosteen shell. *Journal Taiwan Institute Chemical E*, 42 (5): 837–842. doi:10.1016/j.jtice.2011.01.007
- [32] Oliveira, L.C.A.; Pereira, E.; Guimaraes, I.R.; Vallone, A.; Pereira, M.; Mesquita, J.P.; Sapag, K. (2009) Preparation of activated carbons from coffee husks utilizing FeCl<sub>3</sub> and ZnCl<sub>2</sub> as activating agents. *Journal of Hazardous Materials*, 165 (1): 87–94. doi:10.1016/j.jhazmat.2008.09.064
- [33] Shi, Q.; Zhang, J.; Zhang, C.; Li, C.; Zhang, B.; Hu, W.; Xu, J.; Zhao, R. (2010) Preparation of activated carbon from cattail and its application for dyes removal. *Journal Environment Sciences*, 22 (1): 91–97. doi:10.1016/S1001-0742(09)60079-6
- [34] Yorgun, S.; Yıldız, D. (2015) Preparation and characterization of activated carbons from paulownia wood by chemical activation with H<sub>3</sub>PO<sub>4</sub>. *Journal Taiwan Institute Chemical E*, 53: 122–131. doi: 10.1016/j.jtice.2015.02.032
- [35] Yakout, S.M.; Sharaf El-Deen, G. (2016) Characterization of activated carbon prepared by phosphoric acid activation of olive stones. *Arab Journal Chemical*, 9: S1155–S1162. doi: 10.1016/j.arabjc.2011.12.002
- [36] Pereira, R.G.; Veloso, C.M.; Da Silva, N.M.; de Sousa, L.F.; Bonomo, R.C.F.; de Souza, A.O.; Souza, M.O.D.G.; Fontan, R.D.C.J. (2014) Preparation of activated carbons from cocoa shells and siriguela seeds using H<sub>3</sub>PO<sub>4</sub> and ZnCl<sub>2</sub> as activating agents for BSA and α-lactalbumin adsorption. *Fuel Processing Technology*, 126: 476–486. doi: 10.1016/j.fuproc.2014.06.001
- [37] Niticharoenwong, B.; Shotipruk, A.; Mekasuwandumrong, O.; Panpranot, J.; Jongsomjit, B. (2013) Characteristics of activated carbons derived from deoiled rice bran residues. *Chemical Engineering*



# Activated carbon derived from bacterial cellulose and its application as an adsorbent and catalyst support material

A. KHAMKEAW<sup>1,2</sup>, T. ASAVAMONGKOLKUL<sup>1,2</sup>, T. PERNGYAI<sup>1,2</sup>, B. JONGSOMJIT<sup>2</sup> and M. PHISALAPHONG<sup>1</sup>

<sup>1</sup> Chemical Engineering Research Unit for Value Adding of Bioresources, Department of Chemical Engineering, Faculty of Engineering, Chulalongkorn University, Bangkok, Thailand.

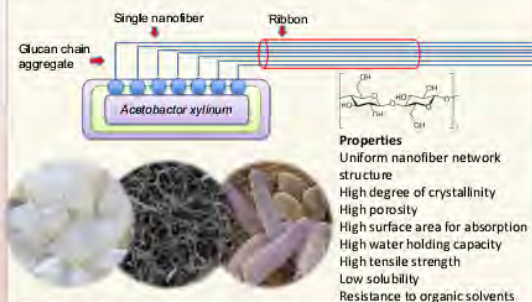
<sup>2</sup> Center of Excellence on Catalyst and Catalytic Reaction Engineering, Department of Chemical Engineering, Faculty of Engineering, Chulalongkorn University, Bangkok, Thailand.

## Abstract

The production of high surface area activated carbon from biomass has attracted attentions due to its wide range of applications. This research focuses on the development and investigation of activated carbons derived from bacterial cellulose (BC) for applications as effective adsorbent and catalyst support material. The activated carbons from BC were prepared by chemical activation using  $H_3PO_4$  and KOH as activating agents. The obtained activated carbons were characterized via BET, SEM, FT-IR and methylene blue adsorption test. The results show that the BC activated carbon has the BET surface area of 340-1316  $m^2/g$ . The adsorption test shows that the activation could generate a mesoporous structure, leading to the high adsorption capacity. The BC activated carbons were applied as a catalyst support for  $H_3PO_4$  catalyst in the ethanol dehydration reaction at the temperature from 200-400°C. At 400°C, the ethanol conversions of 43% to ethylene at could be obtained, whereas the high acetaldehyde selectivity at 52% was obtained at 200°C.

## Bacterial cellulose

Bacterial cellulose (BC) produced by bacteria *Acetobacter xylinum* has been interested as a renewable biomaterial with outstanding properties.



## Experimental methods

1	Bacterial cellulose (BC) preparation – residual bacterial cells and chemicals removal						
2	<table border="0"> <tr> <td>Activation via <math>H_3PO_4</math></td> <td>Activation via KOH</td> </tr> <tr> <td>• Impregnate with 85% <math>H_3PO_4</math> 1:1 w/w</td> <td>• Impregnate with 12M KOH 1:1 w/w</td> </tr> <tr> <td>• Carbonize at 500°C for 1 h</td> <td>• Carbonize at 500°C for 1 h</td> </tr> </table>	Activation via $H_3PO_4$	Activation via KOH	• Impregnate with 85% $H_3PO_4$ 1:1 w/w	• Impregnate with 12M KOH 1:1 w/w	• Carbonize at 500°C for 1 h	• Carbonize at 500°C for 1 h
Activation via $H_3PO_4$	Activation via KOH						
• Impregnate with 85% $H_3PO_4$ 1:1 w/w	• Impregnate with 12M KOH 1:1 w/w						
• Carbonize at 500°C for 1 h	• Carbonize at 500°C for 1 h						
3	<p>Adsorption study</p> <p>BC-ACs of 0.02 g were added into 40 mL of the solution in 100 mL Erlenmeyer flask. The MB absorption experiment was conducted at 30°C and 125 rpm using an incubator-shaker</p>						
4	<p>Acid catalyst preparation</p> <p>BC-ACs were impregnated with <math>H_3PO_4</math> 30 wt. %</p> <p>Catalytic performance study</p> <p>Pack 0.05 g of the prepared catalyst in the reactor. Run ethanol dehydration reaction at 200-400°C with an increment of 50°C</p>						

## Results

Table 1. Nomenclatures, BET results, and activated carbons adsorption capacity.

Activated carbon	Activating agents	Surface area ( $m^2/g$ )	Total pore volume ( $cm^3/g$ )	Average pore diameter ( $\text{\AA}$ )	Adsorption capacity (mg/g)
BC-AC-P	$H_3PO_4$	1,316	0.888	23.7	189.2
BC-AC-K	KOH	340	0.219	25.8	70.2

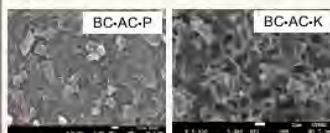


Figure 1 Surface morphology of activated carbon

BC-ACs obtained from both activation showed the mesoporous structure. BC-AC-K exhibited higher pore diameter than BC-AC-P, while BC-AC-P exhibited higher surface area and adsorption capacity than those of BC-AC-K.

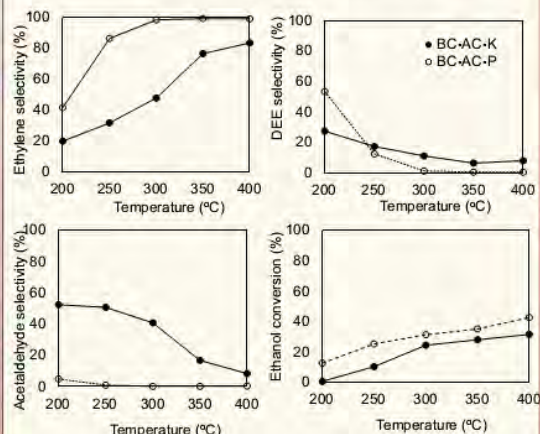


Figure 2 Selectivity of ethylene, DEE, and acetaldehyde, and ethanol conversion.

BC-AC-K exhibited higher selectivity of acetaldehyde (52% at 200°C), while BC-AC-P exhibited higher ethylene selectivity (100% at 350-400°C).

## Conclusion


Both activated carbons derived from BC using difference activating agents showed mesoporous structure (20-500  $\text{\AA}$ ) with different surface area and pore diameter. The difference in porous structure affects adsorption capacity and catalytic performance. BC-AC-P showed larger surface area, better adsorption capacity and higher ethylene selectivity. BC-AC-K exhibited larger pore size and higher acetaldehyde selectivity.

**Acknowledgement** : Grant support from Ratchadaphiseksomphot Endowment Fund, Chulalongkorn University and the National Research Council of Thailand.



## ภาคผนวก(Appendix) 5

ดำเนินการจดอนุสิทธิบัตร ผ่านสถาบันทรัพย์สินทางปัญญา จุฬาลงกรณ์มหาวิทยาลัย


Logoutข้อมูลค่าของเงิน

Dashboard

หน้าหลัก

ข้อมูลส่วนตัว

ติดต่อเจ้าหน้าที่



ถ้าต้องการคำแนะนำเพิ่มเติม สำหรับการกรอกข้อมูลสิทธิบัตรจากเจ้าหน้าที่ กรุณาคลิกด้านล่าง

ติดต่อที่นี่

หน้าหลัก / เลขที่อ้างอิง 01661

### รายละเอียด

เลขที่คำขอ	N/A
ชื่อสิ่งประดิษฐ์/การออก... บทสรุปการประดิษฐ์	ถ่านกัมมันต์จากแบคทีเรียเซลลูโลสด้วยกระบวนการกระตุ้นทางเคมี และกรรมวิธีการผลิต การประดิษฐ์นี้เกี่ยวข้องกับการผลิตถ่านกัมมันต์จากแบคทีเรียเซลลูโลสเพื่อใช้เป็นวัสดุสำหรับดูดซับ สารเคมี และใช้เป็นตัวรองรับตัวเร่งปฏิกิริยา ถ่านกัมมันต์เตรียมโดยการกระตุ้นทางเคมีด้วยกรดฟอสฟอริกความเข้มข้น 50-85 เปอร์เซ็นต์โดยมวลต่อปริมาตร และเผาในเตาเผาภายใต้บรรยากาศ ที่อุณหภูมิ ในช่วง 400-800 องศาเซลเซียส การพัฒนาใช้เป็นตัวรองรับตัวเร่งปฏิกิริยา ทำโดยการเติมหมู่ฟังก์ชัน ของกรดโดยใช้สารละลายกรดซัลฟิวริกหรือกรดฟอสฟอริกที่ความเข้มข้น 50-98 เปอร์เซ็นต์โดยมวล ต่อปริมาตร ลงในถ่านกัมมันต์ โดยวิธีนี้จะทำให้ถ่านกัมมันต์มีกลุ่มฟังก์ชันของกรดกระจายตัวอยู่ภายในรูพรุนและพื้นที่ผิวของถ่านกัมมันต์ สามารถนำไปใช้เป็นตัวเร่งปฏิกิริยาแบบกรด เช่น ใช้ในปฏิกิริยาการ แยกน้ำออกจากเอทานอล โดยผลการทดลองใช้ตัวเร่งปฏิกิริยาในกระบวนการแยกน้ำออกจากเอทานอล ได้ถูกนำมาเปรียบเทียบกับผลการแยกน้ำออกจากเอทานอลที่ใช้ตัวเร่งปฏิกิริยาชนิดอื่นๆ พบว่ามี ประสิทธิภาพสูงกว่าตัวเร่งปฏิกิริยาที่เตรียมจากถ่านกัมมันต์ที่ผลิตเชิงพาณิชย์ และมีประสิทธิภาพใกล้เคียงหรือสูงกว่าตัวเร่งปฏิกิริยาทางเคมีชนิดอื่นๆหลายชนิด
ผู้กรอกข้อมูลสิทธิบัตร	เหมือนเดือน พิศาลพงศ์ +6622186875 Muenduen.p@chula.ac.th
ผู้ประดิษฐ์/ออกแบบ	1. ศาสตราจารย์ (ศ.) เหมือนเดือน พิศาลพงศ์ 02-2186875 Muenduen.p@chula.ac.th 2. ศาสตราจารย์ (ศ.) บรรเจิด จงสมจิตร 02-2186874 Bunjerd.J@chula.ac.th 3. นาย อานนท์ ขำแก้ว 081-7524530 title_fack@hotmail.com
Category	
Keyword	Bacterial cellulose; Activated carbon
รายละเอียดการประดิษฐ์	คลิกดูรายละเอียด

## ภาคผนวก(Appendix) 6

Manuscript  
Click here to view linked References

Activated carbon derived from bacterial cellulose and its use as a catalyst for ethanol dehydration

Arnon Khankeaw<sup>1,2</sup>, Lamphun Phahang<sup>1,2</sup>, Sujit Jongsongit<sup>2</sup>, and Muenduen Phisalaphong<sup>1\*</sup>

<sup>1</sup>Chemical Engineering Research Unit for Value Adding of Bioresources, Department of Chemical Engineering, Faculty of Engineering, Chulalongkorn University, Bangkok, 10330, Thailand.

<sup>2</sup>Center of Excellence on Catalyst and Catalytic Reaction Engineering, Department of Chemical Engineering, Faculty of Engineering, Chulalongkorn University, Bangkok, 10330, Thailand.

\*Corresponding author. Tel: 662 218 6875. E-mail: Muenduen.p@chula.ac.th (Muenduen Phisalaphong)

Activated carbon derived from bacterial cellulose and its use as a catalyst for ethanol dehydration

### Abstract

Activated carbon derived from bacterial cellulose (BC-AC) was modified with various loading of H<sub>3</sub>PO<sub>4</sub> and used as a catalyst for dehydration of ethanol. The BC-AC obtained at a carbonization temperature of 500 °C had a mesoporous structure with surface area and total pore volume of 1734 m<sup>2</sup>/g and 1.0 cm<sup>3</sup>/g, respectively. An increase in the H<sub>3</sub>PO<sub>4</sub> loading from 5% to 40% increased the number of weak acid sites on the catalyst surface, which consequently enhanced ethanol conversion. At a reaction temperature of 400 °C, the modified BC-AC with 30-40% H<sub>3</sub>PO<sub>4</sub> loading (P/BC-AC) gave ethanol conversion at 100% with ethylene selectivity of 100%, whereas high selectivity for DEE at 66%-68%, at ethanol conversion of 49%-51% was obtained at 200 °C. Stability tests with a time-on-stream of 12 h at reaction temperatures of 200 and 400 °C showed that the P/BC-AC catalyst had high thermal stability and stable catalytic activity. Therefore, P/BC-AC was found to be very effective as an inexpensive and environmentally friendly catalyst for ethylene production from ethanol dehydration.

**Keywords:** activated carbon; bacterial cellulose; catalyst; ethanol dehydration; ethylene

## 1. Introduction

Because of environmental concerns, green chemistry and green catalysts have recently been attracting considerable interest. Biomass has been, therefore widely studied as a source of chemicals and catalysts. Bacterial cellulose (BC) produced by the bacterium *Acetobacter xylinum* is a renewable biomass with outstanding properties. This non-photosynthetic organism can convert glucose, sugar, glycerol, and other organic substrates to pure nanocellulose [1]. BC has the same chemical structure as plant cellulose, but has a uniform nanofiber network structure and excellent properties, such as a high degree of crystallinity, high porosity, high surface area for adsorption, high water-retention capacity, high tensile strength, low solubility, and resistance to organic solvents [2–4]. BC is of high purity because its structure does not contain lignin, hemicelluloses, or other complex carbohydrates. These advantageous properties should enable BC to function as an excellent matrix material source of activated carbon. However, so far, there have been only few studies of the production of activated carbon from BC.

Activated carbon is a carbonaceous, porous material, which is prepared by carbonization and activation of organic substances. It is widely used as an adsorbent in water treatment [5], the chemical and petroleum industries [6], separation, and purification [7]. Activated carbon can be usually produced from two different methods, which are chemical activation and physical activation [8]. Chemical activation is a better method than physical activation for activated carbon preparation from organic substances. Chemical activation requires a lower activation temperature, and gives products in higher yields and with higher surface areas [9]. Phosphoric acid ( $H_3PO_4$ ) is commonly used for activation. The use of  $H_3PO_4$ , which is non-toxic, gives high yields of products with high surface areas, high pore volumes, and good pore diameters [9].

Because of its advantageous properties such as a mesoporous structure, high surface area, and high chemical stability, activated carbon provides inexpensive catalyst supports or catalysts.

Carbon materials can be used as catalysts for acid/base reactions because of the presence of acidic and/or basic surface oxygen groups [10]. Porous carbon-supported catalysts are effective and have minimal impact on the environment. Activated carbon has been used as a catalyst or catalyst support in the catalytic dehydration of ethanol for the production of ethylene as the main product and diethyl ether (DEE) as a by-product. Ethylene is preferentially formed at high reaction temperatures, whereas DEE is the main product at lower reaction temperatures [11]. Ethylene is an important raw material in the manufacture of polymers such as polyethylene, polyethylene terephthalate, and polyvinyl chloride [11, 12]. DEE is commonly used as a solvent for waxes, fats, alkaloids, and gums [14]. It is also used as an additive for biodiesel or diesel fuels to improve the engine performance and emission properties [14]. In the catalytic dehydration of ethanol to ethylene, the acid catalyst first protonates the hydroxyl group, which then leaves as a water molecule. The conjugate base of the catalyst then deprotonates the methyl group, and the hydrocarbon rearranges to ethylene. However, the ethylene yields obtained from the catalytic dehydration of ethanol with activated carbon catalysts are still relatively low compared with those achieved with some other catalysts, especially alumina-based catalysts [12,15,16].

$H_3PO_4$  was the first catalyst used for catalytic dehydration of ethanol to ethylene and was prepared by loading  $H_3PO_4$  on clay or coke [17]. The ethylene produced by dehydration of ethanol with a  $H_3PO_4$  catalyst is of high purity [18].  $H_3PO_4$  catalysts are inexpensive and have low preparation costs. Many modified catalysts based on  $H_3PO_4$  have been investigated for use in ethanol dehydration. Recently, Zhang et al. [19] and Ramesh et al. [20] reported that  $H_3PO_4$

1  
2  
3  
4  
5  
6  
7  
8  
9  
10  
11  
12  
13  
14  
15  
16  
17  
18  
19  
20  
21  
22  
23  
24  
25  
26  
27  
28  
29  
30  
31  
32  
33  
34  
35  
36  
37  
38  
39  
40  
41  
42  
43  
44  
45  
46  
47  
48  
49  
50  
51  
52  
53  
54  
55  
56  
57  
58  
59  
60  
61  
62  
63  
64  
65

modification of a HZSM-5 catalyst surface gave high ethylene selectivity and good anti-coking properties because the modification led to the formation of weak acid sites and the elimination of strong acid sites, which are responsible for high hydrocarbon and coking formation. Modification with  $H_3PO_4$  can therefore provide suitable acid sites on catalyst surfaces, and improve the product selectivity and anti-coking ability.

In our previous work, we prepared a novel activated carbon with a mesoporous structure, a high surface area, and a high adsorption capacity from bacterial cellulose by  $H_3PO_4$  activation [21]. In this study, the activated carbon derived from bacterial cellulose was further modified by  $H_3PO_4$  loading for use as a catalyst for ethanol dehydration. The effects of surface changes caused by changes in the  $H_3PO_4$  loading on the catalytic performance in ethanol dehydration were investigated.

**2. Material and methods**

**2.1 Materials**

BC was synthesized by *A. xylinum* 60. The stock culture was kindly provided by Pramote Thammaraad, the Institute of Research and Development of Food Product, Kasetsart University, Bangkok, Thailand. BC hydrogel was treated with 1% w/v NaOH for 24 h. to remove bacterial cells and then it was rinsed with deionized (DI) water until pH was 7.0 and dried at 110°C for 24 hours.

**2.2 Catalyst preparation**

BC was treated with  $H_3PO_4$  at a ratio of 1:1 w/w and then was dried in a general electric oven (SNOL 67/350 LSP01, SNOL, Lithuania) at 110°C for 24 h. The dried BCs were later placed in a furnace (CWF 1100, Carbolite, UK) and carbonized under various temperatures of

5

1  
2  
3  
4  
5  
6  
7  
8  
9  
10  
11  
12  
13  
14  
15  
16  
17  
18  
19  
20  
21  
22  
23  
24  
25  
26  
27  
28  
29  
30  
31  
32  
33  
34  
35  
36  
37  
38  
39  
40  
41  
42  
43  
44  
45  
46  
47  
48  
49  
50  
51  
52  
53  
54  
55  
56  
57  
58  
59  
60  
61  
62  
63  
64  
65

400, 500, and 600°C for 1 h (without inert gas purging) before cooling down. To remove residual chemicals in the porous structure, the obtained activated carbons were washed sequentially with 1M HCl solution under mild stirring at 120 rpm and 70°C for 4 h, before were rinsed with distilled water several times until pH was 7.0. Then the samples were dehydrated at 110 °C for 24 h. Next, the activated carbon with mesoporous structure and the highest surface area was selected for the study of effect of the  $H_3PO_4$  loading on the surface. The activated carbon was impregnated with 5, 10, 20, 30, and 40 wt% of  $H_3PO_4$  by the incipient wetness technique. The solution of  $H_3PO_4$  was dropped slowly onto 0.1 g of activated carbon and then the samples were dehydrated in oven at 110°C for 24 h.

**2.3 Catalyst characterizations**

The surface area, pore volume, and pore diameter of catalysts were determined by nitrogen physisorption-desorption at liquid  $N_2$  temperature of -196°C using a Micromeritics Chemisorb 2750 Pulse instrument (Norcross, GA, USA).

Field emission scanning electron microscope (Model of JSM-7610F, JEOL, USA) and energy dispersive X-ray (Hitachi mode S-3400N, Japan) spectroscopy were used to determine the morphology and elemental distribution of catalysts. The energy dispersive X-ray was performed using Apollo X silicon drift detector series by EDAX.

The X-ray diffraction (XRD) was performed to determine the bulk crystal structure of catalysts using  $CuK\alpha$  radiation with Ni filter in the 2 $\theta$  range of 10 to 80 degree resolution 0.02° (SIEMENS D5000 X-ray diffractometer, Aubrey, USA). The crystallite size was calculated from Scherrer's equation.

6

The Fourier transform infrared (FTIR) spectroscopy (Nicolet 6700 FTIR spectrometer, Thermo Scientific, USA) was used to determine the functional groups of catalyst chemical structure.

The temperature-programmed desorption of ammonia (NH<sub>3</sub>-TPD) was used to investigate the acid properties of catalysts. It was performed using a Micromeritics chemisorp 2750 pulse chemisorption system to study the acid properties of catalysts. In this experiment, 0.05 g of catalyst sample was packed in U-tube glass with 0.03 g of quartz wool and pretreated at 200 °C under helium (He) flow for 1 h. After that, the catalyst sample was saturated with 15% of NH<sub>3</sub>/He and the physisorbed ammonia was desorbed under helium gas flow after saturation. The catalyst sample was heated from 40°C to 500 °C at heating rate of 10 °C/min. The amount of ammonia in effluent was measured via TCD signal as a function of time.

#### 2.4 Catalytic ethanol dehydration reaction

##### 2.4.1 Temperature-programmed reaction

The dehydration of ethanol has been carried out under atmospheric pressure in fixed-bed continuous flow micro-reactor made from a borosilicate glass with inside diameter of 0.7 cm and outside diameter of 0.9 cm. 0.1 g of catalyst and 0.01 g quartz wool were packed in the fixed-bed continuous flow micro-reactor [12,14–16]. Before running the reaction, the catalyst was pre-treated in situ at the reaction temperature of 200 °C for 1 h in N<sub>2</sub> flow (30 ml/min) to remove any moisture on surface of catalyst. The liquid ethanol was vaporized at 120 °C in N<sub>2</sub> flow (30 ml/min) and then introduced to the reactor by controlled injection with a single syringe pump at constant ethanol flow rate of 1.45 ml/h (11.4 g<sub>ethanol</sub>/g<sub>cat</sub> h). The ethanol dehydration reaction was performed at the temperature in the range of 200 to 400 °C. The products (ethanol, ethylene,

acetaldehyde, and diethyl ether) were determined by gas chromatography (GC) using a Shimadzu model GC-14A with flame ionization detector (FID) and capillary column (DB-5).

##### 2.4.2 Stability test

The catalyst that provided the highest catalytic ethanol dehydration from temperature-programmed reaction test was selected to investigate its stability for ethanol dehydration reaction as a function of time on stream (TOS) for 12 h. The experimental apparatus and set-up were similar with temperature-programmed reaction as mentioned above. The ethanol dehydration reactions were conducted at the reaction temperature of 200, and 400 °C. During running the reactions, the products were collected every 1 h for 12 h.

### 3. Results and discussion

#### 3.1 Catalyst characterization

##### 3.1.1 Pore structure and surface area

The dried BC was carbonized with H<sub>3</sub>PO<sub>4</sub> activation at various temperatures (400, 500, and 600 °C). The amount of carbon in all BC-AC samples exceeded 70% with a yield of BC at 26–40% [21]. The samples are denoted by BC-AC<sub>x</sub>, where *x* is the carbonization temperature, i.e., BC-AC400 refers to an activated carbon derived from BC with H<sub>3</sub>PO<sub>4</sub> activation at carbonization temperature of 400 °C. Because BC-AC500 has a mesoporous structure and the highest surface area, it was selected for investigation by the incipient wetness technique of the effects of H<sub>3</sub>PO<sub>4</sub> loadings of 5, 10, 20, 30, and 40 wt%. The samples are denoted by *y*P/BC-AC500, where *y* is the weight percentage loading of H<sub>3</sub>PO<sub>4</sub>, i.e., 5P/BC-AC500 refers to BC-AC500 with a 5 wt% H<sub>3</sub>PO<sub>4</sub> loading.

The pore structures and surface areas of all the catalysts were investigated by N<sub>2</sub> physisorption. According to the International Union of Pure and Applied Chemistry classification of physisorption isotherms, all the catalysts have type IV isotherms with H<sub>4</sub> hysteresis loops at high pressure (figure not shown). This indicates that all the catalysts have mesoporous structures [22]. Table 1 shows the Brunauer–Emmett–Teller (BET) surface areas, pore volumes, and pore diameters of all the catalysts. The BET surface area and the total pore volume of BC-AC increased with increasing carbonization temperature from 400 to 500 °C and then started to decrease slightly from 500 to 600 °C. This is the result of shrinkage and/or partial collapse of the carbon structure, which leads to a reduction in the surface area and pore volume of the activated carbon [23]. The AC-BC with the highest BET surface area and total pore volume (1.734 m<sup>2</sup>/g and 1.0 cm<sup>3</sup>/g, respectively) was obtained by carbonization at 500 °C. The results show that the BET surface areas, total pore volumes, and average pore diameters did not significantly change with changes in the H<sub>3</sub>PO<sub>4</sub> loading. All the catalysts had average pore diameters of 2.3–2.5 nm and the pore diameters are distributed in the range 2–50 nm. The surface areas of the activated carbons derived from BC were about twice that of a commercial activated carbon (AC-com) and the average pore diameters were about 0.6 times that of AC-com.

**Table 1** The surface area, pore volume, and average pore diameter of BC-AC and P/BC-AC catalysts in comparison to a commercial activated carbon (AC-com)

Catalysts	S <sub>BET</sub> (m <sup>2</sup> /g)	V <sub>Micro</sub> <sup>a</sup> (cm <sup>3</sup> /g)	V <sub>Meso</sub> (cm <sup>3</sup> /g)	V <sub>total</sub> (cm <sup>3</sup> /g)	Average pore diameter (nm)
AC-com	851	0.165	0.707	0.872	4.1
BC-AC400	1.540	0.324	0.541	0.865	2.3
BC-AC500	1.734	0.181	0.830	1.011	2.3
BC-AC600	1.702	0.183	0.824	1.007	2.4
5P/BC-AC500	1.749	0.184	0.838	1.022	2.5
10P/BC-AC500	1.754	0.185	0.844	1.029	2.5
20P/BC-AC500	1.719	0.186	0.821	1.007	2.5
30P/BC-AC500	1.740	0.188	0.833	1.021	2.5
40P/BC-AC500	1.718	0.194	0.810	1.004	2.5

<sup>a</sup> Determination by t-plot method

### 3.1.2 Surface morphology and elemental distribution

The surface morphologies of BC after carbonization with  $H_3PO_4$  activation at temperatures of 400, 500, and 600 °C were all similar to that shown in Fig. 1. Because of the evaporation of  $H_3PO_4$  and other volatile matter from the surface during carbonization, BC-AC400, BC-AC500, and BC-AC600 had rough surfaces with irregular pores [24].

Energy dispersive X-ray spectroscopy (EDX) was used to map the elemental distributions and percentages on all the catalyst surfaces. All the catalysts had good surface distributions of phosphorus (figure not shown). The data in Table 2 show that the percentage of phosphorus on the BC-AC surface increased with increasing carbonization temperature from 400 to 600 °C. This is because a higher amount of phosphorus is incorporated into the carbon surface at higher carbonization temperatures [25]. The percentage of phosphorus on the surface of P/BC-AC500 also increased with increasing  $H_3PO_4$  loading.

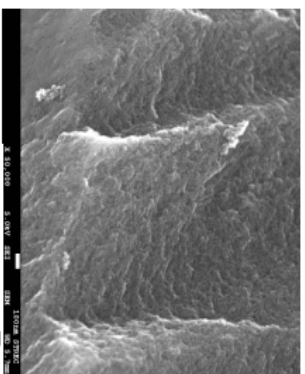


Fig. 1. SEM micrograph of surface morphology of BC-AC.

Catalysts	% Atom*			Acid sites ( $\mu\text{mol NH}_3/\text{g catalyst}$ )**		
	C	P	O	Weak	Moderate to strong	Total
BC-AC400	82.5	1.8	15.7	162.9	182.4	272.3
BC-AC500	87.5	4.3	8.2	206.0	109.4	281.5
BC-AC600	82.6	4.9	12.5	200.0	75.5	273.6
5P/BC-AC500	81.0	7.0	12.0	215.4	73.6	311.4
10P/BC-AC500	73.5	8.1	18.4	239.1	98.9	353.2
20P/BC-AC500	64.8	11.4	23.8	434.6	114.1	581.0
30P/BC-AC500	58.2	12.5	29.3	1140.6	146.4	1434.8
40P/BC-AC500	56.8	20.3	22.9	1249.0	294.3	1898.7

\* Surface elemental composition was determined by EDX analysis.

\*\*Quantities of acid site of catalysts were determined by  $\text{NH}_3$ -TPD with Fiyk program calculation.

### 3.1.3 Acidity

Temperature-programmed  $\text{NH}_3$  desorption ( $\text{NH}_3$ -TPD) was used to determine the surface acidity and the strength of the acid sites of all the catalysts. The desorption temperature indicates the strength of the acid sites. Desorption peaks at low temperatures (<250 °C) denote weak acid sites, whereas peaks at higher temperatures, around 250–500 °C, correspond to moderate to strong acid sites [14]. The numbers of acid sites for all the catalysts are summarized in Table 2. The number of moderate to strong acid sites on BC-AC decreased with increasing carbonization temperature from 400 to 600 °C. The number of weak acid sites increased with increasing

1  
2  
3  
4  
5  
6  
7  
8  
9  
10  
11  
12  
13  
14  
15  
16  
17  
18  
19  
20  
21  
22  
23  
24  
25  
26  
27  
28  
29  
30  
31  
32  
33  
34  
35  
36  
37  
38  
39  
40  
41  
42  
43  
44  
45  
46  
47  
48  
49  
50  
51  
52  
53  
54  
55  
56  
57  
58  
59  
60  
61  
62  
63  
64  
65

13

carbonization temperature from 400 to 500 °C and then decreased with increasing carbonization temperature from 500 to 600 °C. This is because the carbonization temperature affects the surface acidity and surface area of the activated carbon. An increase in the carbonization temperature from 400 to 500 °C increases the surface area of the activated carbon, and this increases the surface acidity of the catalyst [25]. An increase in the carbonization temperature from 500 to 600 °C decreases the surface area of the activated carbon, and this decreases the surface acidity. The BC-AC500 and P/BC-AC500 catalysts had larger numbers of weak acid sites than of moderate to strong acid sites. The surface acidities of weak character could be corresponding to weakly acidic surface of P-OH groups and phosphate ester and/or phenol groups; and moderate to strong characters could be corresponding to H-phosphate groups, which were formed in the carbon surface during the activation process of BC-ACs [10]. The numbers of weak and moderate to strong acid sites increased with increasing H<sub>3</sub>PO<sub>4</sub> loading on BC-AC500 because the surface acidity, which is predominantly derived from Brønsted acid sites, depends on the amount of phosphorus retained on the carbon surfaces [10]. The results indicate that surface modification by loading with H<sub>3</sub>PO<sub>4</sub> can improve the surface acidity of activated carbon. The weak acid sites and moderate to strong acid sites of AC-com were 36.4 and 182.4 μmol NH<sub>3</sub>/g catalyst, respectively. It is important to note that BC-ACs with and without an additional H<sub>3</sub>PO<sub>4</sub> loading had a considerably higher amount of weak acid sites compared to that of AC-com. It has been previously reported that the ethanol conversion to ethylene occurs on weak acid sites, while the oligomerization and the alcohol transformation to higher hydrocarbon correspond to strong acid strength [15–17]. In this study, it was shown that the ratios of weak/moderate to strong acid sites of BC-AC500 and P/BC-AC500 were 9.5-19.5 times that of AC-com. 30P/BC-AC500 was found to be mainly covered by weakly acidic surface with the highest ratio of weak/moderate to

1  
2  
3  
4  
5  
6  
7  
8  
9  
10  
11  
12  
13  
14  
15  
16  
17  
18  
19  
20  
21  
22  
23  
24  
25  
26  
27  
28  
29  
30  
31  
32  
33  
34  
35  
36  
37  
38  
39  
40  
41  
42  
43  
44  
45  
46  
47  
48  
49  
50  
51  
52  
53  
54  
55  
56  
57  
58  
59  
60  
61  
62  
63  
64  
65

14

strong acid sites at 3.9. Therefore, significant improvement in the ethanol conversion to ethylene catalyzed by using 30P/BC-AC500 was expected.

### 3.1.4 X-ray diffraction

X-ray diffraction (XRD) was used to determine the bulk crystal structures of BC-AC produced at various carbonization temperatures and P/BC-AC500 modified with various H<sub>3</sub>PO<sub>4</sub> loadings. The XRD patterns of all the catalysts showed a broad peak at  $2\theta = 24^\circ$  (figure not shown), which represented amorphous carbon composed of aromatic carbon sheets [26]. These XRD patterns are the usual pattern for amorphous carbon derived from cellulose [27,28].

### 3.1.5 Fourier transforms infrared spectroscopy

Fourier-transform infrared (FT-IR) spectroscopy was used to identify the functional groups or chemical bonds in all the catalysts; the spectra are shown in Fig. 2. The FT-IR spectra of all the catalysts show a broad band located at 3700–3260 cm<sup>-1</sup>, which is attributed to the O-H stretching vibration of the hydroxyl group and adsorbed water [29]. The bands at 2921 and 2855 cm<sup>-1</sup> are attributed to aliphatic C-H stretching vibrations [29]. The weak band at approximately 1700 cm<sup>-1</sup> is usually ascribed to the C=O stretching vibrations of ketones, aldehydes, lactones, or carboxyl groups [30]. The strong band at 1580 cm<sup>-1</sup> represents the C-C stretching vibrations of aromatic rings. The broad band at approximately 1200 cm<sup>-1</sup> is assigned to C-O stretching of acids, alcohols, phenols, ethers, and/or esters [29]. The presence of aromatic carbon was confirmed by the peak at 880 cm<sup>-1</sup>, which is associated with aromatic C-H out-of-plane vibrations of various substituted benzene rings [29]. The two bands at 980 and 500 cm<sup>-1</sup> are attributed to the stretching vibrations of hydrogen-bonded P-O-C and O-P-O groups, respectively [30–32]. It has previously been suggested that phosphorus surface groups



preferentially react with molecular oxygen, prior to carbon gasification, through oxidation of the C–P bond to form P–O–C, which is thermally stable at temperatures lower than 700 °C. For BC-AC500, the intensities of the peaks corresponding to P–O–C and O–P–O increased with increasing H<sub>3</sub>PO<sub>4</sub> loading. These bands confirm the presence of phosphorus and phosphorus-containing carbonaceous compounds formed from H<sub>3</sub>PO<sub>4</sub> on the activated carbon surface [31, 33]. The P–O and P–OH formed on the carbon surface during the activation process can act as Bronsted acid sites and have an important effect on the acidic character of the carbon catalysts prepared for ethanol dehydration [10].

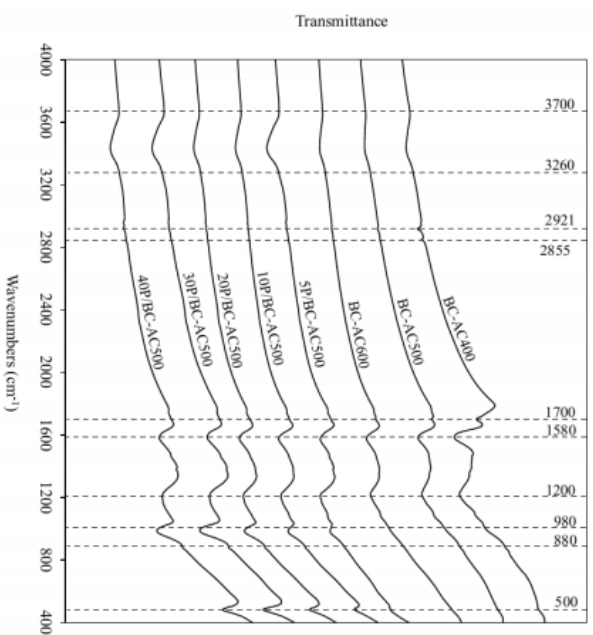


Fig. 2. FT-IR spectra of catalysts

### 3.2 Catalytic dehydration of ethanol

#### 3.2.1 Temperature-programmed reaction

The catalytic activities in ethanol dehydration at atmospheric pressure and reaction temperatures of 200–400 °C of the BC-AC samples obtained at various carbonization temperatures were investigated. The effects of the H<sub>3</sub>PO<sub>4</sub> loading on the catalytic activity were also examined. The activities were compared with those of AC-com. The ethanol conversions of all the catalysts are shown in Fig. 3. Selectivities of ethylene, diethyl ether (DEE), and acetaldehyde (MeCHO) from ethanol dehydration are summarized in Table 3.

The ethanol conversion increased with increasing reaction temperature from 200 to 400 °C (Fig.3). Similar effects of reaction temperature and catalyst acidity on ethanol conversion have previously been reported [11]. At a reaction temperature of 400 °C, ethanol conversions of 100% were obtained with all the BC-AC catalysts, except BC-AC400, which gave an ethanol conversion of 66.6%. The results show that an increase in the H<sub>3</sub>PO<sub>4</sub> loading on BC-AC500 increased the ethanol conversion. It is indicated that the concentration of weakly acidic sites on the catalyst surface has important effects for ethanol conversion and on the product selectivity in the ethanol dehydration reaction. The ethanol conversions obtained with the P/BC-AC500 catalysts were considerably higher than that obtained with the BC-AC500 catalyst. The 30P/BC-AC500 and 40P/BC-AC500 catalysts gave the highest ethanol conversions, i.e., 98.3%–100%, at reaction temperatures of 300–400 °C.

The ethylene selectivity achieved with the BC-AC catalysts was considerably higher than that obtained with AC-com. The ethylene selectivity obtained with BC-AC500 and BC-AC600 was higher than that obtained with BC-AC400. The highest selectivity for ethylene at 100%, was obtained at a reaction temperature of 400 °C with BC-AC500 and BC-AC600. Overall, the

17

1 ethylene selectivity achieved with all the P/BC-AC500 catalysts was higher than that obtained  
2 with BC-AC500. An increase in the H<sub>3</sub>PO<sub>4</sub> loading increased the selectivity for ethylene; the  
3 order was 40P/BC-AC500  $\approx$  30P/BC-AC500 > 20P/BC-AC500 > 10P/BC-AC500 > 5P/BC-  
4 AC500 > BC-AC500. The enhanced ethylene selectivity should be a result of an increase in the  
5 number of weak acid sites. It has previously been suggested that ethanol conversion to ethylene  
6 occurs at weak acid site [12, 31]. In this study, H<sub>3</sub>PO<sub>4</sub> loading on the BC-AC surface can  
7 increase the number of weak acid sites, and therefore increase the selectivity for ethylene.  
8 Ethylene production is an endothermic reaction and therefore favors high temperatures. The  
9 30P/BC-AC500 and 40P/BC-AC500 catalysts gave ethylene selectivity of 92.0%–93.3% at a  
10 reaction temperature of 300 °C. The ethylene selectivity increased to 98.7%–100% at a reaction  
11 temperature of 350–400 °C. The ethylene selectivity was found correspond to the amounts of  
12 weak acid sites as shown in Table 2. Among all the catalysts, 30P/BC-AC500 and 40P/BC-  
13 AC500 contained the largest amounts of weak acid sites, i.e., 1140.6 and 1249.0  $\mu\text{mol NH}_4\text{Y/g}$ ,  
14 respectively. Although 40P/BC-AC500 had the highest number of weak acid sites, the selectivity  
15 for ethylene of 40P/BC-AC500 was close to that of 30P/BC-AC500. It was shown that the  
16 amount of moderate to strong acid sites also increased with increasing H<sub>3</sub>PO<sub>4</sub> loading on the BC-  
17 AC surface. The number of moderate to strong acid sites on 40P/BC-AC500 was 2.2 times that  
18 on 30P/BC-AC500. Previously, it was suggested that an increase in the number of strong acid  
19 sites promoted ethylene polymerization, resulting in a decrease in ethylene concentration [12].  
20 The selectivity for DEE tends to increase with decreasing reaction temperature because it  
21 is an exothermic reaction product. The conversion of ethanol to DEE therefore favors low  
22 temperatures [11]. The highest selectivities for DEE at 65.7%–68.4%, were obtained at 200 °C  
23 with the 30P/BC-AC500 and 40P/BC-AC500 catalysts. However, the DEE selectivities of the

18

1 BC-AC400, BC-AC500, BC-AC600, 5P/BC-AC500, 10P/BC-AC500, and 20P/BC-AC500  
2 catalysts at a reaction temperature of 200 °C were lower than those at a reaction temperature of  
3 250 °C (data not shown) because acetaldehyde selectivity was higher at 200 °C. At higher  
4 reaction temperatures (300–350 °C), the selectivity for DEE rapidly decreased with increasing  
5 H<sub>3</sub>PO<sub>4</sub> loading owing to higher ethylene production and the DEE selectivity was 0 or almost 0  
6 at 400 °C.  
7 The selectivity for acetaldehyde tends to decrease with increasing reaction temperature.  
8 The acetaldehyde selectivities obtained in ethanol dehydration with the BC-AC catalysts were  
9 significantly lower than that achieved with AC-com as the catalyst. By using AC-com, high  
10 selectivities for acetaldehyde at 92.7% and 83.5% were obtained at 200 and 250 °C, respectively.  
11 However, because the ethanol conversion of the AC-com catalyst was quite low at 200–300 °C,  
12 therefore, the acetaldehyde yields were low. The maximum acetaldehyde yield at 29.0% was  
13 obtained with the AC-com catalyst at 400 °C.

Overall, the ethanol conversions, ethylene yields, and DEE yields achieved in the  
reactions with BC-AC400, BC-AC500, and BC-AC600 as the catalyst were considerably higher  
than those obtained with AC-com as the catalyst. In addition, among all the catalysts, 30P/BC-  
AC500 and 40P/BC-AC500 gave the highest ethylene yields (90.5%–100.0%) at reaction  
temperatures of 300–400 °C, and the highest DEE yields (32.1%–34.5%) at reaction  
temperatures of 200 °C. The 30P/BC-AC500 and 40P/BC-AC500 catalysts are therefore  
considered to be promising catalysts for ethanol dehydration, either for ethylene production (at  
350–400 °C) or for DEE production (at 200 °C), with the highest product yields. The 5P/BC-  
AC500, 10P/BC-AC500 and 20P/BC-AC500 catalysts were also effective for DEE production at  
250 °C, and gave DEE yields of 33.9%, 37.9% and 35.0%, respectively.

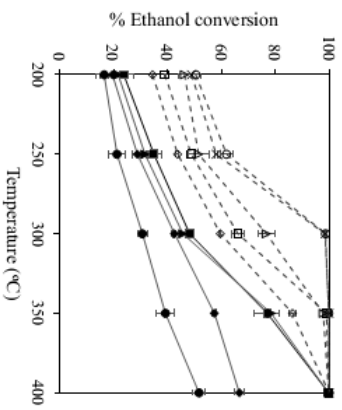


**Fig. 3.** Ethanol conversion in ethanol dehydration at reaction temperatures of 200-400°C catalyzed by: AC-eom (□), BC-AC400 (◆), BC-AC500 (■), BC-AC600 (▲), 5P/BC-AC500 (○), 10P/BC-AC500 (◇), 20P/BC-AC500 (Δ), 30P/BC-AC500 (◊), and 40P/BC-AC500 (×).

**Table 3** Selectivities of ethylene, diethyl ether (DEE), and acetaldehyde (MeCHO) from ethanol dehydration at 200, 300, and 400°C.

Catalysts	200°C			300°C			400°C		
	Ethylene	DEE	MeCHO	Ethylene	DEE	MeCHO	Ethylene	DEE	MeCHO
AC-eom	0.0	7.3	92.7	23.3	1.4	75.3	43.8	0.1	56.1
BC-AC400	0.0	35.5	64.5	40.5	53.2	6.3	86.7	5.7	7.6
BC-AC500	0.0	24.6	75.4	38.6	54.4	7.1	97.4	0.3	2.3
BC-AC600	0.0	24.4	75.6	39.4	58.4	2.2	98.0	0.3	1.7
5P/BC-AC500	1.3	49.2	49.5	50.5	46.8	2.8	97.9	0.5	1.6
10P/BC-AC500	1.7	58.1	40.2	59.8	38.2	2.0	98.3	0.2	1.5
20P/BC-AC500	2.5	52.3	45.2	78.8	19.1	2.1	98.2	0.5	1.3
30P/BC-AC500	13.9	68.4	17.7	92.0	6.9	1.1	100.0	0.0	0.0
40P/BC-AC500	11.0	65.7	23.3	93.3	5.5	1.2	100.0	0.0	0.0

### 3.2.2 Stability test

The 30P/BC-AC500 catalyst was then selected for use in stability tests with a time-on-stream of 12 h. Fig. 4 shows the ethanol conversions during 12 h stability tests at reaction temperatures of 200 and 400 °C. At a reaction temperature of 200 °C, the ethanol conversion and selectivity for DEE were consistent at around 40.4%–50.8% and 67.9%–73.6% respectively. At a reaction temperature of 400 °C, the ethanol conversion was constant at 100%, with an ethylene selectivity of 100%, during the 12 h stability test. This indicates that the 30P/BC-AC500 catalyst has good activity and high stability in ethanol dehydration for the production of ethylene at 400 °C or DEE at 200 °C. In a previous study, chemical activation of olive stones with H<sub>3</sub>PO<sub>4</sub> produced activated carbons with relatively high contents of phosphorus surface groups, which remained stable on the carbon surface at relatively high temperatures (<700 °C) [30]. The data show that 30P/BC-AC500 is a more effective ethanol dehydration catalyst than modified activated carbon catalysts previously reported [35]. The ethanol conversion and ethylene yield achieved with the 30P/BC-AC500 catalyst are comparable to those obtained with modified alumina-based catalysts [15]. This could be because of the highly uniform mesoporous structure, high effective surface area with high concentration of weak acid sites of activated carbon derived from BC loaded with H<sub>3</sub>PO<sub>4</sub>.

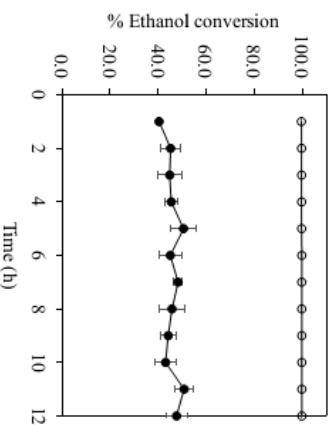


**Fig. 4.** Stability test with a time-on-stream (TOS) for 30P/BC-AC500 catalyst at reaction temperature of 200°C (●) and 400°C (○).

#### 4. Conclusion

Activated carbon derived from BC (BC-AC) with a highly uniform mesoporous structure was successfully prepared by one-step  $H_3PO_4$  activation at a carbonization temperature of 500 °C. The BC-AC500 was modified with various loadings of  $H_3PO_4$  and was used as an inexpensive and environmentally friendly catalyst for ethanol dehydration. The results show that the P/BC-AC500 catalysts had larger numbers of weak acid sites than of moderate to strong acid sites, and the amount of weak acid sites increased with increasing  $H_3PO_4$  loading from 5% to 40%. The modified P/BC-AC catalyst was an efficient catalyst for the dehydration of ethanol to ethylene and DEE. The ethanol conversion of 98-100% and ethylene selectivity of 93-100% were obtained by using 30P/BC-AC500 and 40P/BC-AC500 catalysts at reaction temperature of 300-400°C, whereas the ethanol conversion at 42-50% with the selectivity of DEE at 65.7-68.4% was obtained at reaction temperature of 200°C. Under the stability test for 12 h, 30P/BC-AC500

was shown to act as an effective catalyst with high thermal stability to achieve complete conversion of ethanol with 100% ethylene yield at 400°C. Activated carbon developed from BC was found considerably more effective than those of commercial activated carbons. Unique physicochemical properties of highly pure nanocellulose fiber network structure with high surface area and uniform pore distribution are considered to be beneficial for BC to be used as a source of effective activated carbon catalysts.

#### Acknowledgement

The authors acknowledge the financial support from The 100<sup>th</sup> Anniversary Chulalongkorn University Fund for Doctoral Scholarship and the 90<sup>th</sup> Anniversary of Chulalongkorn University Fund (Ratchadaphiseksomphot Endowment Fund).

#### References

- [1] S. Hestrin, M. Schramm, Synthesis of cellulose by *Acetobacter xylinum*. 2. Preparation of freeze-dried cells capable of polymerizing glucose to cellulose. *Biochem. J.* 58 (1954) 345–352. <https://doi.org/10.1042/bj0580345>.
- [2] S. Taokaew, S. Seetabhaewang, P. Siripong, M. Phisalaphong, Biosynthesis and characterization of nanocellulose-gelatin films. *Materials (Basel)*. 6 (2013) 782-794. <https://doi.org/10.3390/ma6030782>.
- [3] M. Luddace, S. Pivsa-Art, S. Sirisamsameyakul, P. Chiravoojpechyen, Particle size of ground bacterial cellulose affecting mechanical, thermal, and moisture barrier properties of PLA/BC biocomposites. *in: Energy Procedia*, 56 (2014) 211-218. <https://doi.org/10.1016/j.egypro.2014.07.151>.
- [4] F. Çakar, I. Özer, A.Ö. Aytekin, F. Şahin, Improvement production of bacterial cellulose

1 23  
2  
3  
4 by semi-continuous process in molasses medium, *Carbohydr. Polym.* 106 (2014) 7-13.  
5  
6 <https://doi.org/10.1016/j.carbpol.2014.01.103>.  
7  
8  
9  
10  
11 [5] P. Ariyadejwanich, W. Tanhapanichakoon, K. Nakagawa, S.R. Mukai, Preparation and  
12 characterization of mesoporous activated carbon wasted tires, *Carbon N. Y.* 41 (2003)  
13 157-164. [https://doi.org/10.1016/S0008-6223\(02\)00267-1](https://doi.org/10.1016/S0008-6223(02)00267-1).  
14  
15  
16 [6] M. Tawalbeh, M.A. Allawzi, M.I. Kandah, Production of activated carbon from jofpha  
17 seed residue by chemical activation residue using a static bed reactor, *J. Appl. Sci.* 5  
18 (2005) 482-487. <https://doi.org/10.3923/jas.2005.482.487>.  
19  
20  
21 [7] M. Mamoochehri, A. Khorsand, E. Hashemi, Role of modified activated carbon by H<sub>3</sub>PO<sub>4</sub>  
22 or K<sub>2</sub>CO<sub>3</sub> from natural adsorbent for removal of Pb (II) from aqueous solutions, *Carbon*  
23 *Let.* 13 (2012) 115-120. <https://doi.org/10.1109/ISPA.2003.1296917>.  
24  
25  
26 [8] N. Mohammad Nor, L.C. Lau, K.T. Lee, A.R. Mohamed, Synthesis of activated carbon  
27 from lignocellulosic biomass and its applications in air pollution control—a review, *J.*  
28 *Environ. Chem. Eng.* 1 (2013) 658-666. <https://doi.org/10.1016/j.jece.2013.09.017>.  
29  
30  
31 [9] M.A. Yahya, Z. Al-Qodah, C.W.Z. Ngah, Agricultural bio-waste materials as potential  
32 sustainable precursors used for activated carbon production: A review, *Renew. Sustain.*  
33 *Energy Rev.* 46 (2015) 218-235. <https://doi.org/10.1016/j.rser.2015.02.051>.  
34  
35  
36 [10] J. Bodia, R. Ruiz-Rosas, J. Rodriguez-Mirasol, T. Cordero, T.C. J. Bodia, R. Ruiz-Rosas,  
37 J. Rodriguez-Mirasol, Kinetic study of the decomposition of 2-butanol on carbon-based  
38 acid catalyst, *AIChE J.* 56 (2009) 1557-1568. <https://doi.org/10.1002/aic>.  
39  
40  
41 [11] G. Chen, S. Li, F. Jiao, Q. Yuan, Catalytic dehydration of bioethanol to ethylene over  
42 TiO<sub>2</sub>/γ-Al<sub>2</sub>O<sub>3</sub> catalysts in microchannel reactors, *Catal. Today.* 125 (2007) 111-119.  
43 <https://doi.org/10.1016/j.cattod.2007.01.071>.

1 24  
2  
3  
4 [12] T. Kamsuwan, B. Jongsonjti, A comparative study of different al-based solid acid  
5 catalysts for catalytic dehydration of ethanol, *Eng. J.* 20 (2016) 63-75.  
6 <https://doi.org/10.4186/ej.2016.20.3.63>.  
7  
8  
9 [13] J. Becerra, E. Quiroga, E. Tello, M. Figueredo, M. Cobo, Kinetic modeling of polymer-  
10 grade ethylene production by diluted ethanol dehydration over H-ZSM-5 for industrial  
11 design, *J. Environ. Chem. Eng.* 6 (2018) 6165-6174.  
12 <https://doi.org/10.1016/j.jece.2018.09.035>.  
13  
14  
15 [14] M. Ibnu Abdulwahab, A. Khankeaw, B. Jongsonjti, M. Phisalaphong, Bacterial cellulose  
16 supported alumina catalyst for ethanol dehydration, *Catal. Letters.* 147 (2017) 2462-2472.  
17 <https://doi.org/10.1007/s10562-017-2145-y>.  
18  
19  
20 [15] M. Wannarvorworn, P. Prasertkham, B. Jongsonjti, A comparative study of solvothermal  
21 and sol-gel-derived nanocrystalline alumina catalysts for ethanol dehydration, *J.*  
22 *Nanomater.* 2015 (2015) 11 pages. <https://doi.org/10.1155/2015/19425>.  
23  
24  
25 [16] T. Chanachuey, C. Aurtahant, B. Jongsonjti, Effect of Mo-doped mesoporous Al-SSP  
26 catalysts for the catalytic dehydration of ethanol to ethylene, *J. Chem.* 2016 (2016) 8  
27 pages. <https://doi.org/10.1155/2016/9672408>.  
28  
29  
30 [17] M. Zhang, Y. Yu, Dehydration of ethanol to ethylene, *Ind. Eng. Chem. Res.* 52 (2013)  
31 9505-9514. <https://doi.org/10.1021/ie401157c>.  
32  
33  
34 [18] D.E. Pearson, R.D. Tanner, I.D. Picciotto, J.S. Sawyer, J.H. Cleveland, Phosphoric acid  
35 systems. 2. Catalytic conversion of fermentation ethanol to ethylene, *Ind. Eng. Chem.*  
36 *Prod. Res. Dev.* 20 (1981) 734-740. <https://doi.org/10.1021/i300004a028>.  
37  
38  
39 [19] D. Zhang, R. Wang, X. Yang, Effect of P content on the catalytic performance of P-  
40 modified HZSM-5 catalysts in dehydration of ethanol to ethylene, *Catal. Letters.* 124

1 25  
2  
3  
4 (2008) 384-391. <https://doi.org/10.1007/s10562-008-9481-x>.  
5  
6  
7  
8  
9  
10  
11  
12  
13  
14  
15  
16  
17  
18  
19  
20  
21  
22  
23  
24  
25  
26  
27  
28  
29  
30  
31  
32  
33  
34  
35  
36  
37  
38  
39  
40  
41  
42  
43  
44  
45  
46  
47  
48  
49  
50  
51  
52  
53  
54  
55  
56  
57  
58  
59  
60  
61  
62  
63  
64  
65

[20] K. Ramesh, L.M. Hui, Y.F. Han, A. Borgna, Structure and reactivity of phosphorous modified H-ZSM-5 catalysts for ethanol dehydration, *Catal. Commun.* 10 (2009) 567-571. <https://doi.org/10.1016/j.catcom.2008.10.034>.

[21] A. Khankeaw, B. Jongsomjit, J. Robison, M. Phisalaphong, Activated carbon from bacterial cellulose as an effective adsorbent for removing dye from aqueous solution, *Sep. Sci. Technol.* (2018). <https://doi.org/10.1080/01496395.2018.1541906>.

[22] IUPAC, *Pure Appl. Chem.* 57 (1985) 603-619. <https://doi.org/10.1351/pac198557040603>.

[23] M. Armandi, B. Bonelli, F. Geobaldo, E. Garrone, Nanoporous carbon materials obtained by sucrose carbonization in the presence of KOH, *Microporous Mesoporous Mater.* 132 (2010) 414-420. <https://doi.org/10.1016/j.micromeso.2010.03.021>.

[24] H. Demiral, G. Gündüzoglu, Removal of nitrate from aqueous solutions by activated carbon prepared from sugar beet bagasse, *Bioresour. Technol.* 101 (2010) 1675-1680. <https://doi.org/10.1016/j.biortech.2009.09.087>.

[25] J. Bedia, R. Barrionuevo, J. Rodriguez-Mirasol, T. Cordero, Ethanol dehydration to ethylene on acid carbon catalysts, *Appl. Catal. B Environ.* 103 (2011) 302-310. <https://doi.org/10.1016/j.apcatb.2011.01.032>.

[26] T.Y. Jun, S.D. Arumugam, N.H.A. Latip, A.M. Abdullah, P.A. Latif, Effect of activation temperature and heating duration on physical characteristics of activated carbon prepared from agriculture waste, *Environment Asia.* 3 (2010) 143-148. <https://doi.org/10.14456/ea.2010.32>.

[27] I.A. Aguayo-Villarreal, A. Bonilla-Petriciolet, R. Muñiz-Valencia, Preparation of activated carbons from pecan nutshell and their application in the antagonistic adsorption

1 26  
2  
3  
4  
5  
6  
7  
8  
9  
10  
11  
12  
13  
14  
15  
16  
17  
18  
19  
20  
21  
22  
23  
24  
25  
26  
27  
28  
29  
30  
31  
32  
33  
34  
35  
36  
37  
38  
39  
40  
41  
42  
43  
44  
45  
46  
47  
48  
49  
50  
51  
52  
53  
54  
55  
56  
57  
58  
59  
60  
61  
62  
63  
64  
65

of heavy metal ions, *J. Mol. Liq.* 230 (2017) 686-695. <https://doi.org/10.1016/j.molliq.2017.01.039>.

[28] D. Prabas, Y. Karika, N. Indraswati, S. Ismahji, Activated carbon from jackfruit peel waste by H<sub>3</sub>PO<sub>4</sub> chemical activation: Pore structure and surface chemistry characterization, *Chem. Eng. J.* 140 (2008) 32-42. <https://doi.org/10.1016/j.cej.2007.08.032>.

[29] S.M. Yakout, G. Sharaf El-Deen, Characterization of activated carbon prepared by phosphoric acid activation of olive stones, *Arab. J. Chem.* 9 (2016) S1155-S1162. <https://doi.org/10.1016/j.arabjce.2011.12.002>.

[30] S. Yorgun, D. Yildiz, Preparation and characterization of activated carbons from Paulownia wood by chemical activation with H<sub>3</sub>PO<sub>4</sub>, *J. Taiwan Inst. Chem. Eng.* 53 (2015) 122-131. <https://doi.org/10.1016/j.jtice.2015.02.032>.

[31] H. Tounsadi, A. Khalidi, A. Machrouhi, M. Farnane, R. Elmoubarki, A. Elhadi, M. Sadiq, N. Barka, Highly efficient activated carbon from *Glebionis coronaria* L. biomass: Optimization of preparation conditions and heavy metals removal using experimental design approach, *J. Environ. Chem. Eng.* 4 (2016) 4549-4564. <https://doi.org/10.1016/j.jece.2016.10.020>.

[32] V.M. Vučkurović, R.N. Raznovski, M.N. Tekić, Methylene blue (cationic dye) adsorption onto sugar beet pulp: Equilibrium isotherm and kinetic studies, *J. Taiwan Inst. Chem. Eng.* 43 (2012) 108-111. <https://doi.org/10.1016/j.jtice.2011.06.008>.

[33] M.J. Valero-Romero, F.J. García-Mateos, J. Rodríguez-Mirasol, T. Cordero, Role of surface phosphorus complexes on the oxidation of porous carbons, *Fuel Process. Technol.* 157 (2017) 116-126. <https://doi.org/10.1016/j.fuproc.2016.11.014>.

- 1  
2  
3  
4  
5  
6  
7  
8  
9  
10  
11  
12  
13  
14  
15  
16  
17  
18  
19  
20  
21  
22  
23  
24  
25  
26  
27  
28  
29  
30  
31  
32  
33  
34  
35  
36  
37  
38  
39  
40  
41  
42  
43  
44  
45  
46  
47  
48  
49  
50  
51  
52  
53  
54  
55  
56  
57  
58  
59  
60  
61  
62  
63  
64  
65
- [34] C. Krupjiti, B. Jongsonjiti, Catalytic ethanol dehydration over different acid-activated  
montmorillonite clays, *J. Oleo Sci.* 65 (2016) 347-355.  
<https://doi.org/10.5650/jos.sssi15244>.
- [35] J. Ob-eye, P. Prasertdam, B. Jongsonjiti, Dehydrogenation of ethanol to acetaldehyde  
over different metals supported on carbon catalysts, *Catalysts*. 9 (2019) 14 pages.  
<https://doi.org/10.3390/catal9010066>.

## ประวัตินักวิจัยและคณะ พร้อมหน่วยงานสังกัด

หัวหน้าโครงการ	ศาสตราจารย์ ดร.เหมือนเดือน พิศาลพงษ์
ส่วนงาน	ภาควิชาวิศวกรรมเคมี คณะวิศวกรรมศาสตร์
คุณวุฒิ	Ph.D. (Chemical Engineering) Colorado State University, พ.ศ. 2542

## ผลงานทางวิชาการด้าน บทความวิชาการ, ตำรา/หนังสือ

บทความวิชาการ (ปี 2554 – ปัจจุบัน)

1. Bangrak, P., Limtong, S., Phisalaphong, M., “Continuous ethanol production using immobilized yeast cells entrapped in loofareinforced alginate carriers”, Brazilian Journal of Microbiology Vol. 42, p 676-684 (2011).
2. Mongkolkajit, J., Pullsirisombat, J., Limtong, S., Phisalaphong, M., “Alumina-doped alginate gel as a cell carrier for ethanol production in a packed-bed bioreactor”, Biotechnology and Bioprocess Engineering Vol.16, p 505-512 (2011).
3. Chiaoprakobkij, N., Sanchavanakit, N., Subbalekha, K., Pavasant, P., Phisalaphong, M., “Characterization and biocompatibility of bacterial cellulose/alginate composite sponges with human keratinocytes and gingival fibroblasts”, Carbohydrate Polymers Vol.85, p 548-553 (2011).
4. Rattanapan, A., Limtong, S., Phisalaphong, M., “Ethanol production by repeated batch and continuous fermentations of blackstrap molasses using immobilized yeast cells on thin-shell silk cocoons”, Applied Energy Vol.88, p 4400-4404 (2011).
5. Eiadpum, A., Limtong, S., Phisalaphong, M., “High-temperature ethanol fermentation by immobilized coculture of *Kluyveromyces marxianus* and *Saccharomyces cerevisiae*”, Journal of Bioscience and Bioengineering Vol.114, p 325-329 (2012).
6. Taokaew, S., Seetabhawang, S., Siripong, P., Phisalaphong, M., “Biosynthesis and characterization of nanocellulose-gelatin films”, Materials Vol.6, p 782-794 (2013).
7. Phisalaphong, M., Kirdponpattara, S., Kingkaew, J., Taokaew, S., Chiaoprakobkij, N., Sanchavanakit, N., “Modification of bacterial cellulose by adding interfering biopolymers”, Abstracts of papers of the American Chemical Society, Vol. 245 Meeting Abstract: 123-CELL Published: 7 April 2013.



8. Taokaew, S., Phisalaphong, M., Yin, LY, Newby, BMZ. Effects of drying methods of bacterial cellulose membrane on differentiation and proliferation of induced pluripotent stem cells, Abstracts of papers of the American Chemical Society, Volume: 245 Meeting Abstract: 102-CELL Published: 7 April 2013.
9. Kirdponpattara, S., Phisalaphong, M., Newby, B.M.Z., “Applicability of Washburn capillary rise for determining contact angles of powders/porous materials”, Journal of Colloid and Interface Science Vol.397, p 169-176, (2013) .
10. Kirdponpattara, S., Phisalaphong, M., “Bacterial cellulose-alginate composite sponge as a yeast cell carrier for ethanol production”, Biochemical Engineering Journal, 77, p 103-109 (2013).
11. Kirdponpattara, S., Newby, B.Z., Phisalaphong, M., “Effect of oxygen plasma treatment on bacterial cellulose-alginate composite sponge as a yeast cell carrier for ethanol fermentation”, Advanced Materials Research, 724-725, pp. 1150-1153 (2013).
12. Mulalee, S., Chanprasert, J., Kerdpoksup, P., Sawangpanya, N.S., Phisalaphong, M. “Esterification of oleic acid and bioalcohols using immobilized lipase”, Advanced Materials Research, 724-725, p 1154-1157 (2013).
13. Taokaew, S., Phisalaphong, M., Zhang Newby, B.-M., “In vitro behaviors of rat mesenchymal stem cells on bacterial celluloses with different moduli”, Materials Science and Engineering C, Vol.38, p 263-271 (2014).
14. Taokaew, S., Nunkaew, N., Siripong, P., Phisalaphong, M., “Characteristics and anticancer properties of Bacterial cellulose films containing ethanolic extract of mangosteen peel”, Journal of Biomaterials Science: Polymer Edition Vol. 25(9), p. 907-922 (2014).
15. Kingkaew, J.,Kirdponpattara, S.,Sanchavanakit, N.,Pavasant, P., Phisalaphong, M., “Effect of Molecular Weight of Chitosan on Antimicrobial Properties and Tissue Compatibility of Chitosan-impregnated Bacterial Cellulose Films”, Biotechnology and Bioprocess Engineering Vol.19(3), p 534-544 (2014).
16. Mulalee, S., Sena, K., Phisalaphong, M., “Enzymatic esterification of oleic acid and propanol by Novozym 435”, Applied Mechanics and Materials Vol.705, p 29-33 (2015).
17. Kittithanesuan, N., Phisalaphong, M., “Thin-shell silk socoon (TSC) as a nitrogen source of ABE fermentation by Clostridium acetobutylicum”, Applied Mechanics and Materials Vol.705, p14-18 (2015).
18. Kittithanesuan, N., Phisalaphong M. “Enhanced acetone-butanol production from sugarcane juice by immobilized Clostridium acetobutylicum (ATCC 824) on thin-shell silk cocoons”, Biotechnology and Bioprocess Engineering Vol. 20 (3), p 599-607(2015).

19. Suratago, T., Taokaew, S., Kanjanamosit, N., (...), Burapatana, V., Phisalaphong, M. "Development of bacterial cellulose/alginate nanocomposite membrane for separation of ethanol-water mixtures" *Industrial and Engineering Chemistry Vol. 32*, p 305-312 (2015).
20. Taokaew, S., Phisalaphong, M., Zhang Newby, B.-M., "Modification of bacterial cellulose with organosilanes to Improve attachment and spreading of human fibroblasts", *Cellulose Vol. 22 (4)*, p 2311-2324, (2015).
21. Kirdponpattara, S., Khamkeaw, A., Sanchavanakit, N., Pavasant, P., Phisalaphong, M. "Structural modification and characterization of bacterial cellulose-alginate composite scaffolds for tissue engineering", *Carbohydrate Polymers Vol.132* p. 146-155 (2015).
22. Mulalee, S., Srisuwan, P., Phisalaphong, M., "Influences of operating conditions on biocatalytic activity and reusability of Novozym 435 for esterification of free fatty acids with short-chain alcohols: a case study of palm fatty acid distillate (PFAD)", *Chinese Journal of Chemical Engineering Vol.23* p.1851–1856 (2015).
23. Khamkeaw, A., Phisalaphong, M., "Hydrolysis of cassava starch by co-immobilized multi-microorganisms of Loog-Pang (Thai rice cake starter) for ethanol fermentation", *Food Science and Biotechnology Vol. 25(2)*, p. 509-516 (2016).
24. Suratago, T., Panitchakarn, P., Kerdlarpphon, P., Burapatana, V., Phisalaphong, M. "Bacterial cellulose-alginate membrane for dehydration of biodiesel-methanol mixtures" *Engineering Journal Vol. 20(5)*, p. 145-153 (2016)
25. Phomrak, S., Phisalaphong, M., "Reinforcement of Natural Rubber with Bacterial Cellulose via a Latex Aqueous Microdispersion Process", *Journal of Nanomaterials*, 4739793 (2017).
26. Ibnu Abdulwahab, M., Khamkeaw, A., "Jongsomjit, B., Phisalaphong, M. "Bacterial Cellulose Supported Alumina Catalyst for Ethanol Dehydration", *Catalysis Letters Vol. 147(9)*, p. 2462-2472 (2017)
27. Kirdponpattara, S., Phisalaphong, M., Kongruang, S. "Gelatin-bacterial cellulose composite sponges thermally cross-linked with glucose for tissue engineering applications", *Carbohydrate Polymers Vol. 177*, pp. 361-368 (2017)
28. Taokaew, S., Piyaviriyakul, S., Siripong, S., Phisalaphong, M. "Aqueous and Ethanolic Extracts of Mangosteen Peels as Natural Antimicrobial/anticancer Materials Against Pathogenic Microbes and B16F10 Murine Melanoma", *Chiang Mai J. Sci.* 2017 (in press)

ตำรา/หนังสือ (Book Chapter) (ปี 2554 – ปัจจุบัน)

1. Taokaew, S., Phisalaphong, M., Newby, B.-M.Z. Bacterial cellulose: Biosyntheses, modifications, and applications in Applied Environmental Materials Science for Sustainability. Ed. by T. Kobayashi 2016, IGI Global (Hershey, PA 17033, USA).
2. Phisalaphong, M., Tran, T-K, Taokaew, S., Budiraharjo, R., Febriana, G, Nguyen, D-N, Chu-Ky, S., Dourado, F., Nata de coco Industry in Vietnam, Thailand, and Indonesia, in Bacterial Nanocellulose: From Biotechnology to Bio-Economy, Ed. by M. Gama, F. Dourado, S. Bielecki 2016, Elsevier (B.V., Amsterdam, The Netherland).
3. Phisalaphong, M., Kirdponpattara, S., Synthesis and Characterization of Bacterial Cellulose-Based Composites and Their Applications, Handbook of Sustainable Polymers: Processing and Applications. Ed. by V. K. Thakur and M. K. Thakur, 2015, Pan Stanford Publishing Pte. Ltd. (Singapore).
4. Phisalaphong, M., Chiaoprakobkij, N., Applications and Products-Nata de Coco, in Bacterial NanoCellulose; a sophisticated multifunctional material. Ed. by M. Gama, P. Gatenholm and D. Klemm, 2013, CRC Press, Taylor & Francis Group (Florence, KY, USA).
5. Phisalaphong, M.,Jatupaiboon, N., Kingkaew, J., Biosynthesis of Cellulose-Chitosan Composite, in Chitin, Chitosan, Oligosaccharides and Their Derivatives. Ed. By Se-Kwon Kim, 2011, CRC Press, Taylor & Francis Group (Florence, KY, USA).